Soil – Atmosphere Interaction:
Modeling the fate of semi-volatile organic compounds and chemical weathering of marine mudrocks

Dissertation

der Mathematisch-Naturwissenschaftlichen Fakultät

der Eberhard Karls Universität Tübingen

zur Erlangung des Grades eines

Doktors der Naturwissenschaften

(Dr. rer. nat.)

vorgelegt von

Zhongwen Bao

aus Anhui (Lu'an), China

Tübingen

2016

Tag der mündlichen Qualifikation: to date

Dekan: Prof. Dr. Wolfgang Rosenstiel

1. Berichterstatter: Prof. Dr. Peter Grathwohl

2. Berichterstatter: Prof. Dr. David W. Blowes

3. Berichterstatter: Dr. Chuanhe Lu

Abstract

In this dissertation, reactive transport modeling is applied to analyze coupled physical, biological, geochemical and hydrological processes at the soil-atmosphere interface. Focus is on mass transfer of compounds between different environmental compartments (e.g. groundwater, the unsaturated zone, soils, plants and the atmosphere). The influence of soil-atmosphere diffusive gas exchange and water infiltration is addressed with respect to environmental fate of semi-volatile organic compounds (SVOCs) as well as oxidation and carbon turnover during chemical weathering of pyrite- and kerogen-bearing mudrocks. Conceptual models considering soils, plants, and the atmospheric boundary layer were developed and solved numerically with a multicomponent reactive transport code (MIN3P). The models consider eddy diffusion and photochemical oxidation in the atmosphere, changes in the thickness of the atmospheric boundary layer, gas diffusion and heat transport in the soil, temperature dependence of sorption and partitioning in soils and plants as well as solute transport by seepage water. Besides these transport processes, biodegradation and geochemical changes in water and solids are considered. Model results on environmental fate of SVOCs show that on the long term (i.e. for centuries) soils are sinks for atmospheric pollutants because of strong sorption and thus limited bioavailability. Potential re-volatilization back into the atmosphere following declined anthropogenic emissions does not change this finding substantially. Modeling shows also that diurnal, temperature-driven volatilization of SVOCs from soils into the atmosphere cannot account for short-term concentration fluctuations often observed in the atmosphere. The latter can only be simulated if a rapidly-exchanging storage compartment is introduced into the model – a function that can be taken over e.g. by plants in conjuction with fast atmospheric mixing due to eddy diffusion.

Numerical simulations of chemical weathering show that initially diffusion is the main physical control in the chemical weathering of pyrite- and kerogen-bearing mudrocks (e.g. Opalinus Clay of the Swabian Alb, Southwestern Germany). Pyrite and kerogen oxidation cause acidification of seepage water, which consequently leads to dissolution of carbonate minerals, i.e. calcite and siderite, and thus to an increase in porosity, release of CO_2 into the atmosphere as well as elevated groundwater alkalinity. Seepage water chemistry highly depends on water infiltration rates (or fluid residence times). In case

water infiltration rates are low, ions accumulate in the seepage water and finally gypsum precipitation starts. The latter has geotechnical consequences such as swelling of the ground, which is often observed for buildings founded in pyrite bearing mudrocks in Southern Germany.

Overall this dissertation demonstrates the capability of reactive transport modeling to elucidate the controls on pollutant and gas exchange between different environmental compartments by considering various coupled physical, biological, geochemical and hydrological processes. This allows to investigate trends in long term soil and groundwater pollution as well as evolution of seepage water chemistry during chemical weathering of mudrocks including CO_2 release into the atmosphere.

Zusammenfassung

In dieser Dissertation werden mit Hilfe eines numerischen Simulationsmodells für den reaktiven Transport von Wasserinhaltsstoffen physikalische, biologische, geochemische und hydrologische Prozesse im Übergangsbereich Boden - Atmosphäre untersucht.

Der Fokus liegt dabei auf dem Stofftransfer und -austausch der Stoffe zwischen unterschiedlichen Umweltkompartimenten (z.B. Grundwasser/wassergesättigte Zone, vadose Zone, Boden, Pflanzen, Atmosphäre). Im Besonderen wird dabei auf den Einfluss des diffusiven Gasaustausches an der Grenzfläche Boden – Atmosphäre und der Infiltration von Niederschlagswasser in die Bodenzone auf das Verhalten und die Verteilung von sogenannten semi-volatilen organischen Verbindungen (SVOCs), sowie auf Oxidationsdynamik und Kohlenstoffumsatz während der Verwitterung von Pyrit- und Kerogen-haltigen Sedimentgesteinen, eingegangen.

Dazu wurden konzeptionelle Modelle für die Verbindung bzw. Kopplung der Kompartimente Boden, Pflanze und atmosphärische Grenzschicht entwickelt und in Mehrkomponenten-Transportmodelle mit dem Modell-Code MIN3P umgesetzt. Die Modelle berücksichtigen Eddy-Diffusion und photochemische Oxidation in der Atmosphäre, Änderungen der Mächtigkeit der atmosphärische Grenzschicht, Gasdiffusion und Wärmeübertragung in Böden, Temperaturabhängigkeit von Stoffsorption und -verteilung in Böden und Pflanzen sowie den gelösten Stofftransport im Sickerwasser. Neben diesen Prozessen werden zudem der mikrobiologische Abbau der Stoffe und geochemische Änderungen in Wasser und Festphase betrachtet.

Die Modellergebnisse zeigen, dass - langfristig betrachtet - Böden als Senken für SVOCs in der Atmosphäre fungieren. Die vergleichsweise starke Sorption und dementsprechend geringe Bioverfügbarkeit der SVOCs führt zu einer Anreichung im Oberboden. Eine denkbare Ausgasung der SVOCs in die Atmosphäre als Folge rückläufiger anthropogener Schadstoffemissionen ändert diesen Befund nur geringfügig. Die Simulationen zeigen auch, dass die in der Atmosphäre beobachteten kurzfristigen Konzentrationsschwankungen nicht durch die regelmäßige Ausgasung von SVOCs aus dem Boden aufgrund der täglichen Temperaturschwankungen erklärt werden können. In der Simulation ist dies nur dann möglich, wenn im Modell ein Speicherkompartiment eingeführt wird, welches einen schnellen Austausch ermöglicht - eine Funktion, die z.B.

die Pflanzen in Verbindung mit einer schnellen Vermischung durch Eddy Diffusion übernehmen können.

Numerische Simulationen zur chemischen Verwitterung von Pyrit- und Kerogen-haltigen Sedimentgesteinen (z.B. der Opalinuston der Schwäbischen Alb in Südwestdeutschland) belegen, dass die Diffusion der anfänglich kontrollierende physikalische Prozess ist. Pyrit- und Kerogen-Oxidation führen zu einer Versauerung des Sickerwassers, wodurch Karbonatmineralien (z.B. Kalzit und Siderit) gelöst werden und es schließlich zu einer Vergrößerung des Porenraums, einer Ausgasung von CO_2 in die Atmosphäre sowie zu einer erhöhten Alkalinität des Grundwassers kommt. Der Chemismus des Grundwassers ist dabei abhängig von den relevanten Verweilzeiten, d.h. von der Höhe der Grundwasserneubildungsrate. Bei geringer Grundwasserneubildung kann es zur Akkumulation von Ionen im Sickerwasser und in der Folge zur Ausfällung von Gips kommen. Letzteres kann zu einer Volumenvergrößerung und schließlich zu Bodenhebungen führen, deren Folgen häufig an Gebäuden, die auf pyrithaltigem Sedimentgestein in Süddeutschland gebaut sind, zu beobachten sind.

Insgesamt demonstriert diese Dissertation wie die reaktive Stofftransportmodellierung als Werkzeug genutzt werden kann, um die kontrollierenden Faktoren für den Austausch von Schadstoffen und Gasen zwischen verschiedenen Umweltkompartimenten zu ergründen, indem unterschiedliche physikalische, biologische, geochemische und hydrologische Prozesse gekoppelt betrachtet werden. Damit können langfristige Trends der Verunreinigung von Böden und Grundwasser untersucht und erklärt werden, ebenso wie die Entwicklung von Sickerwasserchemismus durch Gesteinsverwitterung und der ggf. resultierenden Freisetzung von CO_2 in die Atmosphäre.

Acknowledgements

Contents

List of Figures

II

III

List of Tables

Notation

The following table lists some of the major symbols used in this work. Generic units of the symbols are given here. Specific units and local notations are given in the text.

Symbol	Definition	Dimension
Greek letters:		
α	van Genuchten model: capillary pressure parameter	[1/L]
α^*	dispersivity	[1/L]
θ	volumetric water content	[-]
λ	reaction rate constant	[1/T]
λ_{biodeg}	reaction rate constant: microbial biodegradation	[1/T]
$\lambda_{photodeg}$	reaction rate constant: photochemical transformation	[1/T]
ρ	solids density	[M/L^3]
ρ_i	density of reactive mineral *i*	[M/L^3]
$\rho_{mudrock}$	density of mudrock	[M/L^3]
ρ_{OPC}	grain density of Opalinus Clay	[M/L^3]
ρ_{plant}	density of plant materials	[M/L^3]
τ	time period of diurnal temperature changes	[T]
ψ_a	matric potential	[L]
φ_i	volume fraction of reactive mineral *i*	[-]
δ	thickness of the stagnant air layer	[L]
$\omega_{particle}$	concentration of atmospheric particles	[M/L^3]
Latin letters:		
C	concentration of a compound in gas or water	[M/L^3]
C_0	initial concentration of a compound in gas or water	[M/L^3]
C/C_0	normalized concentration of a compound in gas or water	[-]
C/C_{ref}	normalized concentration of a compound in gas	[-]
C_g	concentration of a compound in gas	[M/L^3]
C_{ref}	reference concentration	[M/L^3]
C_{plant}	concentration of a compound in plant materials	[M/M bulk phase]
$C_{particle}$	concentration of a compound in atmospheric particles	[M/M bulk phase]
C_s	concentration of a compound in soild phase	[M/M bulk phase]
C_w	concentration of a compound in water	[M/L^3]
$C_{w,in}$	concentration of a compound at the inflow boundary	[M/L^3]
$C_{w,s-s}$	steady-state concentration of a compound in water	[M/L^3]
D	hydrodynamic dispersion coefficient	[L^2/T]
Da	Damköhler number	[-]
D_a	apparent diffusion coefficient	[L^2/T]
D_{eddy}	eddy diffusion coefficient in the atmosphere	[L^2/T]
D_{eg}	effective diffusion coefficient in gas	[L^2/T]
D_{ew}	effective diffusion coefficient in water	[L^2/T]

$D_g{}^*$	free phase diffusion coefficient in gas	[L^2/T]
$D_w{}^*$	free phase diffusion coefficient in water	[L^2/T]
f_{oc}	soil organic carbon content	[-]
H	Henry's law coefficient	[-]
h	soil depth	[L]
h_{ABL}	thickness of the atmospheric boundary layer	[L]
h_{plant}	equivalent depth of plants	[L]
ΔH_{aw}	enthalpy of air-water partitioning	[]
ΔH_{PA}	enthalpy of plant-air partitioning	[]
$\Delta H_{sorption}$	enthalpy of sorption	[]
h_ψ	hydraulic potential	[L]
K	hydraulic conductivity	[L/T]
$K_{1/2S,O_2}$	Monod term of the half-saturation constant	[M/L^3]
k	von Kármán constant	[-]
K_e	empirical factor for calculating diurnal temperature changes	[-]
K_{eq}	equilibrium constant	[-]
k_{eff}	effective rate contant	[M/(L^{3}bulk·T)]
K_d	distribution coefficient	[L/M]
K_{OA}	Octanol-air partition coefficient	[L/M]
K_{oc}	soil organic carbon-water partition coefficient	[L/M]
K_{PA}	plant-air partition coefficinet	[L^3/M]
$K_{particle-air}$	particle-air partition coefficient	[L^3/M]
K_{SG}	soil-air partition coefficient	[L^3/M]
k_{rw}	relative permeability	[-]
K_T	thermal diffusivity	[L^2/T]
l	van Genuchten model: parameter	[-]
M	mass of a compound in the subsurface	[M]
m	mass of the mudrock	[M]
m_i	mass of reactive mineral i	[M]
MW	molecular weight	[-]
N	van Genuchten model: pore	[]
N_m	total number of reactive minerals	[-]
n	porosity	[-]
n_g	gas-filled porosity	[-]
n_{gyp}	total mass of gypsum per square meter surface area	[M/L^2]
n_w	water-filled porosity	[-]
Q	source and sink terms resulting from biogeochemical reactions	[M/(L^3·T)]
Q_{biodeg}	sink terms resulting from microbial biodegradation	[M/(L^3·T)]
$Q_{photodeg}$	sink terms resulting from photochemical transformation	[M/(L^3·T)]
q	groundwater recharge rate or water infiltration rate	[L/T]
R	ideal gas law constant	[L^2/(t·T^2)]
R_j	reaction rate of reaction j	[M/(L^{3}bulk·T)]
S	water solubility	[M/L^3]
S_{ew}	effective water saturation	[-]
S_g	gas saturation	[-]
S_{rw}	residual water saturation	[-]

S_w	water saturation	[-]
S_s	specific storage coefficient	[1/L]
S_{scl}	subcooled liquid solubility	[M/L^3]
u_*	friction or sheer velocity	[L/T]
T	specified temperature	[t]
T_0	standard temperature	[t]
T_A	average temperature	[t]
t	time	[T]
t_a	time scale of flow	[T]
t_c	characteristic time of steady state	[T]
t_r	time scale of biodegradation	[T]
$t_{1/2,biodeg}$	half-life of biodegradation	[T]
$t_{1/2,photodeg}$	half-life of photochemical transformation	[T]
$V_{mudrock}$	volume of mudrock	[L^3]
V_i	volume of mineral i	[L^3]
V_{gyp}	potential volume of gypsum	[L^3]
ΔV_{gyp}	molar volume of gypsum	[L^3]
$v_{i,j}$	stoichiometric coefficient of component i in reaction j	[-]
V_{plant}	effecive volume of plants per square meter land surface	[L^3/L^2]
wt_i	weight fraction of reactive mineral i	[-]

Additional symbols used

IAP	ion activity product	[-]
PCBs	polychlorinated biphenyls	[-]
PAHs	polycyclic aromatic hydrocarbons	[-]
SVOCs	semi-volatile organic compounds	[-]

Chapter 1.

Introduction

1.1 Motivation

Typically, anthropogenic activities, atmospheric deposition, geological sources, temperature changes, biogeochemical transformations, and water-rock interactions pose strong impacts on mass transfer of a compound within/across environmental compartments. Mass transfer of a compound within or across environmental compartments usually takes place by coupled physical, biological, geochemical and hydrological processes, i.e. advection, dispersion, effective and eddy diffusion, sorption, and microbial degradation. For example, anthropogenic activities release many semi-volatile organic compounds (SVOCs) into the environment. Some of these SVOCs may persist as a result of their affinity to soil particles (sorption) and their resistance to photolytic, chemical, and microbial degradation. Hence, these compounds may have a tendency for long-range transport (Bao et al., 2015), eventually causing atmospheric pollution. Some atmospheric pollutants first accumulate in topsoils due to wet and gas deposition, retardation (sorption), advection, dispersion, and diffusion (Cousins et al., 1999), while on the long term they may leach into groundwater when topsoils are fully loaded. Plants may be important in regulating atmospheric concentrations of these pollutants (Jones et al., 1992; Simonich and Hites, 1994a, 1994b, 1995; Kömp and McLachlan, 1997; McLachlan, 1999; Hung et al., 2001; Terzaghi et al., 2015). Changes in land use, temperature and climate, and reduced anthropogenic emissions can cause re-volatilization of pollutants from soils and plants into the atmosphere (Bao et al., 2015, 2016). For instance, at elevated temperatures and/or reduced atmospheric concentrations, pollutants in soils and plants may re-volatilize into the atmosphere by vapor phase diffusion. Therefore, mass transfer of SVOCs across the soil-atmosphere interface is an important mechanism for the environmental fate of SVOCs and environmental safety regarding the quality of soils, groundwater, and the atmosphere.

Mass transfer of inorganic gases (particularly O_2 and CO_2) across the soil-atmosphere interface strongly influences chemical weathering of sedimentary rocks as well as soil and groundwater chemistry. As an example, oxidation of reduced phases (such as pyrite and organic minerals) by O_2 acidifies seepage water, which causes dissolution of carbonates, precipitation of secondary minerals, as well as release of CO_2 and dissolved species. Eventually, porosity, soil structure and other soil properties may be adversely affected.

Fig. 1.1 shows coupled physical, biological, geochemical and hydrological processes that may control mass transfer of SVOCs between different compartments (e.g. soils, plants, and the atmosphere) as well as gas exchange of O_2 and CO_2. As evident from Fig. 1.1, soil-atmosphere exchange is important for many subsurface processes and engineered applications. Typically, using numerical models to address soil-atmosphere exchange is an important research priority. However, numerical models were usually designed focusing on specific aspects of the real-world problem. Therefore, development of numerical models to evaluate comprehensive interactions of coupled physical, biological, geochemical and hydrological processes can provide us with a better understanding of mass transfer dynamics of SVOCs and volatile inorganic gases (e.g. O_2 and CO_2) across compartmental interfaces. Moreover, potential sources of legacy and emerging pollutants as well as potential disasters with respect to geotechnical applications can be identifed. Based on scientific knowledge, such numerical models, hence, can helps us to introduce further environmental regulations and may serve as tools for management and engineering applications, e.g. limiting sources of environmental pollutants, evaluating status of soil and groundwater pollution and remediation, natural attenuation, waste disposal and re-cycling, and bioenergy production and collection (Maier, 2004; Haberer, 2012).
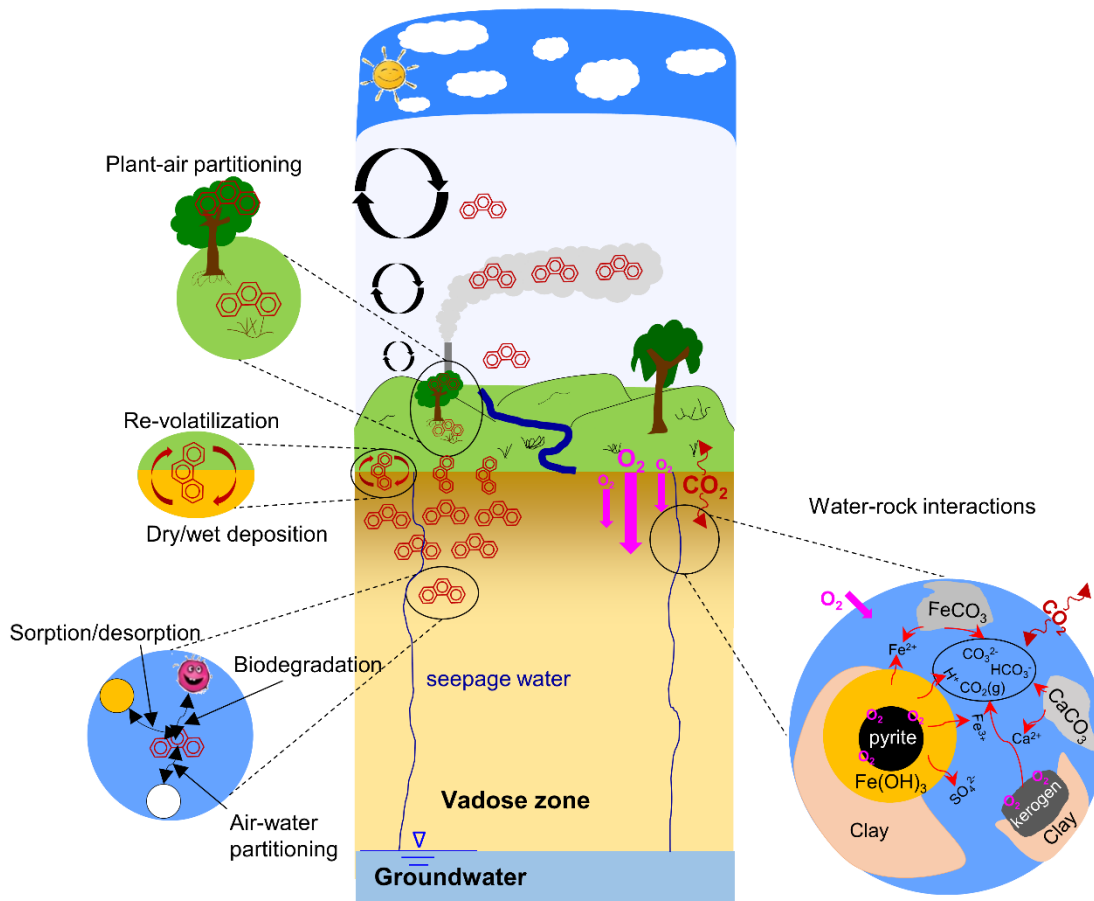
Figure 1.1. Conceptual description of physicochemical processes controlling the environmental fate of SVOCs and chemical weathering of sedimentary mudrocks.

1.2 Scope of this study

To model coupled physical, biological, geochemical and hydrological processes with diffusive gas exchange across the soil-atmosphere interface, the numerical code MIN3P (Mayer et al., 2002) was extended with the atmospheric boundary layer and a plant layer. Two case studies are used for illustration purposes (Fig. 1.1): (*i*) multimedia environmental fate of SVOCs and (*ii*) chemical weathering of sedimentary mudrocks. In the first case study, the code was applied for modeling long-term soil pollution and short-term temperature-driven cycling of SVOCs in the soil–plant–atmosphere system. In the second case study, MIN3P was used to simulate chemical weathering of pyrite- and

3

kerogen-bearing mudstones with focus on gas exchange (O_2 and CO_2), dynamics of carbon, iron and sulfur turnover, mineral transformation (mineral oxidation, dissolution and precipitation and finally increase of porosity) and evolution of water chemistry. Main characteristics of the compounds considered (i.e. SVOCs, O_2 and CO_2) are given below.

1.2.1 Semi-volatile organic compounds (SVOCs)

SVOCs include legacy compounds, such as organochlorine pesticides (OCPs), polycyclic aromatic hydrocarbons (PAHs), polychlorinated biphenyls (PCBs), organochlorine pesticides and brominated flame retardants (PBDEs), as well as some emerging pollutants, i.e. pharmaceuticals and personal care products (PPCPs) and poly- and perfluorinated compounds (PFCs). SVOCs are mainly released into the environment by anthropogenic activities, e.g. agricultural applications, incomplete combustion of organic materials such as natural gas, fuels, and biomass for heating, transportation, etc. Many SVOCs accumulate in the environment due to their affinity to organic matter by sorption and their resistance to microbial degradation and photochemical transformation, and may be widely distributed by atmospheric cycles from local to regional and global scales. However, some SVOCs (such as phenanthrene) are easily degradable chemicals under aerobic conditions; reasons for their persistence in topsoils may depend on comprehensive interactions of underlying physical, biological and hydrological processes, and thus deserve further investigations. In addition, some SVOCs may pose mutagenic, carcinogenic, and toxicological effects to humans and other biological life-forms.

1.2.2 O_2 and CO_2

Oxygen is the richest element in the earth's crust. Furthermore, O_2 is of significant importance for maintaining aerobic organisms. It acts as an important electron acceptor e.g. for oxidation of reduced phases and for aerobic microbial reactions. CO_2 plays an important role in regulating regional and global temperatures, and hence ensures the suitability of the Earth for biological life. Currently, atmospheric partial pressures of O_2 and of CO_2 are at 20.9% and 390 ppm of standard atmospheric pressure. In recent decades partial pressure of CO_2 shows an increasing trend due to anthropogenic activities, which consequently influences the climate, economic development and social stability.

4

1.3 Objectives

The objectives of this PhD study were:

- to extend the multicomponent reactive transport code MIN3P (Mayer et al., 2002) with the atmospheric boundary layer, photochemical oxidation, the plant layer, heat transport in the subsurface and temperature-dependent multiphase partitioning to implement coupled physical, biological, geochemical and hydrological processes in the soil–plant–atmosphere system,

- to propose a new framework to model environmental fate of SVOCs and to clearly identify physicochemical processes and relevant parameters controlling mass transfer across different compartments, particularly the environmental fate of SVOCs in the soil–(plant–)atmosphere system.

- and to apply the code for simulating geochemical water-rock reactions in the subsurface. As an example, chemical weathering of pyrite- and kerogen-bearing marine mudrocks in the Swabian Alb, Southern Germany, was chosen to quantify the role of O_2 and CO_2 in driving the weathering process and to answer the question whether chemical weathering of sedimentary rocks acts as a source or as a sink for atmospheric CO_2. Another focus was on seepage water chemistry, dynamics of carbon, iron and sulfur turnover as well as mineral transformation which may impact porosity.

1.4 Structure of the dissertation

In this PhD thesis, the following subjects are presented:

The implementation of the atmospheric boundary layer into the numerical code MIN3P is described in Chapter 2. Thus, a new numerical model, when compared with fugacity models (Mackay, 2001), is introduced into the field of multimedia fate modeling of SVOCs. The extended version of MIN3P is used to evaluate the long-term environmental fate of SVOCs. In addition, an analytical solution is developed to approximate the time required to reach steady state with respect to long-term soil pollution from atmospheric deposition. To investigate temperature-driven cycling of semi-volatile pollutants between different environmental compartments, in Chapter 3 we develop a physically based model coupling soils, plants, and the atmosphere, and which accounts for heat transport, effective gas

diffusion, sorption and biodegradation in the subsurface, and eddy diffusion and photochemical transformation in the atmosphere. The model is applied to simulate temperature-driven mass transfer and concentration fluctuations of PCB-52 (resistant to photo-degradation) and phenanthrene (photo-sensitive) in the soil-plant-atmosphere system.

In Chapter 4, we extend the model to simulate chemical weathering of pyrite- and kerogen-bearing Opalinus Clay in the Swabian Alb, Southern Germany. Apart from investigating the oxidation of pyrite and kerogen by oxygen, subsequent mineral transformation, weathering front propagation, water chemistry and dynamics of carbon, iron and sulfur turnover are also studied in detail.

Geotechnical application of gypsum precipitation below buildings founded in pyrite bearing mudstones in Southern Germany is discussed in Chapter 5.

Overall conclusions and an outlook are given in Chapter 6.

References

Bao, Z., Haberer, C.M., Maier, U., Beckingham, B., Amos, R.T., Grathwohl, P., 2015. Modeling long-term uptake and re-volatilization of semi-volatile organic compounds (SVOCs) across the soil-atmosphere interface. Sci. Total Environ 538, 789-801.

Bao, Z., Haberer, C.M., Maier, U., Beckingham, B., Amos, R.T., Grathwohl, P., 2016. Modeling short-term concentration fluctuations of semi-volatile pollutants in the soil–plant–atmosphere system. Sci. Total Environ. 569-570, 159-167.

Cousins, I.T., Beck, A.J., Jones, K.C., 1999a. A review of the processes involved in the exchange of semi-volatile organic compounds (SVOC) across the air-soil interface. Sci. Total Environ. 228, 5-24.

Haberer, C.M., 2012. Oxygen transfer in a fluctuating capillary fringe (PhD dissertation). University of Tübingen, Tübingen.

Hung, H., Thomas, G.O., Jones, K.C., Mackay, D., 2001. Grass-air exchange of polychlorinated biphenyls. Environ. Sci. Technol. 35, 4066-4073.

Jones, K.C., Sanders, G., Wild, S.R., Burnett, V., Johnston, A.E., 1992, Evidence of a decline of PCBs and PAHs in rural vegetation and air in the United Kingdom. Nature 356, 137-139.

Kömp, P., McLachlan, M.S., 1997. Influence of temperature on the plant/air partitioning of semivolatile organic compounds. Environ. Sci. Technol. 31, 886-890.

Mackay, D., 2001. Multimedia environmental models: the fugacity approach. CRC press.

Maier, U., 2004. Modeling of natural attenuation in soil and groundwater (PhD dissertation). University of Tübingen, Tübingen.

Mayer, U.K., Frind, E.O., Blowes, D.W., 2002. Multicomponent reactive transport modeling in variably saturated porous media using a generalized formulation for kinetically controlled reactions. Water Resour. Res. 38, 1174.

McLachlan, M.S., 1999. Framework for the interpretation of measurements of SOCs in plants. Environ. Sci. Technol. 33, 1799-1804.

Simonich, S.L., Hites, R.A., 1994a. Vegetation-atmosphere partitioning of polycyclic aromatic hydrocarbons. Environ. Sci. Technol. 28(5), 939-943.

Simonich, S.L., Hites, R.A., 1994b. Importance of vegetation in removing polycyclic aromatic hydrocarbons from the atmosphere. Nature 370, 49-50.

Simonich, S.L., Hites, R.A., 1995. Organic pollutant accumulation in vegetation. Environ. Sci. Technol. 29(2), 2905-2914.

Terzaghi, E., Scacchi, M., Cerabolini, B., Jones, K. C., di Guardo, A., 2015. Estimation of polycyclic aromatic hydrocarbon variability in air using high volume, film, and vegetation as samplers. Environ. Sci. Technol. 49, 5520-5528.

Chapter 2.

Modeling long-term uptake and re-volatilization of semi-volatile organic compounds (SVOCs) across the soil-atmosphere interface
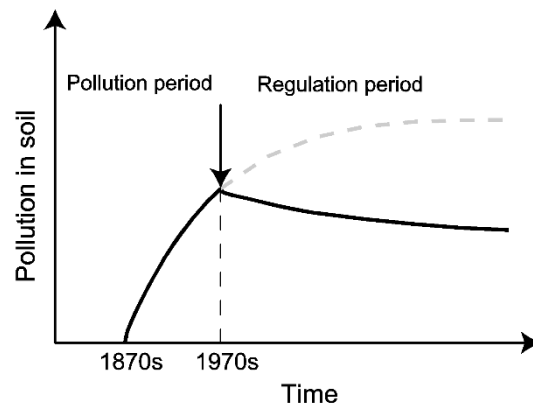
Abstract

Soil-atmosphere exchange is important for the environmental fate and atmospheric transport of many semi-volatile organic compounds (SVOCs). This study focuses on modeling the vapor phase exchange of semi-volatile hydrophobic organic pollutants between soil and the atmosphere using the multicomponent reactive transport code MIN3P. MIN3P is typically applied to simulate aqueous and vapor phase transport and reaction processes in the subsurface. We extended the code to also include an atmospheric boundary layer where eddy diffusion takes place. The relevant processes and parameters affecting soil-atmosphere exchange were investigated in several 1-D model scenarios and at various time scales (from years to centuries). Phenanthrene was chosen as a model compound, but results apply for other hydrophobic organic compounds as well. Gaseous phenanthrene was assumed to be constantly supplied to the system during a pollution period and a subsequent regulation period (with a 50% decline in the emission rate). Our results indicate that long-term soil-atmosphere exchange of phenanthrene is controlled by the soil compartment – re-volatilization thus depends on soil properties. A sensitivity analysis showed that accumulation and transport in soils in the short term is dominated by diffusion, whereas in the long term groundwater recharge and biodegradation become relevant. As expected, sorption causes retardation and slows down transport and biodegradation. If atmospheric concentration is reduced (e.g. after environmental regulations), re-volatilization from soil to the atmosphere occurs only for a relatively short time period. Therefore, the model results demonstrate that soils generally are sinks for atmospheric pollutants. The atmospheric boundary layer is only relevant for time scales of less than one month. The extended MIN3P code can also be applied to simulate fluctuating concentrations in the atmosphere, for instance due to temperature changes in the topsoil.

Keywords: soil and atmosphere pollution, diffusion, sorption, biodegradation, groundwater recharge, phenanthrene.

2.1 Introduction

Over the last two centuries, many semi-volatile organic compounds (SVOCs), such as organochlorine pesticides, polychlorinated biphenyls (PCBs), and polycyclic aromatic hydrocarbons (PAHs), have been produced and intentionally or unintentionally released to the environment due to various anthropogenic activities. For instance, pesticides have been applied on arable land for agricultural production and are still used in developing countries (e.g. DDT for malaria control), PCBs were and still are released into the atmosphere from PCB-containing buildings, electrical equipment and contaminated sediments (Jamshidi et al., 2007), and PAHs are produced as byproducts in combustion of fossil fuels and biomass burning. SVOCs may persist in the environment due to their affinity to natural organic matter in soils or sediments and if they are resistant to photolytic, chemical, and microbial degradation, and can pose risks to ecosystems and human health due to their inherent toxicity, persistence, and tendency for long-range transport and accumulation in organisms.

Since the beginning of industrialization and agriculture intensification, soils became sinks for many SVOCs, some of which are now considered as legacy pollutants. Once applied or released into the atmosphere, SVOCs are transported regionally or globally by atmospheric cycling (van Jaarsveld et al., 1997; Beyer et al., 2000; Totten et al., 2006; Lohmann et al., 2007). As a consequence of atmospheric transport, deposition and re-volatilization, soils have become contaminated at a large scale (Lang et al., 2007). Yet, environmental legislation and technological progress already in place or on the horizon aim to limit emission or application of certain compounds, thus decreasing atmospheric concentrations. Therefore, soils preloaded with SVOCs now may act as secondary sources and SVOCs may re-volatilize to the atmosphere. Soil-atmosphere exchange, therefore, is a critical process determining the long-range/global transport of many SVOCs (Cousins et al., 1999a).

To evaluate the exchange of SVOCs between soil and the atmosphere, several combined soil-atmosphere models (Reichman et al., 2000a, 2000b; Scholtz and Bidleman, 2006, 2007; Komprda et al., 2013) were developed to specifically describe the environmental

fate of surface-applied pesticides as a function of the compound's volatilization rate. In contrast, only few studies have focused on the numerical evaluation of soil-atmosphere exchange of global pollutants such as PAHs and PCBs (Harner et al., 1995; Lee et al., 1998; Wania and Dugani, 2003; Wania et al., 2006; Mackay, 2010; Ghirardello et al., 2010), and even fewer studies investigated the vertical concentration distributions of PAHs and PCBs in soil and the atmosphere (Cousins et al., 1999b, 1999c; Moeckel et al., 2009). Whereas soil-atmosphere exchange has been studied in the field at time scales from hours to seasons (Lee et al., 1998; Bidleman and Leone, 2004; Lang et al., 2007; Tao et al., 2007, 2008; Bozlaker et al., 2008a, 2008b; Schuster et al., 2010; Cabrerizo et al., 2011; Wang et al., 2011; Zhang et al., 2011; Zhong and Zhu, 2013), detailed long-term simulations on pollutant uptake in soils and re-volatilization – specifically that address the vertical concentration distribution across the soil-atmosphere interface – are missing.

In this study, we extended a numerical model to describe the long term vapor phase exchange of SVOCs between soil and the atmosphere under varying boundary conditions. Phenanthrene ($C_{14}H_{10}$) was chosen as a model compound and we specifically focused on the vertical concentration profiles across the soil-atmosphere interface. The main objectives of this study were (*i*) to extend a subsurface multicomponent reactive transport code (MIN3P) by considering an atmospheric boundary layer and taking into account the most relevant transport processes (i.e., advective transport with groundwater recharge, sorption, air-water partitioning, biodegradation, and diffusion), (*ii*) to investigate which processes affect soil-atmosphere exchange of SVOCs in the long term and when steady state will be achieved, and (*iii*) to evaluate the re-volatilization potential after regulations limit input of SVOCs into the atmosphere. Focus of our study was not on matching field data but on the theoretical evaluation of the physico-chemical processes in order to identify the most sensitive parameters in long-term uptake and re-volatilization of organic compounds.

2.2 Background on soil-atmosphere exchange

2.2.1 The atmospheric boundary layer

The atmospheric boundary layer is defined as the lower part of the atmosphere that is in direct contact with the Earth's surface. The height of the atmospheric boundary layer reaches up to 100 - 3000 m above the ground surface, and varies diurnally and seasonally (Wild and Jones, 1995; Harner et al., 1995; Cousins et al., 1999c; Lee et al., 1998; Farrar et al., 2005; Scholtz and Bidleman, 2006, 2007; MacLeod et al., 2007; Tao et al., 2007). Transport of airborne pollutants in the atmospheric boundary layer mainly depends on eddy diffusion, which in turn is related to wind velocity and surface roughness. Wind velocity is dependent on many factors and conditions at varying scales, e.g. on pressure gradients and on local weather conditions. Under neutral or stable atmospheric conditions, i.e. when vertical air movement does not take place beyond the rate of adiabatic heating or cooling, wind velocity and direction primarily varies horizontally. The horizontally moving air carries momentum, water vapor, heat, and chemicals, which results in turbulent transport of these components also perpendicular to the mean wind direction.

2.2.2 Time-dependent accumulation of SVOCs in soils

The history of SVOCs accumulation in soils, especially for PCBs and organochlorine pesticides, can be traced through a simple conceptual model (depicted in Fig. 2.1) that includes two phases: a pollution period and a regulation period. Prior to industrialization, natural emissions had already resulted in a low background pollution of soils with SVOCs, but with the onset of industrial revolution in the 19th century, anthropogenic activities increased the amount in the environment. Generally, the highest concentrations of SVOCs in the environment were observed in the 1960s and 1970s. In the late decades of the 20th century, regulatory policies for responsible energy consumption and economic development as well as international source reduction measures have been enacted to protect the environment. Since then a continuous decrease in concentrations of many environmental pollutants has been observed in industrialized countries (Gocht and Grathwohl, 2004; Prevedouros et al., 2004; Schuster et al., 2010). As a consequence, the concentrations of SVOCs in soils (black solid lines in Fig. 2.1) are expected to decrease when compared to the hypothetical case in which no reduction measures were applied

(grey dashed line in Fig. 2.1). SVOCs present in the soil eventually may undergo degradation by microorganisms, re-volatilize to the atmosphere because of reduced atmospheric concentrations, and/or leach to the underlying groundwater. In early-industrialized countries such as Germany, over the last two centuries a similar trend with respect to the accumulation of PAHs in soils or sediments was observed (Gocht and Grathwohl, 2004). In fact, due to technological progress and regulation nowadays significantly less PAHs are emitted into the atmosphere than in the middle of the last century.
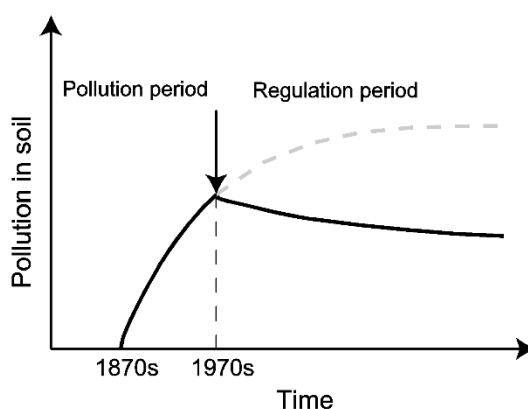
Figure 2.1. Simplified temporal trend for the accumulation of SVOCs in soils during the high emission period (from ca. 1870 to 1970) and the subsequent regulation period (since ca. 1970). Eventually, steady-state conditions will establish because of biodegradation and leaching towards groundwater; the grey dashed line refers to the case in which no environmental reduction measures have been applied, whereas the black solid line accounts to a 50% decrease of pollutant input (after the 1970s), e.g. because of environmental regulations (from numerical simulation).

2.3 Numerical simulations and parameters

2.3.1 Physicochemical parameters of phenanthrene

Phenanthrene was chosen as a representative model compound, because it has physico-chemical properties (hydrophobic, lipophilic) similar to many other SVOCs. Furthermore, phenanthrene is widely spread in the atmosphere and, thus, significantly contributes to the high concentrations of this pollutant in topsoils, e.g. in Germany (Gocht et al., 2001, 2007). As phenanthrene is a relatively easily degradable compound under aerobic

13

conditions, the role of biodegradation on the long-term fate of this compound in soils can be studied.

Several studies on the environmental fate and the transport of phenanthrene in soils provide reliable data on sorption and biodegradation processes. Phenanthrene is mainly present as vapor in the free atmosphere or sorbed to the soil organic carbon. Sorption/desorption equilibrium of phenanthrene in fine grained soils or sediments (particle size less than 0.1 mm) was shown to occur in typical time scales of few weeks, and certainly in less than one year (Rügner et al., 1999; Kleineidam et al., 1999, 2002, 2004; Karapanagioti et al., 2000; Wang et al, 2007; Kuntz and Grathwohl, 2009). Therefore, for the time periods relevant in this study (years to centuries) sorption/desorption at the grain scale can be considered as a local equilibrium process. Table 2.1 summarizes the relevant physicochemical properties of phenanthrene used in the numerical simulations.

Table 2.1. Physicochemical properties of phenanthrene at 25 °C.

Chemical name	Unit	Value	Reference
Molecular weight, MW	g/mol	178.2	Schwarzenbach et al. (2003)
Overall half-life of biodegradation, $t_{1/2,biodeg}$	Hours	1.60×10^3	Gouin et al. (2000)
Aqueous diffusion coefficient, D_w^*	m^2/s	6.71×10^{-10}	Grathwohl (1998)
Gaseous diffusion coefficient, D_g^*	m^2/s	5.97×10^{-6}	Grathwohl (1998)
Water solubility, S	g/m^3	1.1	Schwarzenbach et al. (2003)
Subcooled liquid solubility, S_{scl}	g/m^3	3.05	Liu et al. (2013b)
Henry's law coefficient, H	dimensionless	1.0×10^{-3}	Verschueren (1983)
Enthalpy of air-water partitioning, ΔH_{aw}	kJ/mol	47	Schwarzenbach et al. (2003)
Enthalpy of sorption, $\Delta H_{sorption}$	kJ/mol	-30	Wang and Grathwohl (2013)

2.3.2 Conceptual model

A vertical 1-D model was applied to describe soil-atmosphere exchange of SVOCs (Fig. 2.2). We considered an open two-compartment model, in which a 100 m thick atmospheric boundary layer overlies a soil compartment with two soil layers, namely a 0.1 m thick topsoil layer with elevated organic carbon content and the vadose zone (subsoil layer) above a groundwater table at 5 m depth.
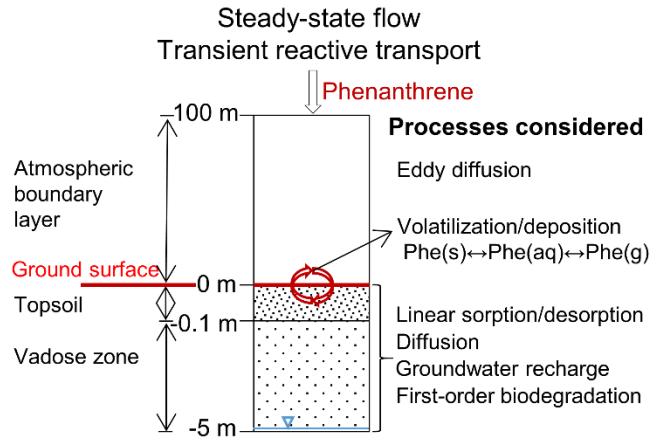
Figure 2.2. Conceptual model of soil-atmosphere exchange of phenanthrene ('Phe') with a 100 m thick atmospheric boundary layer (not drawn to scale), a 0.1 m thick topsoil layer, and a 4.9 m thick vadose zone above the groundwater table.

The two soil layers primarily consist of sandy material and are distinct from each other by different porosity, organic carbon content, and water saturation (Table 2.2). An average value of the organic carbon content of 3% (mean f_{oc}-case) was chosen for the topsoil layer, which approximates the average for European countries (Panagos et al., 2013). The organic carbon content in the subsoil was assumed to be ten times smaller than that in the topsoil. Low and high f_{oc}-cases (1% to 10%) were simulated since data on the spatial distribution of organic carbon content in soils, collected by the European Soil Data Centre, indicate a high natural variability of organic carbon contents ranging from 0.01% to over 35%. Potential co-transport of phenanthrene with dissolved organic carbon (DOC) in the soil water would be less significant than the effect of variability in soil organic carbon content and therefore was not considered (with DOC concentrations of less than 20 mg/L, the expected change in sorption of phenanthrene would be less than 20%). Potential changes in the organic carbon content of soils were accounted for by comparing the three different levels of f_{oc}.

A vertical water saturation profile was implemented using the well-known van Genuchten parameterization (e.g., Carsel and Parrish, 1988). The values of the van Genuchten parameters used in this study are given in Table 2.2.

Table 2.2. Physical and hydraulic parameters used in our conceptual model for the two soil layers.

Input parameter	Unit	Subsoil layer	Topsoil layer
Porosity, n	dimensionless	0.33	0.40
Organic carbon content, f_{oc} (low f_{oc}-case)	dimensionless	0.1%	1%
Organic carbon content, f_{oc} (mean f_{oc}-case)	dimensionless	0.3%	3%
Organic carbon content, f_{oc} (high f_{oc}-case)	dimensionless	1%	10%
Residual water saturation, S_{rw}	dimensionless	0.2	
van Genuchten parameter, α	1/m	14.5	
van Genuchten parameter, N	dimensionless	2.68	
van Genuchten parameter, l	dimensionless	0.5	
Hydraulic conductivity, K	m/s	8.3×10^{-5}	
Dispersivity, α^*	m	0.01	
Groundwater recharge rate, q	mm/year	200	
Solids density, $\boldsymbol{\rho}$	kg/m³	2650	

The soil compartment was implemented as a 3-phase system with solid, aqueous, and gaseous phases. Phenanthrene is transported in the gaseous and aqueous phases, and partitions among the three different phases. In the atmosphere gaseous and aqueous phase transport was considered, whereas particle-associated deposition of airborne phenanthrene was not investigated in our study.

By implementing a first-order chemical reaction in the aqueous phase, we accounted for microbial degradation of phenanthrene in the subsurface:

$$C_{14}H_{10}(aq) + 16.5O_2 + 9H_2O \rightarrow 14CO_3{}^{2-} + 28H^+$$
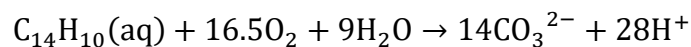
The reaction rate for microbial degradation of aqueous phenanthrene, with a half-life ($t_{1/2,biodeg} = \ln(2)/\lambda$ [s]), was assumed to be temperature independent.

In addition, bioturbation in soils (i.e., by feeding and burrowing of earthworms or other animals) (Cousins et al., 1999c) or ploughing activities on agricultural land may have a strong effect on vertical mixing, and thus on mass transport. Bioturbation is very species specific and hence hard to quantify (Hedman, 2008). In this study, therefore, we focus on undisturbed soils, i.e. without additional mixing due to bioturbation and ploughing. Modelling was limited to steady-state flow of water and temperature was assumed to stay

constant. In an earlier study, Kuntz and Grathwohl (2009) showed that the assumption of steady-state flow is justified to be representative for the prediction of long-term average concentrations of compounds in seepage water (i.e. average concentrations obtained from transient simulations are very close to concentrations from steady-state simulations in most cases of mid latitude precipitation frequency and intensity). At the upper boundary of the domain (Fig. 2.2), water infiltrates at a fixed rate and is allowed to discharge freely via the bottom boundary (i.e. free seepage boundary at z = -5 m). A groundwater recharge rate of 200 mm/year and an average annual temperature of 10 °C were assumed, representative for the weather conditions in Germany (data from the German Weather Service, DWD, and the Federal Institute for Geosciences and Natural Resources, BGR).

2.3.3 Model description

The numerical code MIN3P was used to simulate the soil-atmosphere exchange of phenanthrene and its reactive transport towards the groundwater table. MIN3P couples Richards' equation, the governing equation for water flow under variably saturated conditions, with reactive advective-dispersive transport in the aqueous phase and diffusive transport in the gaseous phase (Mayer et al., 2002). A generalized formulation for multicomponent, kinetically controlled and equilibrium biogeochemical reactions is integrated in the model.

2.3.3.1 Governing equations for flow

The governing differential equation for the simulation of variably saturated water flow is:

$$S_w S_s \frac{\partial h_\psi}{\partial t} + n \frac{\partial S_w}{\partial t} - \frac{\partial}{\partial z}\left[k_{rw} K \frac{\partial}{\partial z} h_\psi\right] = 0 \tag{2.1}$$

where S_w [-] and S_s [1/m] refer to the water saturation and the specific storage coefficient, and k_{rw} [-] and K [m/s] identify the relative permeability and the hydraulic conductivity, respectively. h_ψ [m] is the hydraulic potential, n [-] denotes the porosity, and t [s] is the time. In Eqn. 2.1, we used the van Genuchten model to parameterize the vertical distributions of water saturation and relative permeability:

$$S_w = S_{rw} + \frac{1 - S_{rw}}{(1 + |\alpha\psi_a|^N)^m} \tag{2.2}$$

$$k_{rw} = S_{ew}^l[1 - (1 - S_{ew}^{1/m})^m]^2 \tag{2.3}$$

with

$$m = 1 - 1/N \qquad (2.4)$$

$$S_{ew} = \frac{S_w - S_{rw}}{1 - S_{rw}} \qquad (2.5)$$

where S_{ew} [-] and S_{rw} [-] are the effective and the residual water saturation, ψ_a [m] denotes the matric potential, and l [-], α [1/m], m [-] and N [-] are the van Genuchten parameters (e.g., Carsel and Parrish, 1988). The same equations outlined above were also applied in the atmospheric boundary layer, where we assumed a uniform distribution of the aqueous phase with a very low water saturation of 3×10^{-5} (Fig. 2.3). Flow was at steady state and fixed to a rate of 200 mm/year.
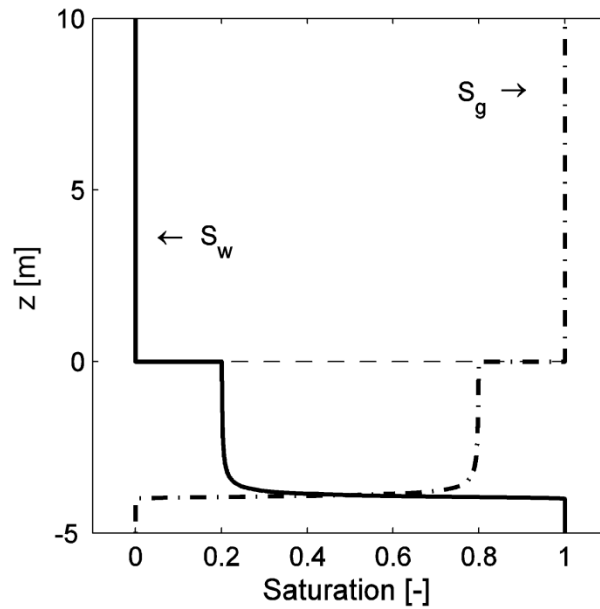
Figure 2.3. Vertical profiles of water saturation (S_w) and gas saturation ($S_g = 1 - S_w$) across the soil-atmosphere interface (horizontal dashed line at $z = 0$ m).

2.3.3.2 Reactive transport modeling

The reactive transport process includes advective-dispersive transport of dissolved species, vapor phase diffusion, and the contributions from biogeochemical reactions that involve gaseous, aqueous, and mineral species in soil and the atmosphere:

$$\frac{\partial}{\partial t}[n_w C_w] + \frac{\partial}{\partial t}[n_g C_g] + \frac{\partial}{\partial z}[q C_w] - \frac{\partial}{\partial z}\left[D_{ew}\frac{\partial}{\partial z}C_w\right] - \frac{\partial}{\partial z}\left[D_{eg}\frac{\partial}{\partial z}C_g\right] - Q = 0 \qquad (2.6)$$

18

where C_w [kg/m³] and C_g [kg/m³] respectively are the concentrations of the compound of interest in the aqueous and gaseous phase; n_w [-] and n_g [-] denote the water-filled and gas-filled porosity, q [m/s] is the groundwater recharge rate, and Q [kg/(m³·s)] represents the source and sink terms that result from biogeochemical reactions. In the present case, the parameter Q accounts for

$$Q = \lambda\, n_w\, c_w \tag{2.7}$$

where λ [1/s] refers to the biogeochemical reaction rate constant.

In Eqn. 3.6, D_{eg} [m²/s] and D_{ew} [m²/s] are the effective diffusion coefficients in the gaseous and aqueous phases. The effective diffusion coefficient in the gaseous phase, D_{eg} [m²/s], is estimated according to the empirical correlation from Moldrup et al. (2000):

$$D_{eg} = D_g^* \frac{n_g^{2.5}}{n} \tag{2.8}$$

Where D_g^* [m²/s] is the molecular diffusion coefficient of the diffusing compound in the free gaseous phase.

To compute the effective diffusion/dispersion coefficient in the aqueous phase, D_{ew} [m²/s], we extended Eqn. 2.8 (Moldrup et al., 2000, 2001):

$$D_{ew} = \alpha^*|q| + D_w^* \frac{n_w^{2.5}}{n} \tag{2.9}$$

where α^* [m] is the dispersivity of the porous medium and D_w^* [m²/s] denotes the molecular diffusion coefficient of the transported compound in the free aqueous phase. The values of D_g^* (Eqn. 2.8) and D_w^* for phenanthrene at 25 °C are listed in Table 2.1.

At the soil-atmosphere interface, hence, the dominating transport mechanism shifts from pure diffusion in the soil to eddy diffusion in the atmosphere. Typically, the eddy diffusion coefficient, D_{eddy} [m²/s], is used to describe turbulent mixing in the atmospheric boundary layer. Under neutral or stable atmospheric conditions, D_{eddy} was shown to linearly increase with height (Foken, 2008):

$$D_{eddy} = k\, u_*\, z \tag{2.10}$$

where k [-] represents the von Kármán constant (here $k = 0.4$), u_* [m/s] is the friction or shear velocity (here 0.3 m/s), and z [m] refers to the height above the ground surface (with $z = 0$ m at the surface). To account for the turbulent mixing in MIN3P, D_{eg} in Eqn. 2.6 was replaced by D_{eddy} (Eqn. 2.10) in the atmospheric boundary layer. Fig. 2.4 shows

19

the effective diffusion coefficients used in the model at 10 °C and at a bare soil site (comparable values for eddy diffusion in the atmosphere depicted by Meixner et al., 2003). The linear model for eddy diffusion is based on the assumption that atmospheric conditions are neutral or stable, i.e. vertical air movement does not take place beyond the rate of adiabatic heating or cooling. Non-linear parameterizations would cause more mixing due to increased eddy diffusion.
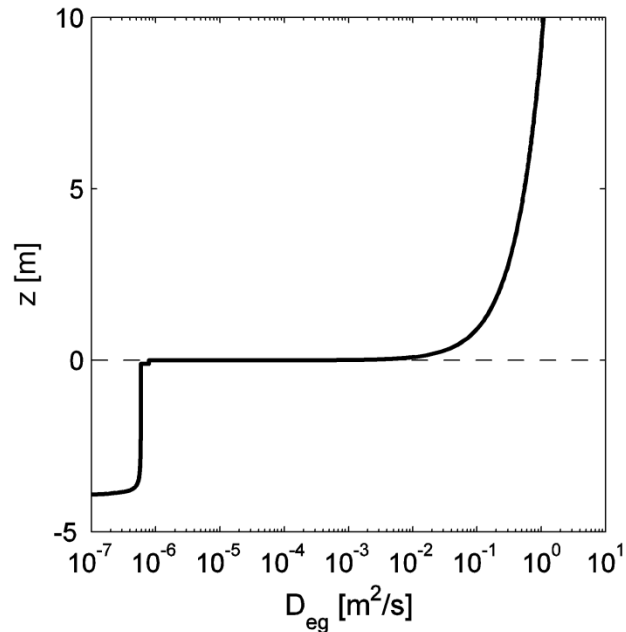
Figure 2.4. Vertical profile of the effective diffusion coefficient of gaseous phenanthrene across the soil-atmosphere interface (horizontal dashed line at $z = 0$ m) at 10 °C at a bare soil site. The *x*-axis is shown in log-scale.

2.3.3.3 Distribution in the 3-phase System

We assumed that phenanthrene distributes linearly among the solid, aqueous, and gaseous phases. Partitioning of phenanthrene between the aqueous and the gaseous phases is described by Henry's law:

$$C_g = HC_w \qquad\qquad (2.11)$$

in which H [-] is the temperature-dependent Henry's law coefficient.

Distribution of phenanthrene between the aqueous and the solid phases is described by:

$$C_s = K_d C_w \qquad (2.12)$$

where C_s [kg/kg bulk phase] denotes the solid phase concentration and K_d [L/kg] is the distribution coefficient calculated for organic compounds by:

$$K_d = K_{OC} f_{OC} \qquad (2.13)$$

where f_{oc} [-] is the organic carbon content of the soil and K_{OC} [L/kg] is the soil organic carbon-water partition coefficient. The latter was calculated by a linear regression, reported in Razzaque and Grathwohl (2008), which is based on the subcooled liquid solubility, S_{scl} [kg/L], of the compound of interest:

$$log K_{OC} = -0.85 \, log S_{scl} - 0.55 \qquad (2.14)$$

with an average absolute error of 0.23 log units in predicted K_{OC} values.

2.3.3.4 Temperature dependence of parameters

In Table 2.1 the physico-chemical parameters for phenanthrene were given for 25 °C. To account for low subsurface temperatures of 10 °C, the molecular diffusion, sorption and Henry's law coefficients were converted by applying empirical relationships. Temperature dependence of the molecular gas diffusion coefficient according to Lyman et al. (1990) is:

$$\frac{D_g(T)}{D_g(T_0)} = \left(\frac{T}{T_0}\right)^{1.75} \qquad (2.15)$$

where T [K] is the specified temperature and T_0 [K] refers to the standard temperature (298.15 K).

The temperature dependence of the molecular diffusion coefficient in water was computed according to Atkins (1986):

$$\frac{D_w(T)}{D_w(T_0)} = \frac{T}{T_0} \times 10^{\frac{247.8(T-T_0)}{(T-140)(T_0-140)}} \qquad (2.16)$$

In addition, to account for the temperature dependence of the sorption distribution coefficient, K_d [L/kg], we applied the van't Hoff equation:

$$\frac{K_d(T)}{K_d(T_0)} = \exp\left[-\frac{\Delta H_{sorption}}{R}\left(\frac{1}{T} - \frac{1}{T_0}\right)\right] \qquad (2.17)$$

where $\Delta H_{sorption}$ [kJ/mol] is the enthalpy of sorption with a representative value of -30 kJ/mol for phenanthrene for anthropogenic and mineral soil samples (see Wang and

Grathwohl, 2013). R [J/(mol K)] refers to the ideal gas constant with a value of 8.314 J/(mol K).

To calculate the temperature dependence of Henry's law coefficient, the van't Hoff equation (Eqn. 2.17) was used again, accounting for the enthalpy of air-water partitioning, ΔH_{aw} [kJ/mol], of 47 kJ/mol for phenanthrene (see Schwarzenbach, 2003).

2.3.4 Model simulations performed

As the base scenario, we started from clean soil (initial condition $C_w(z, t_0) = 0$) and allowed pollution of the soil during a 100 years pollution period (Fig. 2.1). This assumption seems justified since preindustrial emission rates were at least ten times smaller than during industrialization as shown by the sedimentary record in lakes and estuaries (Müller, 1977; Sanders et al., 1993; Simcik et al., 1996; Schneider et al., 2001; Lima et al., 2003). The vertical concentration profile, observed at the end of the pollution period then was taken as the initial condition for the subsequent regulation period, where we assumed 50% reduced concentrations of pollutants in the atmosphere. This is a reasonable assumption for early-industrialized countries such as Germany. In newly industrialized countries such as China as well as developing countries atmospheric concentrations may still increase (Liu et al., 2013a).

The atmospheric concentrations of phenanthrene during the pollution and regulation periods were predefined in the model (boundary conditions). We calculated the average gaseous concentration of phenanthrene in the atmosphere, with a value of 2.24 ng/m^3, from data of 85 passive sampler stations in 32 European countries in 2006 (EMEP database) (regulation period). Before environmental regulations came into effect (pollution period), the gaseous concentration of phenanthrene was assumed to be twice as high (Gocht and Grathwohl, 2004).

2.3.4.1 Model verification and scenarios

Verifications of the numerical model with analytical solutions are shown in Section S1.1. Excellent agreement of the numerical results with analytical solutions proved the applicability of our numerical model to simulate soil-atmosphere exchange. We used the extended version of the numerical code to investigate the long-term environmental fate of SVOCs between soils and the atmosphere. Model runs were performed in order:

22

(*i*)   to investigate the importance of the atmospheric boundary layer for the uptake of airborne phenanthrene in soil (Table 2.2) during the early pollution period.

(*ii*)   to quantify the relative importance of sorption, groundwater recharge, biodegradation, and diffusion on the uptake of airborne phenanthrene in soil. To do so, we performed a local sensitivity analysis on the relevant parameters by comparing vertical concentration profiles for the mean f_{oc}-case as well as the change in total mass of phenanthrene present in the soil compartment for the high and low f_{oc}-cases (Table 2.2).

(*iii*)   to evaluate the change in vertical concentration profiles of phenanthrene in the soil due to reduced anthropogenic emissions and, hence, temporary re-volatilization from the soil to the atmosphere, following the 100 years pollution period. Our model results are qualitatively compared to field observations from several studies in Europe.

(*iv*)   to estimate the time scales needed to reach steady state for three different levels of f_{oc}.

Vertical concentration profiles are shown as relative gaseous concentration, C/C_0 [-], in which C_0 is the atmospheric concentration of phenanthrene (4.48 ng/m^3) applied as a boundary condition at the upper limit of the model domain during the pollution period. The time-dependent accumulation of phenanthrene in the soil compartment is shown as the relative mass, $M/M_{100year}$ [-], in which $M_{100year}$ [kg] is the total mass of phenanthrene, present in the soil, at the end of the 100 years pollution period.

2.4 Results and discussion

2.4.1 Effect of the atmospheric boundary layer

To evaluate the importance of the atmospheric boundary layer for uptake and re-volatilization of SVOCs in soils, we placed the upper boundary condition directly at the ground surface ($z = 0$ m) and compared the results to the outcomes of a second simulation with a 100 m thick atmospheric boundary layer ($z = 100$ m). Fig. 2.5 shows the vertical concentration profiles of gaseous phenanthrene for the two simulations at 1 day, 30 days, and 1000 days.
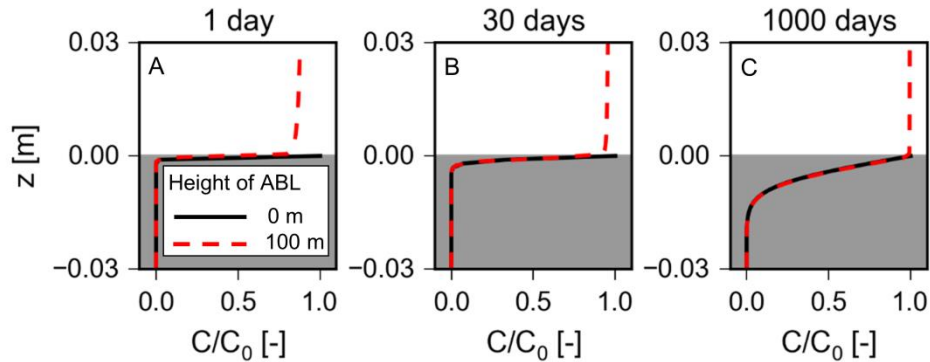
Figure 2.5. Impact of the atmospheric boundary layer on uptake of vapor phase phenanthrene into the soil (mean f_{oc}-case, Table 2.2); black solid lines: concentration profiles in the absence of the atmospheric boundary layer, i.e. upper boundary condition at $z = 0$ m; red dashed lines: concentration profiles in the presence of the atmospheric boundary layer, i.e. upper boundary condition at $z = 100$ m. The grey-shaded areas indicate the location of the topsoil layer enriched in organic carbon.

Due to fast eddy diffusion, the atmospheric boundary layer is well mixed as shown by the straight vertical concentration profiles (red dashed lines) in Fig. 2.5. Only at early times (1 day and 30 days, Figs. 2.5-A and 2.5-B), mixing near the soil-atmosphere interface is not complete, which thus affects the concentration distribution in the soil compartment underneath. In fact, by comparing the two simulation results with each other in Figs. 2.5-A and 2.5-B, for short time periods we observe a slight lag in mass transport of phenanthrene in the soil in case the atmospheric boundary layer is included. However, for 1000 days (Fig. 2.5-C), the lag between the two simulations has disappeared. The shape of the breakthrough curves in the soil indicates that at early times (i.e. within the first month) transport of phenanthrene is dominated by vapor phase diffusion in the soil. Generally, our results show that at time scales larger than one month the atmospheric boundary layer has a negligible effect on mass transport of atmospheric pollutants into soils – provided that pollutants are constantly supplied to the atmosphere. In the following, we therefore neglect the atmospheric boundary layer. It should be noted, however, that for highly volatile less sorbing compounds ("gases") and for indoor situations the atmospheric boundary layer may be important for mass transfer.

2.4.2 Sensitivity analysis on the relevant transport parameters

To determine which physico-chemical parameters are decisive for soil-atmosphere exchange of atmospheric pollutants, we performed a local sensitivity analysis by subsequently changing one of the following parameters: the sorption distribution coefficient (sorption, +50%), the groundwater recharge rate (advection, +50%), the first-order biodegradation rate (biodegradation, +50%), and the diffusion coefficients in the gaseous and aqueous phases (diffusion, +50%). Such changes may be due to temperature fluctuations by 5 to 10 °C or uncertainty in parameter estimations. We investigated the impact of these parameters on the long-term vertical concentration profiles of phenanthrene in the soil at 1 year, 10 years, and 100 years during the pollution period.

Fig. 2.6 shows the concentration profiles in the soil (solid lines) as well as the results of our sensitivity analysis (dashed lines). With increasing organic carbon content in the soil, i.e. with increasing sorption to the solid phase, retardation increases and phenanthrene propagates more slowly into the soil (Group S in Fig. 2.6). In contrast, increasing the groundwater recharge rate (Group A in Fig. 2.6) results in more rapid downward advective transport of phenanthrene, whereas biodegradation hardly affects transport of phenanthrene at this time scale (Group B in Fig. 2.6; concentration profiles overlap each other almost entirely). In accordance to the findings of McKelvie et al. (2013), these results demonstrate how strong sorption and unsaturated conditions limit the effect of biodegradation on the propagation of phenanthrene in the soil, due to reduced bioavailability of the pollutant. Also, an increase in diffusion coefficients impacts the propagation of phenanthrene in the soil (Group D in Fig. 2.6). The shape of the breakthrough curves in Group D indicates that vapor phase diffusion and sorption dominate the transport process during the pollution period for the mean f_{oc}-case. Since diffusion and sorption are temperature sensitive and effective groundwater recharge is highly dependent on the local climate, diurnal and seasonal changes in temperature and groundwater recharge will introduce some dynamics in uptake and re-volatilization of SVOCs in/from soils. Model simulations considering diurnal changes of temperature and atmospheric boundary layer thickness are subject of ongoing work.
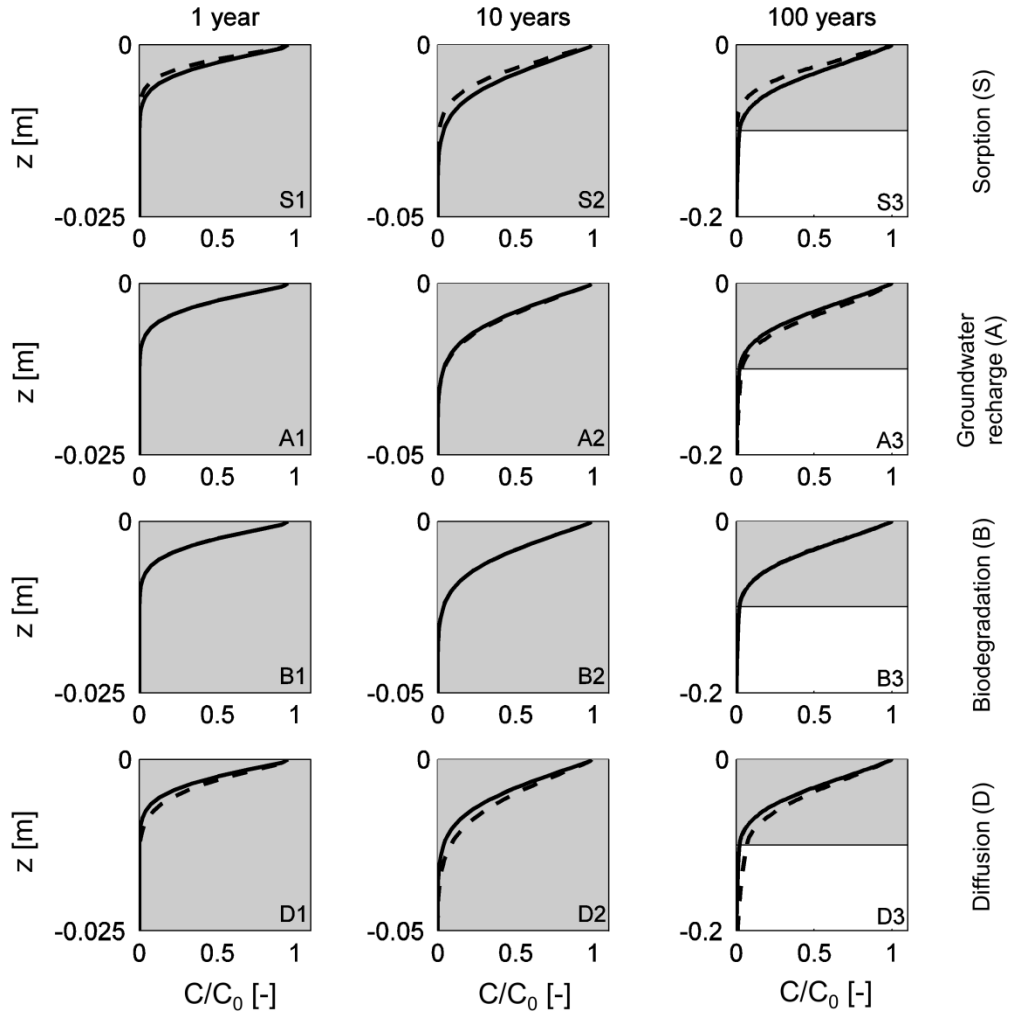
Figure 2.6. Concentration profiles of phenanthrene in the soil at three time points during the uptake (pollution) period. The solid lines refer to concentration profiles for the mean f_{OC}-case, whereas the dashed lines refer to those with 50% increase in the respective parameter(s) investigated. Note different scales on the vertical axis. The grey-shaded areas indicate the location of the topsoil layer enriched in organic carbon.

To quantify the impact of the different parameters on the total mass of phenanthrene accumulated in the soil, we also calculated the local sensitivity, which is defined as the relative deviation of the output value due to a change in an input value (Webster et al., 1998; Meyer et al., 2005). Local sensitivity, $S(X_i)$ [-], therefore, was computed as the relative deviation of the total mass, $\partial M(t) / M(t)$ [-], in the soil due to a 50% increase in the respective parameter, X_i (i.e. sorption distribution coefficient, groundwater recharge rate, biodegradation rate, and gaseous and aqueous diffusion coefficients):

26

$$S(X_i) = \left| \frac{\partial M(t) / M(t)}{\partial X_i / X_i} \right|$$

where $M(t)$ [kg] refers to the total mass of phenanthrene present in the soil at a selected time point, t [s]. In case $S(X_i) \leq 0.1$, the total mass present in the soil is assumed to be non-sensitive to the input variable. With increasing local sensitivity, the total mass accumulated is increasingly affected by the input variable.

Fig. 2.7 shows the time-dependent local sensitivity of each parameter based on the total mass of phenanthrene accumulated in the soil for 7 time points (0.3 year, 1 year, 3 years, 10 years, 30 years, 50 years, and 100 years) and for the three levels of f_{oc}. We found that sorption (Fig. 2.7-A) significantly affects mass accumulation at all times. In addition, diffusion (Fig. 2.7-D) clearly dominates only at early times (up to 10 years), whereas it diminishes at later times and groundwater recharge (Fig. 2.7-B) becomes more important. For the mean and the high f_{oc}-cases, accumulation is still not advection-dominated at the end of the pollution period (at 100 years); while for the low f_{oc}-case, advection already dominates the transport at 100 years. In fact, the higher the organic carbon content in the soil, the more delayed in time is the observed pattern in local sensitivity due to increased retardation from stronger sorption properties. As illustrated in Fig. 2.7-C, the effect of biodegradation on mass accumulation is strongly constrained over the 100 years pollution period for the three levels of f_{oc} since steady state is not achieved yet. However, on even longer time scales biodegradation would take over and determine long-term mass accumulation (the stronger the sorption the longer that takes).
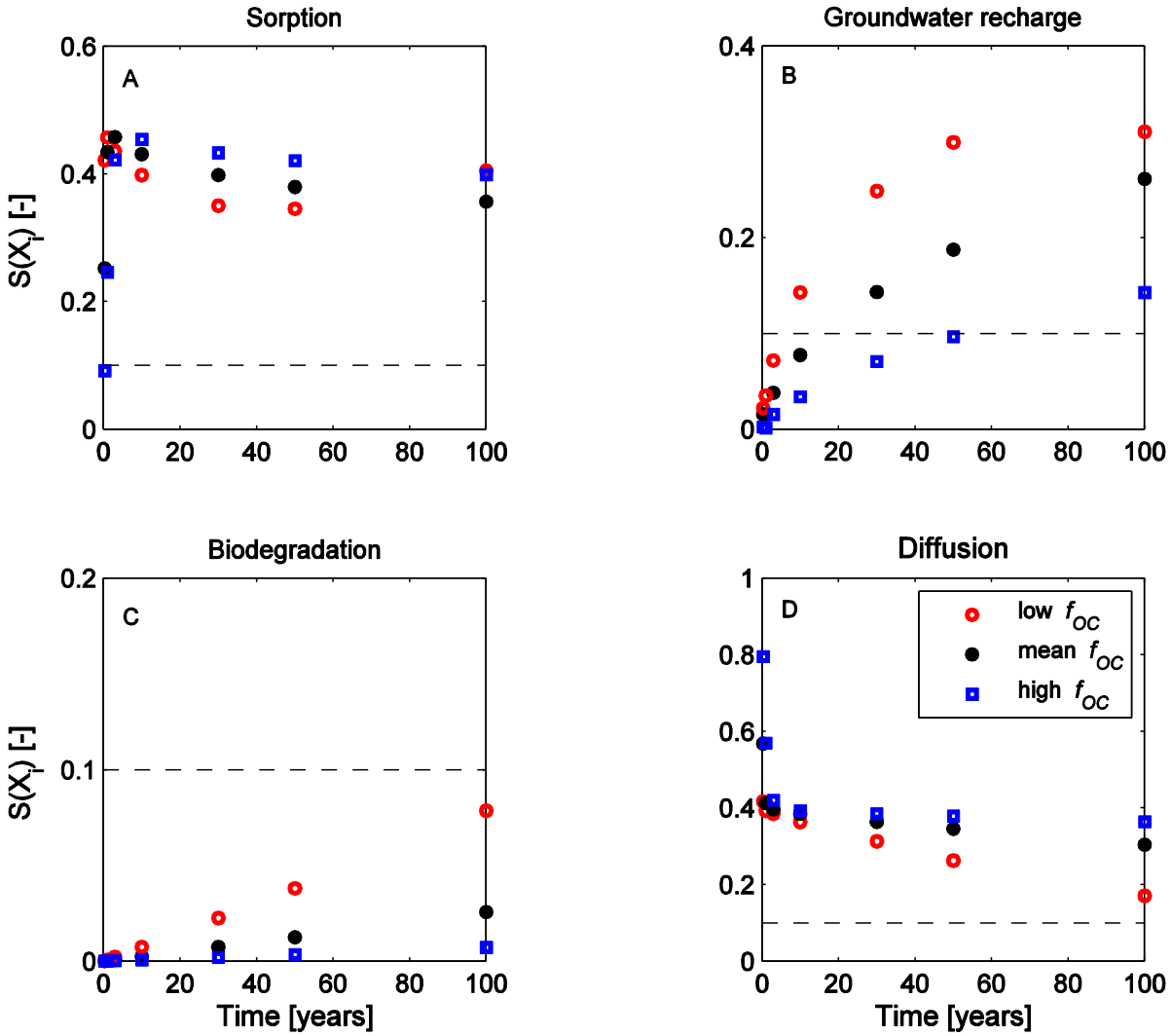
Figure 2.7. Time-dependent local sensitivity ($S(X_i)$) of each parameter based on the total mass accumulated in the soil for the three levels of f_{oc}. The horizontal dashed line refers to a local sensitivity of 0.1 (below, the total mass in the soil is assumed to be non-sensitive to the input parameter). Note, different scales on the vertical axis.

As to be expected, the total mass of phenanthrene in the soil is highly dependent on sorption at all times. Groundwater recharge and biodegradation determine the total mass present in the soil in the long term, while diffusion dominates the transport process at early times. Note, that for less sorbing compounds time scales would be much shorter.

2.4.3 Impact of reduced emissions: re-volatilization from soils

In the following, we investigate how a regulation period with a 50% reduction in anthropogenic emissions of phenanthrene after 100 years of pollution influences the concentration distribution across the soil-atmosphere interface. Fig. 2.8 shows the vertical concentration profiles across the soil-atmosphere interface at 1 year and 30 years after environmental protection measures became effective for the three levels of f_{OC} considered.
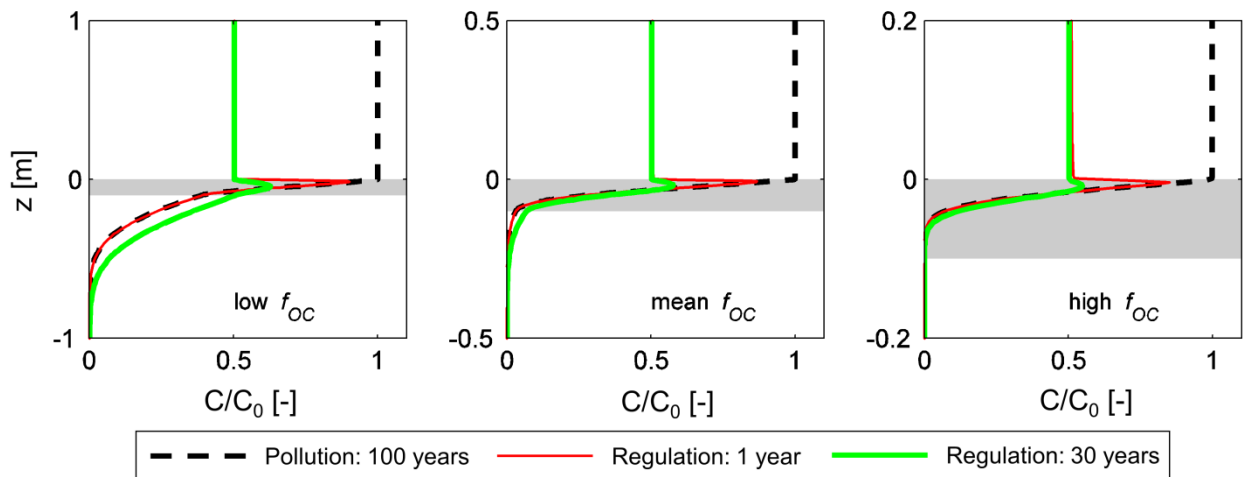
Figure 2.8. Concentration profiles at the end of the pollution period (black dashed line), and 1 year and 30 years after environmental reduction measures became effective (solid lines) for the three levels of f_{oc}. On the vertical axis different scales are shown and the grey-shaded areas indicate the location of the topsoil layer. Only in the low organic carbon case the pollution penetrated the high organic topsoil.

If the concentration in the atmosphere is reduced, re-volatilization of phenanthrene from the soil to the atmosphere occurs. In Fig. 2.8 this is indicated by a reversed concentration gradient that develops directly at the soil-atmosphere interface. Peak concentrations of phenanthrene are observed just below this interface. Over time, the peak shifts downwards and diminishes as phenanthrene re-volatilizes into the atmosphere and also migrates into deeper soil layers by diffusion and advection. The propagation of phenanthrene in the soil layers is affected by the organic carbon content of the soil. From the low f_{oc}-case, to the mean f_{oc}-case, to the high f_{oc}-case, advective transport of

phenanthrene into the deeper soil layers is increasingly retarded while more phenanthrene diffuses back to the atmosphere if f_{oc} is high.

We qualitatively compared the results of our numerical simulations, shown in Fig. 2.8, to field observations of the vertical distribution of phenanthrene in soils, published in the late 1990s and early 2000s (Wilcke et al., 1996; Cousins et al. 1999b, 1999c; Krauss et al., 2000; Gocht et al., 2001; Vikelsøe et al., 2002; Atanassova and Brümmer, 2004). In several field studies (Wilcke et al., 1996; Krauss et al., 2000; Gocht et al., 2001; Vikelsøe et al., 2002; Atanassova and Brümmer, 2004) higher concentrations of phenanthrene in the topsoil than in the underlying subsoil were found, which generally matches results from our model scenario. Moreover, Cousins et al. (1999b) detected the highest concentration of total PAHs (with phenanthrene being the principal component in the upper soil layers according to Atanassova and Brümmer, 2004) at a depth of 5 cm below the ground surface. This finding is also in agreement with our model results at 30 years after the start of the regulation period. In particular, Cousins et al. (1999b) reported values for temperature and organic carbon content that were similar to the values used for the mean f_{oc}-case in our study. The authors hypothesized that bioturbation is the main reason for the lower concentrations in the soil layer close to the ground surface. However, our model results indicate that re-volatilization and limited bioavailability because of strong sorption lead to a peak concentration at shallow depths below the ground surface.

2.4.4 Time scales for re-volatilization and for steady state in the soil

To estimate the time scale for re-volatilization from the soil, several model scenarios with and without environmental regulation measures or biodegradation were investigated. We extended our simulation period to 2500 years to account for long time scales involved.

Fig 2.9 shows the accumulation of phenanthrene in the soil during the 100 years pollution period (black solid line) and the subsequent 900 years regulation period (black dot-dash line). As environmental reduction measures become effective, we observe a significant change in transport across the soil-atmosphere interface when compared to the non-regulated scenario (grey dashed line in Fig. 2.9). The reduced atmospheric concentration of phenanthrene during the regulation period results in a significantly lower amount of phenanthrene accumulating in the soil. With the onset of reduced anthropogenic

emissions of phenanthrene to the atmosphere, we also observe re-volatilization of phenanthrene from the soil to the atmosphere that lasts for about 20 years (compare black dot-dash and dashed lines in Fig. 2.9) - after that the soil becomes a sink again.
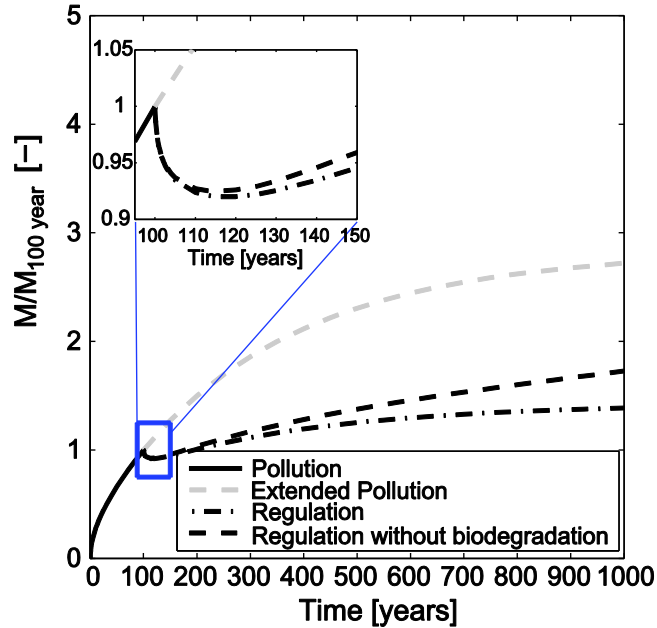
Figure 2.9. Accumulation of phenanthrene in the soil (mean f_{oc}-case) for constant emission (solid black line or grey dashed line), and a reduction of emission rates by 50% after 100 years with and without biodegradation.

Fig 2.10 compares the accumulation of phenanthrene in the soil for the three levels of f_{oc}. In all three cases, retarded diffusion limits the transport of phenanthrene in the topsoil layer during the 100 years pollution period, resulting in the same mass accumulation of phenanthrene accumulating in the soil (linear partitioning). After the concentration of phenanthrene in the atmosphere is reduced by half, re-volatilization of phenanthrene from the soil to the atmosphere occurs and for a limited time period the soil becomes a secondary source for pollution. In the long term, however, the soil becomes a sink again and mass transport is determined by biodegradation and groundwater recharge. As expected, with increasing organic carbon content more phenanthrene accumulates in the soil (due to increased sorption). Also, the time needed to eventually reach steady state extends with increasing f_{oc}. We define the characteristic time for steady state, t_c [s], by

the time period needed to reach 63.21% of the total mass in the soil at steady state (see details in the Section S1.2 where the governing equation was derived for a box model). For the low f_{oc}-case, the mean f_{oc}-case, and the high f_{oc}-case, the characteristic times for steady state following the reduction in atmospheric concentration are 143 years, 430 years, and 1430 years, respectively (calculated by applying Eqn. S1.10, with a Damköhler number, Da, of 10).
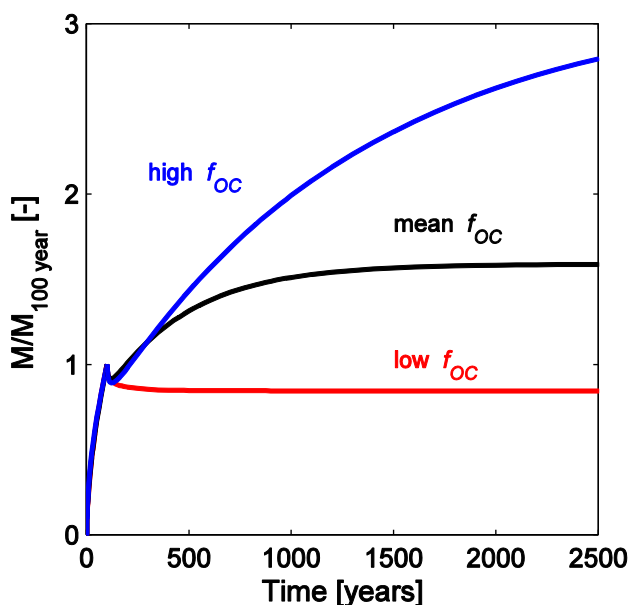
Figure 2.10. Time-dependent mass accumulation of phenanthrene in the soil for the three levels of f_{oc}. Values of the sorption distribution coefficient K_d in the topsoils are 261.0 L/kg for the low-f_{oc} case (1%), 782.9 L/kg for the mean-f_{oc} case (3%), and 2609.8 L/kg for the high-f_{oc} case (10%), respectively.

2.5 Summary and conclusions

In this study, we extended the multicomponent reactive transport code MIN3P by an atmospheric boundary layer accounting for eddy diffusion. We used a vertical 1-D model (Fig. 2.1) to study soil-atmosphere exchange of SVOCs for non-disturbed soils with varying boundary conditions in the atmosphere (i.e. a decrease of pollutant concentration). Phenanthrene was used as a representative compound for SVOCs and was assumed to be supplied by continuous anthropogenic emissions to the atmosphere. Average values for temperature (10 °C) and groundwater recharge (200 mm/year) were applied in our

model, and three cases with different organic carbon contents were analyzed for the specific base scenario in Germany.

We found that in the long term, the soil properties limited re-volatilization of phenanthrene into the atmosphere. Due to fast eddy diffusion and continuous anthropogenic emissions of gaseous phenanthrene, the atmospheric boundary layer is always mixed and thus has a negligible effect on the soil uptake of atmospheric pollutants, except for time periods < 1 month. This indicates that the atmospheric boundary layer is only relevant for short-term changes in the boundary conditions (emission rates, temperatures). Temperature-driven diurnal concentration changes and the height and the stability of the atmospheric boundary layer do not affect the long term uptake and release of pollutants from soils.

A sensitivity analysis showed that sorption/desorption was the most relevant process at all times, whereas vertical transport by diffusion was relevant only in the short term (years to decades) whereas groundwater recharge dominated transport in the long term (decades to centuries). Biodegradation was slowed down by sorption, and thus was of lower relevance.

Re-volatilization of SVOCs from soils to the atmosphere occurs only for a relatively short time period after environmental regulation measures came into effect (i.e. only over two decades for the specific exposure scenario investigated in this study with an abrupt drop in atmospheric concentrations). Gradually decreasing pollutant levels in the atmosphere would cause even less re-volatilization. Thus, soils are more or less infinite sinks for atmospheric pollutants even if concentrations are reduced by 50%. A simple analytical solution can be applied to estimate the time periods needed to reach steady state between input and biodegradation rates (see Section S1.2) and the concentration levels in the soil at steady-state conditions. For phenanthrene (representative for many PAHs) steady-state time scales amount to centuries to millennia depending on soil organic carbon content and the thickness of the soil layer considered. The extended MIN3P code presented in this study can also be applied to simulate soil-atmosphere exchange of other atmospheric pollutants (e.g. further PAHs, PCBs, pesticides) or (semi-)volatile compounds (e.g. O_2, CO_2).

Supporting Information S1

Results of model verification, using the extended MIN3P code and well-known analytical solutions.

References

Atanassova, I., Brümmer, G.W., 2004. Polycyclic aromatic hydrocarbons of anthropogenic and biopedogenic origin in a colluviated hydromorphic soil of Western Europe. Geoderma 120, 27-34.

Atkins, P.W., 1986. Physical chemistry. 3rd ed. Oxford University, New York.

Beyer, A., Mackay, D., Matthies, M., Wania, F., Webster, E., 2000. Assessing long-range transport potential of persistent organic pollutants. Environ. Sci. Technol. 34, 699-703.

BGR, R. Mittlere järhliche Grundwasserneubildung (Tafel 5.5). Bundesanstalt für Geowissenschaften und Rohstoffe (BGR) in Hannover. Access time: Nov. 20, 2014. URL: www.bgr.bund.de.

Bidleman, T.F., Leone, A.D., 2004. Soil-air exchange of organochlorine pesticides in the Southern United States. Environ. Pollut. 128, 49-57.

Bozlaker, A., Muezzinoglu, A., Odabasi, M., 2008a. Atmospheric concentrations, dry deposition and air-soil exchange of polycyclic aromatic hydrocarbons (PAHs) in an industrial region in Turkey. J. Hazard. Mater. 153, 1093-1102.

Bozlaker, A., Odabasi, M., Muezzinoglu, A., 2008b. Dry deposition of soil-air exchange of polychlorinated biphenyls (PCBs) in an industrial area. Environ. Pollut. 156, 784-793.

Cabrerizo, A., Dachs, J., Moeckel, C., Ojeda, M.J., Caballero, G., Barcelo, D., et al., 2011. Ubiquitous net volatilization of polycyclic aromatic hydrocarbons from soils and parameters influencing their soil-air partitioning. Environ. Sci. Technol. 45, 4740-4747.

Carsel, R.F., Parrish, R.S., 1988. Developing joint probability distributions of soil water retention characteristics. Water Resour. Res. 24, 755-769.

Cousins, I.T., Beck, A.J., Jones, K.C., 1999a. A review of the processes involved in the exchange of semi-volatile organic compounds (SVOC) across the air-soil interface. Sci. Total Environ. 228, 5-24.

Cousins, I.T., Gevao, B., Jones, K.C., 1999b. Measuring and modelling the vertical distribution of semi-volatile organic compounds in soils. 1: PCB and PAH soil core data. Chemosphere 39, 2507-2518.

Cousins, I.T., Gevao, B., Jones, K.C., 1999c. Measuring and modelling the vertical distribution of semi-volatile organic compounds in soils. 2: model development. Chemosphere 39, 2519-2534.

Deutscher Wetterdienst (DWD). Temperatur: langjährige Mittelwerte 1981 – 2010. Deutscher Wetterdienst. Access time: Nov. 20, 2014. URL: www.dwd.de.

Farrar, N.J., Harner, T., Shoeib, M., Sweetman, A., Jones, K.C., 2005. Field deployment of thin film passive air samplers for persistent organic pollutants: a study in the urban atmospheric boundary layer. Environ. Sci. Technol. 39, 42-48.

Foken, T., 2008. Micrometeorology. Springer-Verlag, Heidelberg, Germany.

Ghirardello, D., Morselli, M., Semplice, M., Di Guardo, A., 2010. A dynamic model of the fate of organic chemicals in a multilayered air/soil system: development and illustrative application. Environ. Sci. Technol. 44, 9010-9017.

Gocht, T., Grathwohl, P., 2004. Polyzyklische aromatische Kohlenwasserstoffe aus diffusen Quellen. Umweltwiss. Schadst. Forsch. 16:245-254.

Gocht, T., Moldenhauer, K.M., Püttmann, W., 2001. Historical record of polycyclic aromatic hydrocarbons (PAH) and heavy metals in floodplain sediments from the Rhine River (Hessisches Ried, Germany). Appl. Geochem. 16:1707-1721.

Gocht, T., Klemm, O., Grathwohl, P., 2007. Long-term atmospheric bulk deposition of polycyclic aromatic hydrocarbons (PAHs) in rural areas of Southern Germany. Atmos. Environ. 41, 1315-1327.

Gouin, T., Mackay, D., Webster, E., Wania, F., 2000. Screening chemicals for persistence in the environment. Environ. Sci. Technol. 34, 881-884.

Grathwohl, P., 1998. Diffusion in natural porous media: contaminant transport, sorption/desorption and dissolution kinetics. Kluwer, Boston, Massachusetts.

Harner, T., Mackay, D., Jones, K.C., 1995. Model of the long-term exchange of PCBs between soil and the atmosphere in the southern U.K. Environ. Sci. Technol. 29, 1200-1209.

Hedman, J.E., 2008. Fate of contaminants in Baltic Sea sediment ecosystems: the role of bioturbation (PhD Dissertation). Stockholm University, Stockholm.

Jamshidi, A., Hunter, S., Hazrati, S., Harrad, S., 2007. Concentrations of chiral signatures of polychlorinated biphenyls in outdoor and indoor air and soil in a major U.K. conurbation. Environ. Sci. Technol. 41, 2153-2158.

Karapanagioti, H.K., Kleineidam, S., Sabatini, D.A., Grathwohl, P., Ligouis, B., 2000. Impacts of heterogeneous organic matter on phenanthrene sorption: equilibrium and kinetic studies with aquifer material. Environ. Sci. Technol. 34, 406-414.

Kleineidam, S., Rügner, H., Ligouis, B., Grathwohl, P., 1999. Organic matter facies and equilibrium sorption of phenanthrene. Environ. Sci. Technol. 33, 1637-1644.

Kleineidam, S., Schüth, C., Grathwohl, P., 2002. Solubility-normalized combined adsorption-partitioning sorption isotherms for organic pollutants. Environ. Sci. Technol. 36, 4689-4697.

Kleineidam, S., Rügner, H., Grathwohl, P., 2004. Desorption kinetics of phenanthrene in aquifer material lacks hysteresis. Environ. Sci. Technol. 38, 4169-4175.

Komprda, J., Komprdova, K., Sanka, M., Mozny, M., Nizzetto, L., 2013. Influence of climate and land use change on spatially resolved volatilization of persistent organic pollutants (POPs) from background soils. Environ. Sci. Technol. 47, 7052-7059.

Krauss, M., Wilcke, W., Zech, W., 2000. Polycyclic aromatic hydrocarbons and polychlorinated biphenyls in forest soils: depth distribution as indicator of different rate. Environ. Pollut. 110, 79-88.

Kuntz, D., Grathwohl, P., 2009. Comparison of steady state and transient flow conditions on reactive transport of contaminants in the vadose zone. J. Hydrol. 369, 225-233.

Lang, C., Tao, S., Wang, X., Zhang, G., Li, J., Fu, J., 2007. Seasonal variation of polycyclic aromatic hydrocarbons (PAHs) in Pearl River Delta region, China. Atmos. Environ. 41, 8370-8379.

Lee, R.G.M., Hung, H., Mackay, D., Jones, K.C., 1998. Measurement and modeling of the diurnal cycling of atmospheric PCBs and PAHs. Environ. Sci. Technol. 32, 2172-2179.

Lima, A.L.C., Eglinton, T.I., Reddy. C,M., 2003. High-resolution record of pyrogenic polycyclic aromatic hydrocarbon deposition during the 20th century. Environ. Sci. Technol. 37, 53-61.

Liu, Y., Beckingham, B., Rügner, H., Li, Z., Ma, L., Schwientek, M., et al.,, 2013a. Comparison of sedimentary PAHs in the Rivers of Ammer (Germany) and Liangtan (China): Differences between early- and newly industrialized countries. Environ. Sci. Technol. 47, 701-709.

Liu, L., Wu, F., Haderlein, S., Grathwohl, P., 2013b. Determination of the subcooled liquid solubilities of PAHs in partitioning batch experiments. Geosci. Front. 4, 123-126.

Lohmann, R., Breivik, K., Dachs, J., Muir, D., 2007. Global fate of POPs: current and future research directions. Environ. Pollut. 150, 150-165.

Lyman, W.L., Reehl, W.F., Rosenblatt, D.H. (Eds.), 1990. Handbook of chemical property estimation methods: Environmental behavior of organic compounds. 2nd. ed. Mc Graw – Hill, New York.

Mackay, D., 2010. Multimedia environmental models: The fugacity approach. 2nd ed. CRC Press, Florida, USA.

MacLeod, M., Scheringer, M., Podey, H., Jones, K.C., Hungerbuehler, K., 2007. The origin and significance of short-term variability of semivolatile contaminants in air. Environ. Sci. Technol. 41, 3249-3253.

Mayer, U.K., Frind, E.O., Blowes, D.W., 2002. Multicomponent reactive transport modeling in variably saturated porous media using a generalized formulation for kinetically controlled reactions. Water Resour. Res. 38, 1174.

McKelvie, J.R., Åslund, M.W., Celejewski, M.A., Simpson, A.J., Simpson, M.J., 2013. Reduction in the earthworm metabolomics response after phenanthrene exposure in soils with high soil organic carbon content. Environ. Pollut. 175, 75-81.

Meixner, F.X., Andreae, M.O., van Dijk, S.M., Gut, U.A., Rummel, U.K., Scheibe, M., Welling, M., 2003. Biosphere-atmosphere exchange of reactive trace gases in a primary rainforest ecosystem: studies on interlinking scales. Rep. Ser. Aerosol Sci. 62A, 269-274.

Meyer, T., Wania, F., Breivik, K., 2005. Illustrating sensitivity and uncertainty in environmental fate models using partitioning maps. Environ. Sci. Technol. 39, 3186-3196.

Moeckel, C., Nizzetto, L., Strandberg, B., Lindroth, A., Jones, K.C., 2009. Air-boreal forest transfer and processing of polychlorinated biphenyls. Environ. Sci. Technol. 43, 5282-5289.

Moldrup, P., Olesen, T., Gamst, J., Schjønning, P., Yamaguchi, T., Rolston, D.E., 2000. Predicting the gas diffusion coefficient in repacked soil water-induced linear reduction model. Soil Sci. Soc. Am. J. 64 1588-1194.

Moldrup, P., Olesen, T., Komatsu, T., Schjønning, P., Rolston, D.E., 2001. Division S-1 — Soil physics: Tortuosity, diffusivity, and permeability in the soil liquid and gaseous phase. Soil Sci. Soc. Am. J. 65 613-623.

Müller, G., Grimmer, G., Böhnke, H., 1977. Sedimentary record of heavy metals and polycyclic aromatic hydrocarbons in Lake Constance. Naturwissenschaften 64, 427-431.

Panagos, P., Hiederer, P., Van Liedekerke, M., Rampa, F., 2013. Estimating soil organic carbon in Europe based on data collected through an European network. Ecol. Indic. 24, 439-450.

Prevedouros, K., Brorstrom-Lunden, E., Halsall, C.J., Jones, K.C., Lee, R.G.M., Sweetman, A.J., 2004. Seasonal and long-term trends in atmospheric PAH concentrations: evidence and implications. Environ. Pollut. 128, 17-27.

Razzaque, M.M., Grathwohl, P., 2008. Predicting organic carbon-water partitioning of hydrophobic organic chemicals in soils and sediments based on water solubility. Water Res. 42, 3775-3780.

Reichman, R., Wallach, R., Mahrer, Y., 2000a. A combined soil-atmosphere model for evaluating the fate of surface-applied pesticides. 1. Model development and verification. Environ. Sci. Technol. 34, 1313-1320.

Reichman, R., Mahrer, Y., Wallach, R., 2000b. A combined soil-atmosphere model for evaluating the fate of surface-applied pesticides. 2. The effect of varying environmental conditions. Environ. Sci. Technol. 34, 1321-1330.

Rügner, H., Kleineidam, S., Grathwohl, P., 1999. Long term sorption kinetics of phenanthrene in aquifer materials. Environ. Sci. Technol. 33, 1645-1651.

Sanders, G., Jones, K.C., Hamilton-Taylor, J., Dorr, H., 1993. Concentrations and deposition fluxes of polynuclear aromatic hydrocarbons and heavy metals in the dated sediments of a rural english lake. Environ. Toxicol. Chem. 12(9), 1567-1581.

Schneider, A.R., Stapleton, H.M., Cornwell, J., Baker, J.E., 2001. Recent declins in PAH, PCB, and toxaphene levels in the Northern Great Lakes as determined from high resolution sediment cores. Environ. Sci. Technol. 35(19), 3809-3815.

Scholtz, M.T., Bidleman, T.F., 2006. Modelling of the long term fate of pesticide residues in agricultural soils and their surface exchange with the atmosphere: Part 1. Model description and evaluation. Sci. Total Environ. 368, 823-838.

Scholtz, M.T., Bidleman, T.F.,2007. Modelling of the long term fate of pesticide residues in agricultural soils and their surface exchange with the atmosphere: Part 2. Projected long-term fate of pesticide residues. Sci. Total Environ. 377, 61-80.

Schuster, J.K., Gioia, R., Sweetman, A.J., Jones, K.C., 2010. Temporal trends and controlling factors for polychlorinated biphenyls in the UK atmosphere (1991-2008). Environ. Sci. Technol. 44, 8068-8074.

Schwarzenbach, R.P., Gschwend, P.M., Imboden, D.M, 2003.. Environmental organic chemistry. 2nd ed. John Wiley & Sons Inc., New Jersey.

Simcik, M.F., Eisenreich, S.J., Golden, K.A., Liu, S., Lipiatou, E., Swackhamer, D.L., Long, D.T., 1996. Atmospheric loading of polycyclic aromatic hydrocarbons to Lake Michigan as recorded in the sediments. Environ. Sci. Technol. 30, 3039-3046.

Tao, S., Wang, Y., Wu, S., Liu, S., Dou, H., Liu, Y., et al., 2007. Vertical distribution of polycyclic aromatic hydrocarbons in atmospheric boundary layer of Beijing in winter. Atmos. Environ. 41, 9594-9602.

Tao, S., Liu, W., Li, Y., Yang, Y., Zuo, Q., Li, B., et al., 2008. Organochlorine pesticides contaminated surface soil as reemission source in the Haihe plain, China. Environ. Sci. Technol. 42, 8395-8400.

Totten, L.A., Stenchikov, G., Gigliotti, C.L., Lahoti, N., Eisenreich, S.J., 2006. Measurement and modeling of urban atmospheric PCB concentrations on a small (8 km) spatial scale. Atmos. Environ. 40, 7940-7952.

van Jaarsveld, J.A., van Pul, W.A.J., De Leeuw, F.A.A.M., 1997. Modelling transport and deposition of persistent organic pollutants in the European region. Atmos. Environ. 31, 1011-1124.

Verschueren, K., 1983. Handbook of Environmental Data on Organic Chemicals. 2nd ed. van Nostrand Reinhold Company Inc., New York.

Vikesøe, J., Johansen, E., Thomsen, M., Carlsen, L., 2002. Persistent organic pollutants in soil, sludge and sediment: a multianalytical field study of selected organic chlorinated and brominated compounds. National Environmental Research Institute Denmark, Roskilde. Report no. 402.

Wang, G., Grathwohl, P., 2013. Isosteric heats of sorption and desorption of phenanthrene in soils and carbonaceous materials. Environ. Pollut. 175, 110-116.

Wang, G., Kleineidam, S., Grathwohl, P., 2007. Sorption/desorption reversibility of phenanthrene in soils and carbonaceous materials. Environ. Sci. Technol. 41, 1186-1193.

Wang, W., Simonich, S., Giri, B., Chang, Y., Zhang, Y., Jia, Y., et al., 2011. Atmospheric concentrations and air-soil gas exchange of polycyclic aromatic hydrocarbons (PAHs) in remote, rural village and urban areas of Beijing-Tianjin region, North China. Sci. Total Environ. 409, 2942-2950.

Wania, F., Dugani, C., 2003. Assessing the long-range transport potential of polybrominated diphenyl ethers: A comparison of four multimedia models. Environ. Toxicol. Chem. 22, 1252–1261.

Wania, F., Breivik, K., Persson, N.J., McLachlan, M.S., 2006. CoZMo-POP 2 – A fugacity-based dynamic multi-compartmental mass balance model of the fate of persistent organic pollutants. Environ. Model. Softw. 21, 868-884.

Webster, F., Mackay, D., Wania, F., 1998. Evaluating environmental persistence. Environ. Toxicol. Chem. 17, 2148-2158.

Wild, S.R., Jones, K.C., 1995. Polynuclear aromatic hydrocarbons in the United Kingdom environment: A preliminary source inventory and budget. Environ. Pollut. 88, 91-108.

Wilcke, W., Zech, W., Kobza, J., 1996. PAH-pools in soils along a PAH-deposition gradient. Environ. Pollut. 92, 307-313.

Zhang, Y., Deng, S., Liu, Y., Shen, G., Li, X., Cao, J., et al., 2011. A passive air sampler for characterizing the vertical concentration profile of gaseous phase polycyclic aromatic hydrocarbons in near soil surface air. Environ. Pollut. 159, 694-699.

Zhong, Y., Zhu, L., 2013. Distribution, input pathway and soil-air exchange of polycyclic aromatic hydrocarbons in Banshan Industry Park, China. Sci. Total Environ. 444, 177-182.

Chapter 3.

Modeling short-term concentration fluctuations of semi-volatile pollutants in the soil–plant–atmosphere system
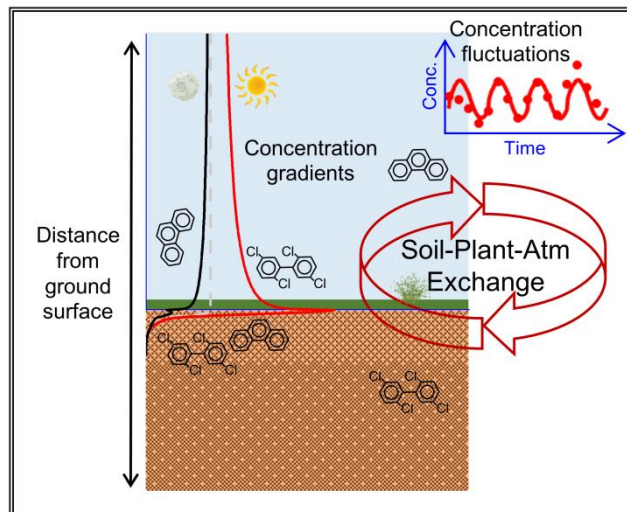
Abstract

Temperature changes can drive cycling of semi-volatile pollutants between different environmental compartments (e.g. atmosphere, soil, plants). To evaluate the impact of daily temperature changes on atmospheric concentration fluctuations we employed a physically based model coupling soil, plants and the atmosphere, which accounts for heat transport, effective gas diffusion, sorption and biodegradation in the soil as well as eddy diffusion and photochemical oxidation in the atmospheric boundary layer of varying heights. The model results suggest that temperature-driven re-volatilization and uptake in soils cannot fully explain significant diurnal concentration fluctuations of atmospheric pollutants as for example observed for polychlorinated biphenyls (PCBs). This holds even for relatively low water contents (high gas diffusivity) and high sorption capacity of the topsoil (high organic carbon content and high pollutant concentration in the topsoil). Observed concentration fluctuations, however, can be easily matched if a rapidly-exchanging environmental compartment, such as a plant layer, is introduced. At elevated temperatures, plants release organic pollutants, which are rapidly distributed in the atmosphere by eddy diffusion. For photosensitive compounds, e.g. some polycyclic aromatic hydrocarbons (PAHs), decreasing atmospheric concentrations would be expected during daytime for the bare soil scenario. This decline is buffered by a plant layer, which acts as a ground-level reservoir. The modeling results emphasize the importance of a rapidly-exchanging compartment above ground to explain short-term atmospheric concentration fluctuations.

Keywords: soil and atmosphere pollution, plants, diurnal temperature changes, photochemical transformation, numerical modeling

3.1 Introduction

Semi-volatile organic compounds (SVOCs), for example polychlorinated biphenyls (PCBs) and polycyclic aromatic hydrocarbons (PAHs), have been released into the environment by various anthropogenic activities and are now widely distributed. Soils represent a terrestrial reservoir for legacy SVOCs and may (temporarily) act as secondary sources, re-volatilizing pollutants to the atmosphere due to changes in land use (Komprda et al., 2013), reduced anthropogenic emissions (Jones and Voogt, 1999; Kurt-Karakus et al., 2006; Bao et al., 2015), and temperature changes. Re-volatilization happens due to changes in seasons and climate on the long term (Lamon et al., 2009; Ma et al., 2010 and 2011; Komprda et al., 2013) or because of the diurnal cycle of solar radiation in the short term (Wallace and Hites, 1996; Lee et al., 1998; Gouin et al., 2002; Totten et al., 2002; Mandalakis et al., 2003; MacLeod et al., 2007; Gasic et al., 2009; Morselli et al., 2011); both are relevant for the environmental fate of SVOCs because they may influence volatilization rates from soils. Plants may play an important role as short-term sources and sinks of semi-volatile pollutants in the atmosphere depending on species and growing seasons (Buckley, 1982; Jones et al., 1992; Simonich and Hites, 1994a, 1994b, 1995; Kömp and McLachlan, 1997; Böhme et al., 1999; McLachlan, 1999; Hung et al., 2001; Moeckel et al., 2001; Barber et al., 2003, 2004; Terzaghi et al., 2015).

Commonly, numerical models are used to investigate temperature-driven soil–plant– atmosphere exchange of SVOCs by simulating sorption and diffusion in soils, partitioning to plants, and the temperature dependence of these processes (Cousins et al., 1999; Prevedouros et al., 2000; Hung et al., 2001; Scholtz et al., 2002a, 2002b; Dalla Valle et al., 2004; MacLeod and Mackay, 2004; van den Berg and Leistra, 2004; Wegmann et al., 2004; MacLeod et al., 2007; Gasic et al., 2009; Collins and Finnegan, 2010; Morselli et al., 2011; Garcia et al., 2014; Loizeau et al., 2014; Trapp, 2015; Bao et al., 2015; Lichiheb et al., 2016). For instance, several models (i.e. Cousins et al., 1999; Scholtz et al., 2002a, 2002b; Gasic et al., 2009; Loizeau et al., 2014; Bao et al., 2015) have addressed soil-atmosphere exchange of SVOCs (two compartments; without plants) considering integrated physico-chemical parameters. Previous studies (i.e. MacLeod et al., 2007; Gasic et al., 2009; Morselli et al., 2011) have identified controls (such as temperature,

local atmospheric stability, hydroxyl radical concentrations, and source type) for short-term concentration fluctuations of SVOCs in the atmosphere. In addition, numerical models describing plant uptake of SVOCs from soils and the atmosphere have been developed (Trapp 1995, 2002, 2007, and 2015; Trapp and Eggen, 2013), the development of which eventually facilitated numerical investigations of plant uptake of organic pollutants in the soil–plant–atmosphere system (van den Berg and Leistra, 2004; Collins and Finnegan, 2010; Lichiheb et al., 2016). However, relevance of plant-atmosphere partitioning compared to soil-atmosphere partitioning has hardly been explored with respect to short-term atmospheric concentration fluctuations. Moreover, steep and dynamic temperature-dependent concentration gradients of SVOCs may form in the lower part of the atmospheric boundary layer and topsoils, depending on the source-sink function of soils and plants as well as meteorological conditions. Although such concentration gradients have been observed in several studies (Farrar et al., 2005; Tao et al., 2007; Zhang et al., 2011), fluxes in the soil–plant–atmosphere system so far have not been addressed in numerical studies in detail. In fact, semi-volatile pollutants usually have been assumed to be well mixed within the atmosphere (Lee et al., 1998).

In this study, therefore, we extended a previous version of a numerical model MIN3P (Bao et al., 2015) to consider the impact of time- and depth-dependent temperature changes as well as photochemical oxidation in the atmosphere on short-term concentration fluctuations of SVOCs in the soil–plant–atmosphere system, using PCB-52 and phenanthrene as model compounds. We focus on a grassland or agricultural-type system, and do not include a forest canopy. We use the model results and comparison to observed daily concentration fluctuations of PCB-52 found in the literature (Lee et al., 1998) to elucidate sources and processes, which are relevant for atmospheric concentration fluctuations and cross-compartmental concentration gradients in a quantitative way.

3.2 Model setup and numerical methods

3.2.1 Model compounds

PCB-52 and phenanthrene were chosen as model compounds. PCB-52 was selected because it is fairly resistant to photochemical oxidation in the atmosphere (with atmospheric half-life times ranging from 3 to 120 days for all PCB congeners, and 62.5

days for PCB-52 specifically, Sinkkonen et al., 2000). Phenanthrene was selected for comparison because of similar physicochemical properties and its photosensitivity, with a much shorter atmospheric half-life of 5.6 hours (Atkinson and Arey, 1994). The relevant physicochemical properties of the two compounds (e.g. thermodynamic properties, half-lives, and diffusion and partitioning coefficients) are summarized in Table S2.1 (Supporting Information S2).

3.2.2 Conceptual model

The conceptual model used to simulate the soil–plant–atmosphere fluxes of SVOCs driven by diurnal temperature changes is shown in Fig. 3.1. It accounts for two distinct soil horizons (high organic carbon topsoil and sandy subsoil), a plant layer, and the atmospheric boundary layer with varying heights. Fig. 3.1 additionally shows how diurnal temperature changes in the atmosphere propagate into the soil over a time period of 1.5 days. For the sake of simplicity, we assumed a sinusoidal temperature change with the minimum and maximum daily temperatures at 3 am and 3 pm, respectively.

Changes in temperature over a day result in changes in the height of the atmospheric boundary layer as well as in vertical mixing. In fact, even under fair weather conditions the height of the atmospheric boundary layer still exhibits strong diurnal changes (Stull, 2000). During daytime, solar radiation leads to surface warming, and hence to the formation of convective thermal eddies that influence mass transport of atmospheric pollutants. Due to turbulence, the atmospheric boundary layer may reach heights of thousands of meters and eddy diffusion is the dominating mass transport process. At night the height of the atmospheric boundary layer decreases due to an inverse temperature field (i.e., increasing temperature with increasing height), caused by radiative cooling of surface air. In the model, the atmospheric boundary layer was simplified with a thickness of 1,000 m during daytime and 100 m at night.
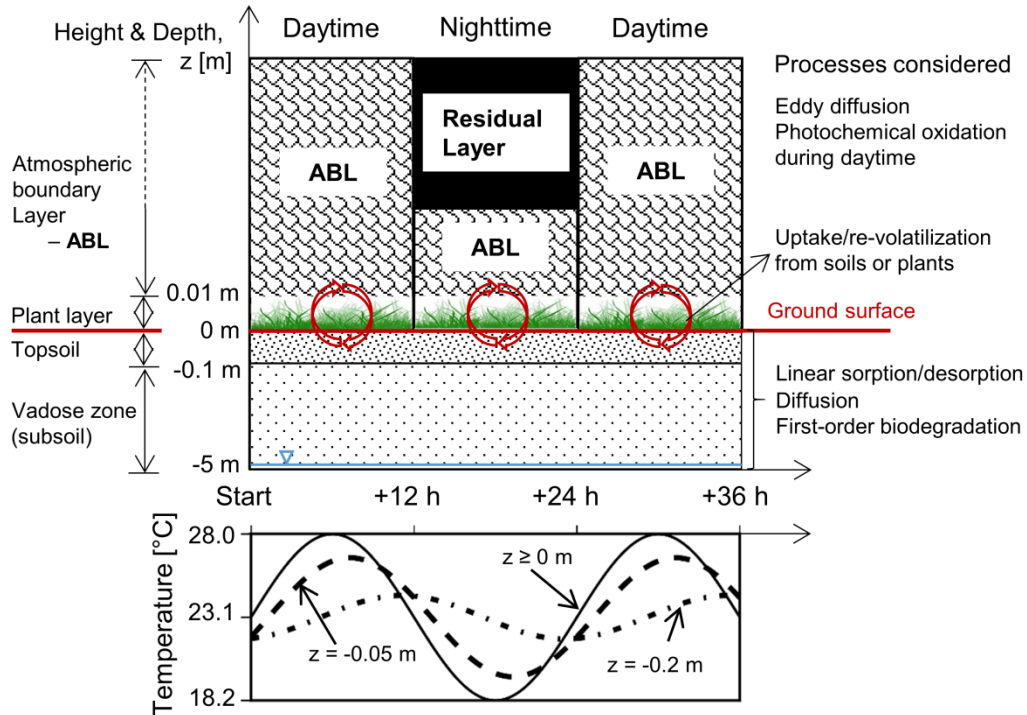
Figure 3.1. Conceptual model (not drawn to scale) and processes used to simulate temperature-driven concentration fluctuations of semi-volatile pollutants in the soil–plant–atmosphere system; changes in the height of the atmospheric boundary layer are simplified by assuming fixed heights during daytime (1,000 m) and at night (100 m); the lower boundary represents the groundwater level. The temperature evolution (bottom) is shown at/above ground surface ($z \geq 0$ m) and for two different soil depths: 0.05 m (topsoil), 0.2 m (subsoil).

The plant layer may act as potential source-sink term at ground level for atmospheric concentration fluctuations, the parameterization of which depends on the species, total biomass, leaf area, age, and effective lipid content (or sorption capacity). Root uptake of pollutants from soils was not considered for the short-term diurnal simulations but may play a role for seasonal fluxes of pollutants. The focus was placed on the ground-level plant layer and the influence of the amount of plant layer that, in terms of quantity of biomass per square meter, varies significantly with dependence on the types of land cover, site-specific plant species, season, and plant ages (e.g. Mackay, 2001). Mackay (2001) recommended 1 cm as the equivalent "height" of plant biomass, mainly composed of water (50%), cellulose, starch, ligneous material, and some lipid-like material (1%), the latter of which is responsible for the uptake and re-volatilization of atmospheric pollutants

44

and may change over time as well. In our study, we simplified this ground-level source-sink term as an equivalent volume of 1 L plant layer per square meter land surface (1 cm equivalent height at 10% land coverage). A subset of parameters that describe the compartments and chemical properties are shown in Table 3.1, and extensively in Table S2.1.

Table 3.1. Overview of mass transfer parameters and selected physical properties in soils, plants and the atmosphere for PCB-52 and phenanthrene (Phe) at 25 °C.

Layer	Lipid/organic carbon content	Water saturation S_w [-]	Porosity n [-]	Partition coefficient [L/kg]		Effective gas diffusion coefficient D_{eg} [m²/s]	
				PCB-52	Phe	PCB-52	Phe
Atm. boundary layer	NA	0 [d]	NA	NA	NA	Variable - Fig. S2.1 [d]	Variable - Fig. S2.1 [d]
Plant layer	1.0% [a]	0 [d]	NA	$\log K_{PA}$ = 5.40	$\log K_{PA}$ = 5.14	> 5.2×10⁻⁶ [d]	> 6.0×10⁻⁶ [d]
Topsoil	2.0% [b]	≈ 0.3 [e]	0.40	$\log K_d$ = 3.56	$\log K_d$ = 2.44	5.3×10⁻⁷	6.1×10⁻⁷
Vadose zone (subsoil)	0.2% [c]	≈ 0.3 [e]	0.33	$\log K_d$ = 2.56	$\log K_d$ = 1.44	4.0×10⁻⁷	4.6×10⁻⁷

[a] lipid content in the plant layer (Mackay, 2001)
[b] data obtained from the European Soil Portal – Soil Data and Information Systems from the website of the European Commission http://eusoils.jrc.ec.europa.eu/
[c] 10 times lower organic carbon content is assumed in the subsoil than in the topsoil
[d] implementation of the atmospheric boundary layer following Bao et al. (2015) and Foken (2008). Fig. S2.1 shows the vertical profile of effective gas and eddy diffusion of vapor phase PCB-52 in soils and in the atmosphere while the vertical profile of vapor phase phenanthrene is similar, following the same procedure in Bao et al. (2015).
[e] mean water saturation calculated for sandy soils predicted by van Genuchten model (Section S2.3) with α = 14.5 m⁻¹, N = 2.68, and l = 0.5 (Carsel and Parrish, 1988)
Note: NA = not applicable.

As shown in Fig. 3.1, the model is 1-D vertically. For the short-term simulations, the mass of conservative compounds (i.e. PCB-52) in the system is preserved. Photosensitive compounds (here phenanthrene) are photochemically reduced by over 90% mass in the atmosphere during daytime, but this is re-compensated at night, and thus ongoing anthropogenic emissions of PAHs are considered to maintain the typical range of observed atmospheric concentrations. In the subsurface, both compounds (PCB-52 and phenanthrene) partition between the aqueous, the gaseous, and the solid phases and are transported by diffusion (pure diffusion in the aqueous and the gaseous phases). In the atmosphere, the two compounds are present in the vapor phase and partition between

plants and air at the temperatures of interest. Partitioning to atmospheric particles was not considered because less than 5% of the two compounds would be involved (assuming e.g. 0.1 mg/m^3 atmospheric particles and local equilibrium, 76% mass of PCB-52 is present in the atmosphere, 19% mass in plants, and 2% mass in atmospheric particles; for details refer to Section S2.7). Vertical exchange of pollutants between different compartments is mainly driven by diffusion (or eddy diffusion) and vertical concentration gradients in the gas phase; for partitioning between air, water, soil solids and plant materials local equilibrium was assumed.

Similar to gas exchange across the soil-atmosphere interface, temperature-driven uptake and re-volatilization of atmospheric pollutants by plants can be simulated with a numerical model. McLachlan (1999) proposed a model framework to describe the uptake of SVOCs in plants via one of the following three processes with dependence on the chemical properties of the compounds: equilibrium partitioning into plants, kinetically limited gaseous deposition, and particle-bound deposition. Böhme et al. (1999) experimentally verified the concept (McLachlan, 1999) of uptake of atmospheric pollutants by plants and demonstrated that the uptake for the compounds with $\log K_{OA} < \sim 9$ may be described by equilibrium partitioning. Values of $\log K_{OA}$ are $< \sim 9$ for the two compounds in our study, PCB-52 ($\log K_{OA} = 7.73$) and phenanthrene ($\log K_{OA} = 7.60$). Terzaghi et al. (2015) also found that concentrations of PAHs in plants reflect actual concentrations in the atmosphere due to fast equilibration. Thus, for numerical simulations, we implemented a plant layer as an additional compartment in the model assuming local equilibrium between plants and air for PCB-52 and phenanthrene (McLachlan, 1999; Böhme et al., 1999).

3.2.3 Model parameterization and solution

The multicomponent reactive transport code MIN3P (Mayer et al., 2002) was initially developed for simulating flow, reactive transport and biogeochemical reactions in the subsurface. It integrates Richard's equation (Eqn. S2.1 in Section S2.3) for simulating flow under unsaturated/saturated conditions and multicomponent reactive transport by advection, dispersion and diffusion in variably saturated porous media. A global implicit solution method following the direct substitution approach (Steefel et al., 2015) was implemented to solve the multicomponent transport equation and biogeochemical

reactions, while finite difference method was used to perform spatial discretization in 1-dimension. The code MIN3P extended with an atmospheric boundary layer (Bao et al., 2015), where eddy diffusion is the dominating mass transport process, was employed in all simulations. The model describes the cross-compartmental kinetic exchange of semi-volatile pollutants between soils, plants and the atmosphere as a function of soils, plants and compound properties:

$$\frac{\partial}{\partial t}[n_w C_w] + \frac{\partial}{\partial t}[n_g C_g] + \frac{\partial}{\partial t}[\rho(1-n)C_s|_{z<0}] + \frac{\partial}{\partial t}\left[\rho_{plant} C_{plant}|_{0<z<h_{plant}}\right]$$
$$- \frac{\partial}{\partial z}\left[D_{ew}\frac{\partial}{\partial z}C_w\right] - \frac{\partial}{\partial z}\left[D_{eg}\frac{\partial}{\partial z}C_g\right] - Q_{biodeg}|_{z<0}$$
$$- Q_{photodeg}|_{z>0,t=daytime} = 0$$

(3.1)

where n_w [-], n_g [-], and n [-] denote the water-filled, the gas-filled, and the total porosity. t [s], z [m], and h_{plant} [m] represent the time, the vertical coordinate, and the equivalent height of the plant layer (which is introduced into the model for numerical settings; and the equivalent height of 1 L/m^2 plants is 1 cm with a plant coverage of 10% per square meter land surface). ρ [2,650 kg/m^3] and ρ_{plant} [1,000 kg/m^3] are the density of soil solids and plant materials. C_w [kg/m^3], C_g [kg/m^3], C_s [kg/kg bulk phase] and C_{plant} [kg/kg bulk phase] are the concentrations of the compound in the aqueous, gas and solid phases as well as in the plant materials. Q_{biodeg} [kg/(m^3·s)] and $Q_{photodeg}$ [kg/(m^3·s)] refer to sink terms that result from microbial biodegradation in the soil water and from photochemical oxidation in the atmosphere (both assumed as pseudo first-order chemical reactions in our study, where $Q_{biodeg} = \lambda_{biodeg}\, n_w\, C_w$ and $Q_{photodeg} = \lambda_{photodeg}\, C_g$ with λ_{biodeg} [1/s] and $\lambda_{photodeg}$ [1/s] representing the reaction rate constants for microbial biodegradation and photochemical oxidation, respectively). Reaction rates for microbial degradation and photochemical oxidation are not well known and for simplicity, both were assumed temperature independent. Microbial biodegradation is only relevant for long-term fate and transport of pollutants in the soil (Bao et al., 2015) - therefore this is not further discussed in this study. Photochemical oxidation is only applied during daytime when solar radiation is present.

The atmospheric boundary layer was implemented in the model as described previously (refer to details in Bao et al., 2015). A 5-mm thick stagnant air layer (Jury et al., 1983;

McKone, 1996; Loizeau et al., 2014) was used above ground, within which effective gas diffusion changes from pure diffusion in the soil to eddy diffusion in the atmosphere. As an example, the vertical profile of effective gas and eddy diffusion coefficients for PCB-52 across the soil-atmosphere interface is presented in Fig. S2.1. The stagnant air layer influences the mass transfer coefficient during soil-atmosphere exchange but was found to influence concentration fluctuations of vapor phase pollutants mainly in the stagnant air layer rather than the atmosphere (see Fig. S2.4 in Section S2.8).

In Eqn. 3.1, D_{eg} [m^2/s] and D_{ew} [m^2/s] denote the effective diffusion coefficients in gas and water, respectively, which are determined following empirical relationships accounting for pore space tortuosity in the soil (Moldrup et al., 2000, 2001):

$$D_{eg} = D_g^* \frac{n_g^{2.5}}{n} \tag{3.2}$$

$$D_{ew} = D_w^* \frac{n_w^{2.5}}{n} \tag{3.3}$$

where D_g^* [m^2/s] and D_w^* [m^2/s] are the molecular diffusion coefficients in the free gaseous and aqueous phases.

Linear distribution of the pollutants between solid, gaseous, and aqueous phases is described by:

$$K_d = \frac{C_s}{C_w} \tag{3.4}$$

$$H = \frac{C_g}{C_w} \tag{3.5}$$

where K_d [L/kg] refers to the sorption distribution coefficient and H [-] is the Henry's law coefficient. The sorption distribution coefficient can be calculated by $K_d = K_{OC} f_{OC}$, with f_{OC} [-] being the soil organic carbon content and K_{OC} [L/kg] being the soil organic carbon-water partition coefficient. The latter is computed from water solubility based on the following empirical relationship (Razzaque and Grathwohl, 2008):

$$\log K_{OC} = -0.85 \log S_{scl} - 0.55 \tag{3.6}$$

where S_{scl} [kg/L] denotes the subcooled liquid solubility.

Partitioning between plants and the atmosphere was implemented analogously by introducing the plant-air partition coefficient, K_{PA} [L/kg], following:

$$K_{PA} = \frac{C_{plant}}{C_g} \qquad\qquad (3.7)$$

Diurnal temperature changes were considered by modeling heat transport in the soil layer (Hillel, 1998). Particularly, we assumed a sinusoidal change in atmospheric temperature over a day that is characterized by an average temperature, T_A [°C] and an amplitude, A [°C] between the average and the minimum/maximum temperature (see Section S2.4). The temperatures were updated at 1-min time intervals. To account for temperature dependence of partitioning and diffusion, the van't Hoff equation and empirical relationships were used (details are provided in Section S2.5).

3.2.4 Initial condition, numerical settings and field data

To set up the initial conditions for short-term simulations, we focused on undisturbed soils and allowed several decades (40 to 100 years) of soil contamination by wet and gas deposition, followed by reduced pollutant concentrations in the atmosphere to replicate declining emissions following regulation and shifts in technology at the end of last century in industrialized countries (Table S2.2). Initial conditions are characterized by steep concentration gradients in the topsoil as shown in Fig. 3.2. Spatial discretization for the layers of subsoil, topsoil, plants and the atmosphere were 1 cm ($z < $ -0.1 m, subsoil), 5 mm (-0.1 m $\leq z < 1$ m, topsoil, plants and lower atmospheric boundary layer), and 0.5 m ($z \geq 1$ m, atmosphere). The short-term model time was five days with temporal resolution of 1 minute and quasi-stable atmospheric concentration fluctuations were achieved during the last four days. The computational time of each model run took around 2 hours.

Model results were compared between the bare soil scenario ('bare soil') and the scenario containing an additional 1 L/m² plant layer ('soil & plant'). In addition, we compared model results for PCB-52 with field measurements from Lee et al., 1998, which were collected at an agricultural site in a rural area in Hazelrigg (outside Lancaster), UK. In this study air samplers were placed at an approximate height of 1.5 m above ground and sampled every 6 hour precisely every day from August 17 to 24 in 1995 to analyze atmospheric concentrations of PCBs and PAHs. Stable patterns in atmospheric concentration fluctuations of several PCBs as well as in temperature cycling were obtained for the first five days (August 17 to 22). In our simulations, we adjusted temperature changes in the

atmosphere to 23.1 ± 4.9 °C (Lee et al., 1998) that had been measured at the near-by meteorological station. Temperatures and initial conditions for numerical simulations are summarized in Figs. S2.2 and S2.3. In particular, model results in concentration fluctuations of PCB-52 at 1.5 m height in the atmosphere were validated with field measurements collected from August 18 to 22, 1995.

3.3 Results and discussion

3.3.1 Vertical concentration profile across the soil–plant–atmosphere interface(s)

Temperature-driven changes in distribution/partitioning and diffusion coefficients change the concentrations in the water and gas phase as well as the fluxes of pollutants. Photochemical transformations reduce concentrations of photosensitive pollutants in the air during daytime, which is here considered for phenanthrene. Results are shown in Fig. 3.2 for normalized gas phase concentrations of PCB-52 and phenanthrene for different times and locations in the soil–plant–atmosphere system. In soil air, concentrations follow changes in temperature due to desorption from soil solids and volatilization from pore water at higher temperatures as well as sorption to soil solids and diffusion into pore water at lower temperatures. Soil gas phase concentration fluctuations are virtually the same regardless whether plants or just bare soils are considered.

In contrast to the observed fluctuations in soil gas concentrations, atmospheric concentrations for the bare soil scenario stay practically constant for PCB-52. This is explained by the fact that only a few millimeters of topsoil actually are involved in the diurnal soil-atmosphere exchange (see the accompanying movie entitled 'Movie S2.1.avi', and Section S2.7). Nevertheless, the soil is always a source for the atmospheric pollutants, except in the bare soil scenario at the minimum temperature at night, where the gradient is reversed and the fluxes are temporarily from the atmosphere into the soil. Concentration fluctuations of PCB-52 in the atmosphere follow temperature changes only if the plant layer is added (soil & plant scenario). Compounds released from plants are rapidly mixed into the atmosphere due to eddy diffusion; only with plants are concentration gradients in the atmosphere expected (see vertical concentration profiles of PCB-52 in Fig. S2.5 in Section S2.9 and animation entitled 'Movie S2.2.avi'). For photosensitive compounds (here phenanthrene) atmospheric concentrations are

50

significantly depleted during daytime due to photochemical oxidation, but restored at night to the original levels due to ongoing emissions into the environment (Fig. 3.2). The atmosphere acts as a strong sink for photosensitive compounds during daytime while the sun is shining. This sink function is buffered in the soil & plant scenario, where the plant material rapidly replenishes the loss of pollutants to some extent. With photochemical transformation a slightly steeper atmospheric concentration gradient of phenanthrene compared to PCB-52 is observed (refer to the second row of Fig. S2.5 in Section S2.9). Vertical concentration gradients of PAHs in the atmosphere were also found in several field observations (Farrar et al., 2005; Tao et al., 2007; Zhang et al., 2011).
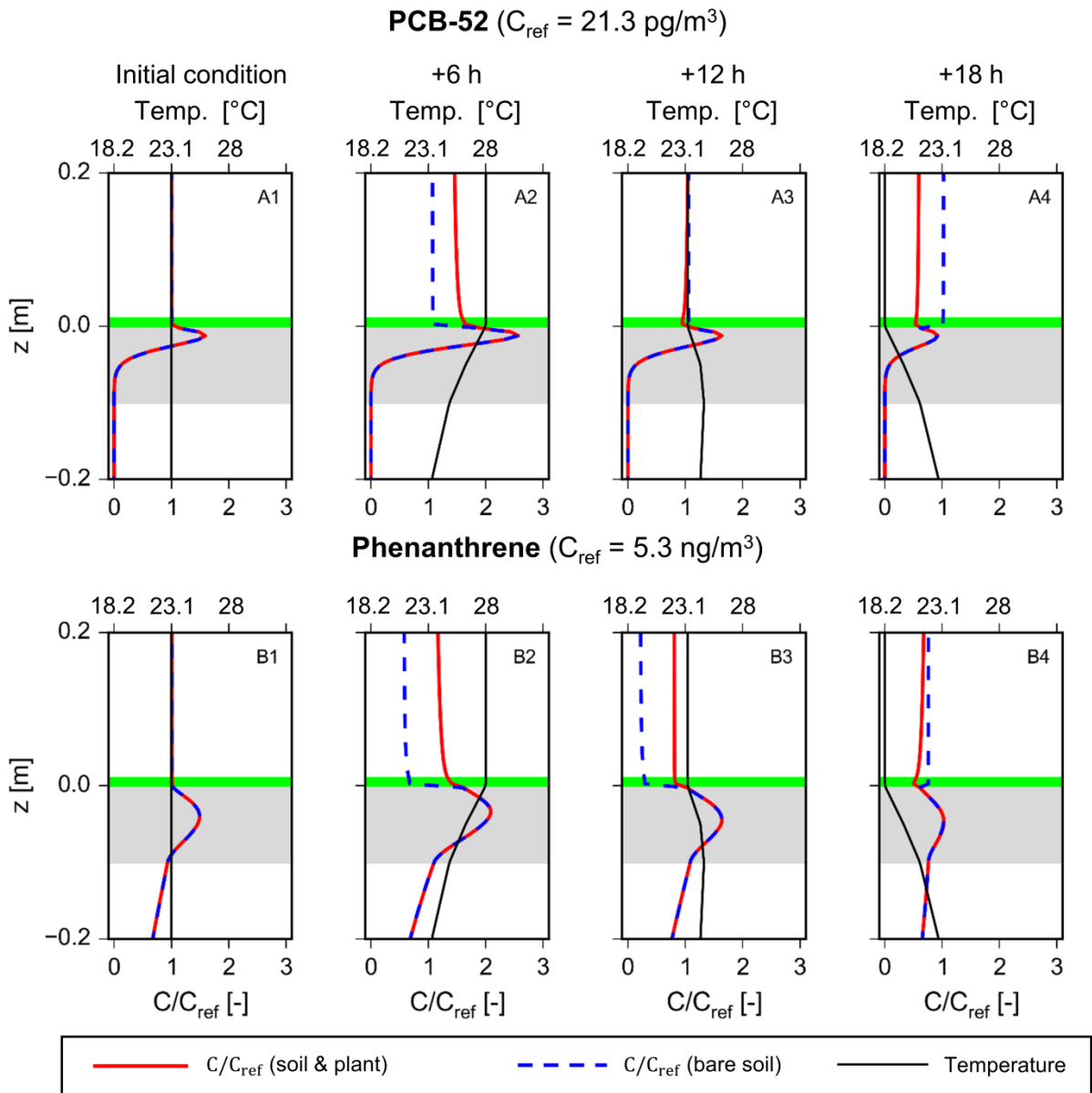
Figure 3.2. Vertical concentration profiles of vapor phase PCB-52 (top) and phenanthrene (bottom) when quasi-stable atmospheric concentrations were achieved. Blue dashed lines: the bare soil scenario; red solid lines: the soil & plant scenario. The grey-shaded area represents the topsoil high in organic carbon (2%), while the green-shaded area refers to the plant layer. Normalized concentration C_{ref} [mass/volume] is based on the initial concentration in the atmosphere.

3.3.2 Diurnal concentration changes in soils and in the atmosphere

For detailed illustration of dynamics at five different vertical locations across the compartmental interfaces, Fig. 3.3 shows modeled results of normalized vapor phase

concentrations at high temporal resolution over 4 days at 1.5 m (top, atmosphere), ±0.005 m (at the soil-atmosphere interface), -0.05 m (topsoil), and -0.2 m (bottom, subsoil). In the soil, PCB-52 and phenanthrene behave similarly since both compounds have similar physicochemical properties and the relative concentration fluctuations in soil air are almost the same for both compounds. Due to the large storage capacity in the soil (or strong retardation), the total mass in the soil remains practically constant over the time period of the short-term model simulations. Generally, and as to be expected, concentrations in the soil follow the temperature changes that are most pronounced at the soil surface (Figs. 3.3-A3 and 3.3-B3); with increasing soil depth, the concentration fluctuations are dampened and shifted in phase. There is a slight asymmetry between the concentration increase during daytime compared to the decrease at night (i.e., rapid increase vs. slower decrease), which is due to changes in partitioning coefficients calculated with the exponential van't Hoff relationship. This slight asymmetry is more pronounced for PCB-52, which has the higher enthalpies of phase changes than phenanthrene (Table S2.1). Below ground, surface concentration fluctuations are the same for both scenarios (bare soil and soil & plant) and are not influenced by plants and photochemical oxidation in the atmosphere, which is due to the high storage capacity of pollutants in the soil.
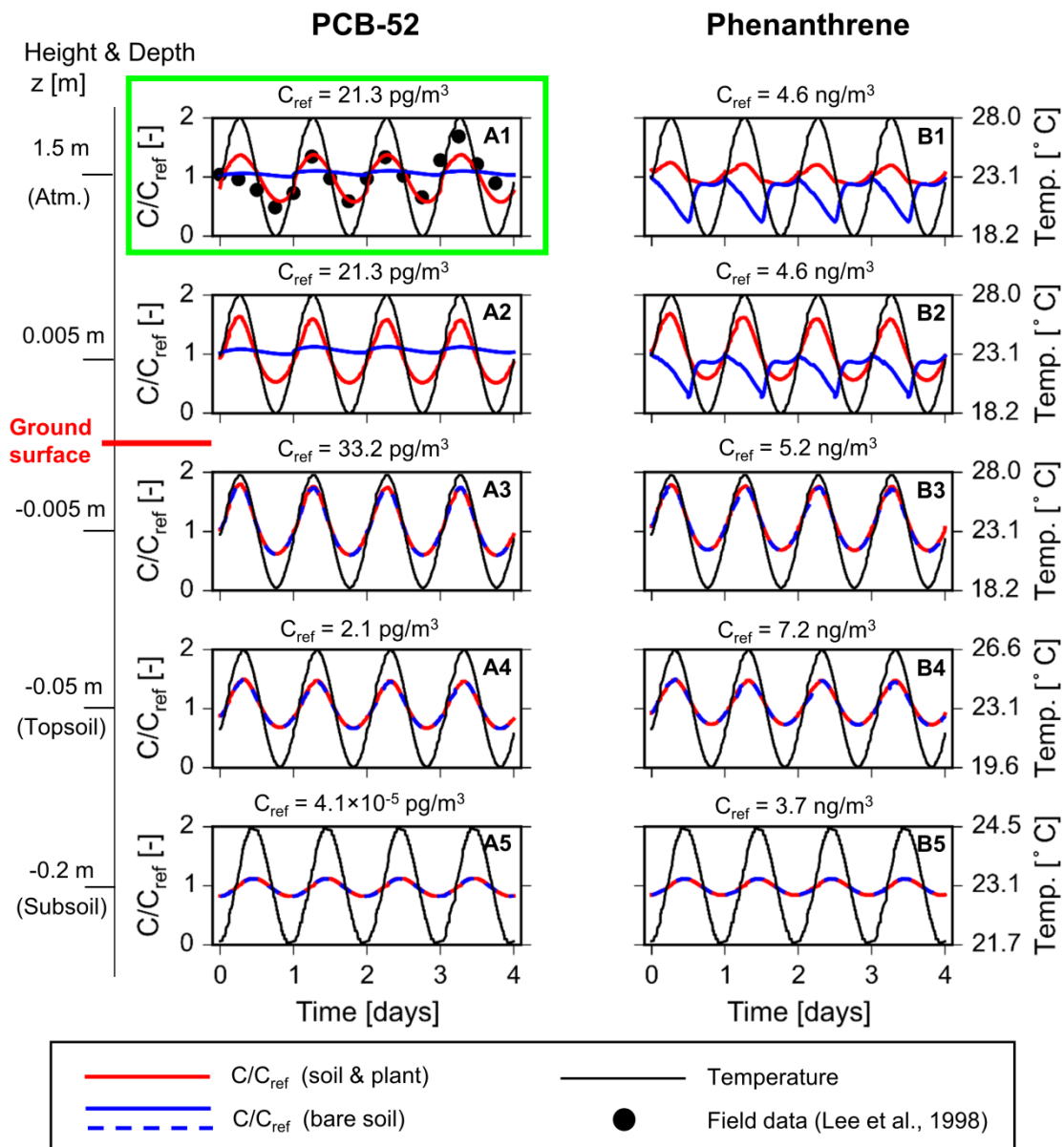
Figure 3.3. Temperature-driven concentration fluctuations in vapor phase over a time period of four days for PCB-52 (left) and phenanthrene (right) at five vertical locations across the soil – atmosphere interface. Blue solid (in the soil) and dashed (in the atmosphere) lines: bare soil scenario; red solid lines: soil & plant. In Plot A1, highlighted in the solid green box, PCB results are compared with data obtained in Hazelrigg, UK (black dots, from Lee et al. (1998) normalized to 21.3 pg/m³). Different reference concentrations, C_{ref} [mass/volume], are used for normalization as shown in the subplots at that respective location based on the initial conditions (for details see Section S2.6).

Since PCB-52 is assumed to be resistant to photochemical oxidation in contrast to phenanthrene, the two compounds show a different behavior in the atmosphere, i.e. lower concentrations for phenanthrene during daytime (for a more detailed comparison of atmospheric concentration fluctuations see Fig. S2.6 in Section S2.9). The main differences in concentration fluctuations are observed in the bare soil scenario (blue solid lines in Fig. 3.3-A1 and 3.3-B1) where phenanthrene shows an opposite trend with temperature changes when compared to PCB-52 because of photochemical transformation. In particular, low phenanthrene concentrations are observed during daytime, (different from PCB-52), yet concentrations of phenanthrene increase again to the original levels at night because of additional emissions (Fig. 3.3-B1). The model output also explains the field observations of temperature-mediated reversible soil-atmosphere exchange of SVOCs (Gouin et al., 2002; Totten et al., 2002) for some sites of stronger photochemical oxidation and for photosensitive compounds.

For the soil & plant scenario (red solid lines in Fig. 3.3-A1 and 3.3-B1), model results indicate that the sorption capacity of a thin plant layer is high enough to cause atmospheric concentration fluctuations as observed for PCB-52 in the field study (Lee et al., 1998). The model fits measured concentrations reasonably well (*RMSE* = 0.235) as shown in Fig. 3.3-A1. Rapid release of phenanthrene from plants buffers the impact of photochemical oxidation and slightly elevated concentrations of phenanthrene are observed during daytime. Field studies (Lee et al., 1998) reporting unstable and fluctuating concentrations of phenanthrene are supported by model results accounting for photochemical oxidation and fast mass exchange from plants, as well as potential emissions to the site. In summary, the model results indicate that soil has relatively low impacts on diurnal atmospheric concentration fluctuations and cannot explain observed variability in the field for PCB-52 (black dots in Figs. 3.3-A1); while a rapidly-exchanging storage compartment such as a plant layer above ground could pose significant impacts to short-term atmospheric concentration fluctuations.

3.3.3 Effect of different initial conditions, water contents, and sorption on pollutant flux in the bare soil scenario

Water saturation for the topsoil (sandy soil) in our scenarios is 0.3, which results in fairly high gas diffusivity and thus would allow relatively rapid exchange of pollutants with the atmosphere. Fig. 3.4 illustrates how different initial conditions, i.e. different concentration gradients in the soil, water contents and elevated levels of organic carbon, influence concentrations of PCB-52 at a height of 1.5 m above ground when compared with the bare soil scenario (base scenario). As to be expected, diffusion fluxes in the gas phase increase from wet soils to dry soils (increasing gas diffusivity), but during half a day volatilization still would contribute less than 1% to the overall mass present in the atmosphere and thus cannot account for significant changes in atmospheric concentrations. In addition, different initial conditions (different concentration profiles e.g. caused by bioturbation or by plowing that result in well-mixed soils) do not change findings drawn from the base scenario. This also applies for elevated levels of organic carbon (i.e. 10% f_{OC}) in the topsoil, which increases the sorption capacity of the soil strongly. In general, model outcomes for different initial conditions, water contents, and sorption, show that temperature-driven soil-atmosphere exchange of pollutants cannot explain significant short-term concentration fluctuations in the atmosphere. Pronounced changes of SVOCs in the atmosphere such as observed at the Hazelrigg field site (Lee et al., 1998) can only be obtained when a plant layer is present or if changes in emissions in close-by sources are considered (MacLeod et al., 2007).
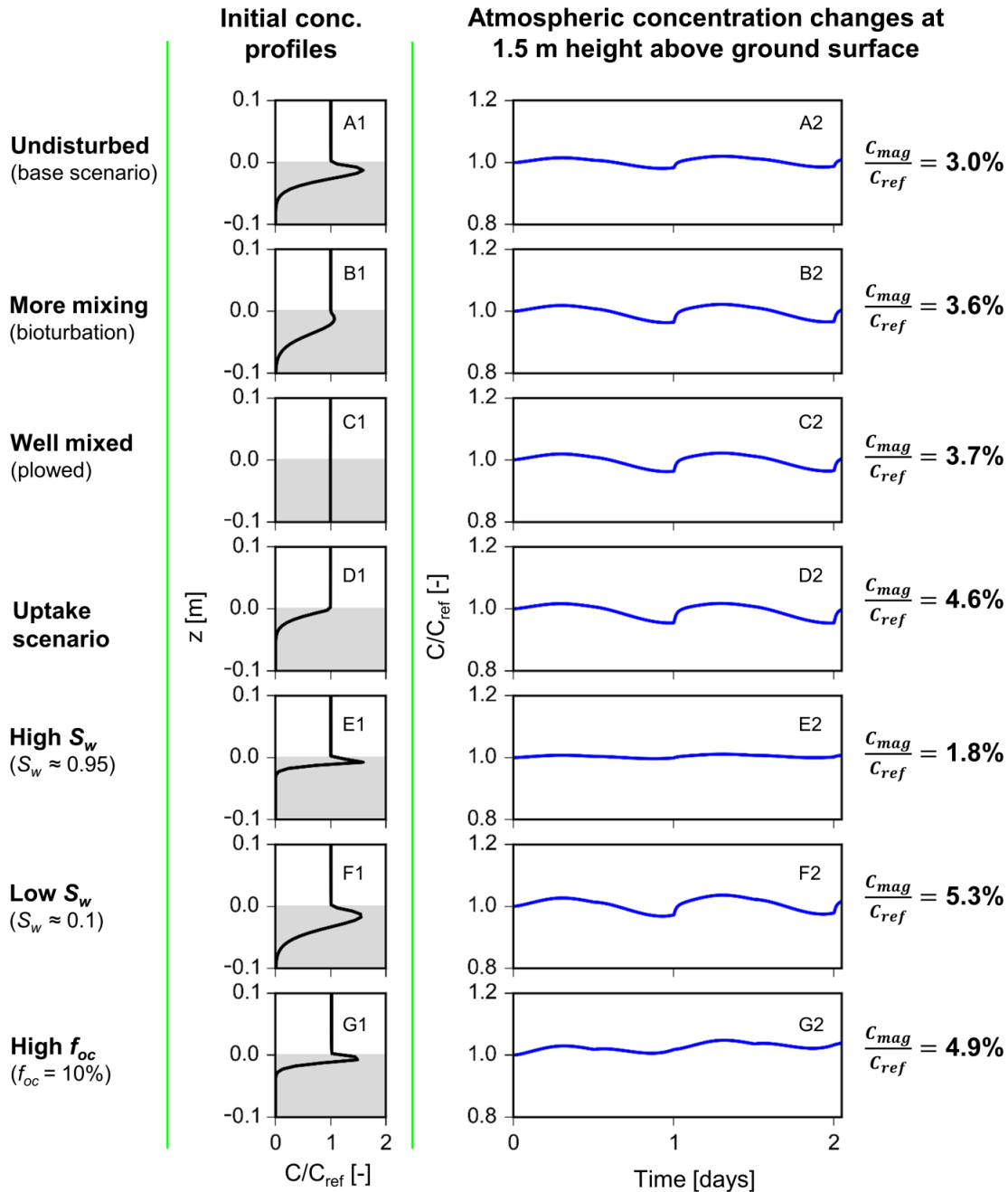
Figure 3.4. Effect of different initial conditions, water contents, and sorption (left) on concentration fluctuations of PCB-52 at 1.5 m height (right) in the bare soil scenario. For normalization the initial concentration at the upper boundary was used (C_{ref} = 21.3 pg/m³). C_{mag} = max{| C_{max} − C_{ref} | , | C_{min} − C_{ref} |} and C_{mag}/C_{ref} [-] denotes the maximum magnitude in atmospheric concentration fluctuations with C_{max} [pg/m³] and C_{min} [pg/m³] being the maximum and minimum concentrations of vapor phase PCB-52 over a day and night cycle. All scenarios produce about the same negligible concentration fluctuations in the atmosphere (C_{mag}/C_{ref} < ~5%).

3.4 Conclusions and model uncertainties

Physically based cross-compartmental models as employed in this study for the soil–plant–atmosphere system help to understand the relevance of different physicochemical processes controlling mass transfer of semi-volatile pollutants between soils, plants and the atmosphere. While soils typically represent a long-term terrestrial reservoir of SVOCs, low effective gas diffusion coefficients in soils limit mass transfer of vapor phase pollutants and thus hardly affect diurnal atmospheric concentration fluctuations. Rapidly exchanging reservoirs of SVOCs at ground level near the soil-atmosphere interface such as plants are needed when accounting for short-term atmospheric concentration fluctuations. However, even though the model accounts for various coupled processes and is able to reproduce field observations very well, significant uncertainties still exist about the parameters involved. Diffusion and sorption of SVOCs in soils are well understood and parameters may be derived from well-established empirical relationships. Variations in the height of the atmospheric boundary layer in principle can influence atmospheric concentration fluctuations but this was not detectable for the bare soil scenario due to limited fluxes from soils. Also turbulent mixing caused by eddy diffusion can influence mass transfer from ground-level source-sink terms to the upper atmosphere – pronounced vertical concentration gradients of SVOCs may form if eddy diffusion is low (Farrar et al., 2005; Tao et al., 2007). Numerical simulations (sensitivity analysis) show that our findings on the role of rapidly exchanging reservoirs at ground level (plant layers) are not significantly affected by uncertainties in the height of the atmospheric boundary layer (also illustrated in MacLeod et al., 2007) and mixing efficiency. Major uncertainties are connected to plant-air partitioning, especially the kinetics, as well as to biomass specifications such as the plant species (e.g. grasses, shrubs, or mosses) and the influence of leaf area, plant height and age; additionally, the lipid content of plants may change seasonally (Mackay, 2001). While equilibrium partitioning of PCB-52 and phenanthrene between plants and the atmosphere was applied following others (Kömp and McLachlan, 1997; Böhme et al., 1999; McLachlan, 1999), temperature-induced uptake and release kinetics of semi-volatile pollutants from plant tissues are not known very well. This is probably plant and compound specific. Nevertheless, model results

indicate the importance of a rapidly exchanging compartment as cause for short-term atmospheric concentration fluctuations.

Additional sources such as particle-associated pollutants in the atmosphere may also contribute to atmospheric concentration fluctuations (Liu et al., 2013), but high uncertainties with respects to site-specific particle densities in the atmosphere and compound-specific particle-air partitioning may exist (Section S7). Moreover, biogenic production, root uptake from soils and subsequent mass transfer to leaf surfaces and final the atmosphere, as well as increased fluxes from soils to the atmosphere at extremely high temperatures (~ 50 – 60 °C) at "surface skins" (upper few millimeters) of top soils may impact atmospheric concentration fluctuations. These factors are highly specific to site location, composition of microbial and plant communities, plant coverage as well as solar radiation. For instance, based on the results of two different studies in which the same methods at uncultivated grassland sites were applied, the authors hypothesized that a biogenic source cause steep soil-atmosphere gradients of some PAHs in temperate locations in Spain and England (Cabrerizo et al., 2011), but not in Hungary (Degrendele et al., 2016). It is known that perylene and possibly phenanthrene, for example, may be produced by the activity of termites in tropical soils (Wilcke et al., 2002), or microbial reactions under anaerobic conditions (Venkatesan, 1988; Wilcke et al., 1999), but the importance of this in temperate, unsaturated soils is unclear. Further work should focus on the quantification of these potentially contributing sources by better identification of compound-specific mass transfer coefficients between plants and air, and better characterization of on-site ground-level source-sink terms, the physical, and the biological properties of soils as well as other so-far little understood storage and flux terms.

Acknowledgements

for helpful discussions. The Integration and Application Network (ian.umces.edu/imagelibrary/) at the University of Maryland Center for Environmental Science is also acknowledged for symbols contributing to the graphical abstract.

Supporting Information S2

Physicochemical properties of PCB-52 and phenanthrene, parameterization of the vertical water distribution, temperature changes, and effective gas and eddy diffusion in soils and in the atmosphere are described in more detail in the Supporting Information S2. S2 also includes detailed model results of vertical concentration profiles in the atmosphere of the two compounds, and atmospheric concentration fluctuations at three heights in the atmosphere. In addition, two movies ("Movie S2.1.avi" and "Movie S2.2.avi") are provided that show dynamics of vertical concentration profiles for vapor phase PCB-52 across the soil-atmosphere interface in the bare soil and soil & plant scenarios.

References

Atkinson, R., Arey, J., 1994. Atmospheric chemistry of gas-phase polycyclic aromatic hydrocarbons: Formation of atmospheric mutagens. Environ. Health Perspect. 102(Suppl 4), 117-126.

Bao, Z., Haberer, C.M., Maier, U., Beckingham, B., Amos, R.T., Grathwohl, P., 2015. Modeling long-term uptake and re-volatilization of semi-volatile organic compounds (SVOCs) across the soil-atmosphere interface. Sci. Total Environ 538, 789-801.

Barber, J.L., Thomas, G.O., Kerstiens, G., Jones, K.C., 2003. Study of plant-air transfer of PCBs from an evergreen shrub: implications for mechanisms and modeling. Environ. Sci. Technol. 37, 3838-3844.

Barber, J.L., Thomas, G.O., Kerstiens, G., Jones, K.C., 2004. Current issues and uncertainties in the measurement and modelling of air-vegetation exchange and within-plant processing of POPs. Environ. Pollut. 128, 99-138.

Böhme, F., Welsch-Pausch, K., McLachlan, M.S., 1999. Uptake of airborne semivolatile organic compounds in agricultural plants: field measurement of interspecies variability. Environ. Sci. Technol. 33, 1805-1813.

Buckley, E.H., 1982. Accumulation of airborne polychlorinated biphenyls in foliage. Science 216, 520-522.

Cabrerizo, A., Dachs, J., Moeckel, C., Ojeda, M.-J., Caballero, G., Barcelo, D., Jones, K.C., 2011. Ubiquitous net volatilization of polycyclic aromatic hydrocarbons from soils and parameters influencing their soil-air partitioning. Environ. Sci. Technol. 45, 4740-4747.

Carsel, R.F., Parrish, R.S., 1988. Developing joint probability distributions of soil water retention characteristics. Water Resour. Res.24, 755-769.

Collins, C.D., Finnegan, E., 2010. Modeling the plant uptake of organic chemicals, including the soil-air-plant pathway. Environ. Sci. Technol.44, 998-1003.

Cousins, I.T., Gevao, B., Jones, K.C., 1999. Measuring and modelling the vertical distribution of semi-volatile organic compounds in soils. 2: model development. Chemosphere 39, 2519-2534.

Dalla Valle, M., Dachs, J., Sweetman, A.J., Jones, K.C., 2004. Maximum reservoir capacity of vegetation for persistent organic pollutants: Implications for global cycling. Glob. Biogeochem. Cycles 18, 1-12.

Degrendele, C., Andy, O., Hofman, J., and et al., 2016. Diurnal variations of air-soil exchange of semivolatile organic compounds (PAHs, PCBs, OCPs, and PBDEs) in a central European receptor area. Environ. Sci. Technol. 50, 4278-4288.

Farrar, N.J., Harner, T., Shoeib, M., Sweetman, A., Jones, K.C., 2005. Field Deployment of thin film passive air samples for persistent organic pollutants: a study in the urban atmospheric boundary layer. Environ. Sci. Technol. 39, 42-48.

Foken, T., 2008. Micrometeorology. Springer-Verlag, Heidelberg, Germany.

Garcia, L., Bedos, C., Génermont. S., Benoit, P., Barriuso, E., Cellier, P., 2014. Modeling pesticide volatilization from bare soil: additional effect of gaseous adsorption on soil solid surface. Environ. Sci. Technol. 48, 4991-4998.

Gasic, B., Moeckel, C., MacLeod, M., Brunner, J., Scheringer, M., Jones, K.C., Hungerbühler, K., 2009. Measuring and modelling short-term variability of PCBs in air and characterization of urban source strength in Zurich, Switzerland. Environ. Sci. Technol. 43, 769-775.

Gouin, T., Mackay, D., Webster, E., Wania, F., 2002. Air-surface exchange of polybrominated diphenyl and polychlorinated biphenyls. Environ. Sci. Technol. 36, 1426-1434.

Hillel, D., 1998. Environmental Soil Physics: Fundamentals, applications, and environmental considerations. Academic Press, CA, USA.

Hung, H., Thomas, G.O., Jones, K.C., Mackay, D., 2001. Grass-air exchange of polychlorinated biphenyls. Environ. Sci. Technol. 35, 4066-4073.

Jones, K.C., de Voogt, P., 1999. Persistent organic pollutants (POPs): state of the science. Environ. Pollut. 100(1-3), 209-221.

Jones, K.C., Sanders, G., Wild, S.R., Burnett, V., Johnston, A.E., 1992, Evidence of a decline of PCBs and PAHs in rural vegetation and air in the United Kingdom. Nature 356, 137-139.

Jury, W., Spencer, W., Farmer, W., 1983. Behavior assessment model for trace organics in soil: I: Model description. J. Environ. Qual. 12, 558-564.

Kömp, P., McLachlan, M.S., 1997. Influence of temperature on the plant/air partitioning of semivolatile organic compounds. Environ. Sci. Technol. 31, 886-890.

Komprda, J., Komprdova, K., Sanka, M., Mozny, M., Nizzetto, L., 2013. Influence of climate and land use change on spatially resolved volatilization of persistent organic pollutants (POPs) from background soils. Environ. Sci. Technol. 47, 7052-7059.

Kurt-Karakus, P.B., Bidleman, T.F., Staebler, R.M., Jones, K.C., 2006. Measurement of DDT fluxes from a historically treated agricultural soil in Canada. Environ. Sci. Technol. 40, 4578-4585.

Lamon, L., von Waldow, H., MacLeod, M., Scheringer, M., Marcomini, A., Hungerbühler, K., 2009. Modeling the global levels and distribution of polychlorinated biphenyls in air under a climate change scenario. Environ. Sci. Technol. 43(15), 5818-5824.

Lee, R.G.M., Hung, D., Mackay, D., Jones, K.C., 1998. Measurement and modeling of the diurnal cycling of atmospheric PCBs and PAHs. Environ. Sci. Technol. 32, 2171-2179.

Lichiheb, N., Personne, E., Bedos. C., van den Berg, F., Barriuso, E., 2016. Implementation of the effects of physicochemical properties on the foliar penetration of pesticides and its potential for estimating pesticide volatilization from plants. Sci Total Environ. 550, 1022-1031.

Liu, J., Li, J., Lin, T., Liu, D., Xu, Y., Chaemfa, C., Qi, S., Liu, F., Zhang, G., 2013. Diurnal and nocturnal variations of PAHs in the Lhasa atmosphere, Tibetan Plateau: Implication for local sources and the impact of atmospheric degradation processing. Atmos. Res. 124, 34-43.

Loizeau, V., Ciffroy, P., Roustan, Y., Musson-Genon, L., 2014. Identification of sensitive parameters in the modeling of SVOC reemission processes from soil to atmosphere. Sci. Total Environ. 493, 419-431.

Ma, J., Hung, H., Tian, C., Kallenborn, R., 2011. Revolatilization of persistent organic pollutants in the Arctic induced by climate change. Nat. Clim. Chang. 1, 255-260.

Ma, J., Cao, Z., 2010. Quantifying the perturbations of persistent organic pollutants induced by climate change. Environ. Sci. Technol. 44, 8567-8573.

Mackay, D., 2001. Multimedia environmental models: the fugacity approach; CRC press.

MacLeod, M., Mackay, D., 2004. Modeling transport and deposition of contaminants to ecosystems of concern: a case study for the Laurentian Great Lakes. Environ. Pollut. 128, 241-250.

MacLeod, M., Scheringer, M., Podey, H., Jones, K.C., Hungerbühler, K., 2007. The origin and significance of short-term variability of semivolatile contaminants in air. Environ. Sci. Technol. 41, 3249-3253.

Mandalakis, M., Berresheim, H., Stephanou, E.G., 2003. Direct evidence for destruction of polychlorobiphenyls by OH radicals in the subtropical troposphere. Environ. Sci. Technol. 37, 542-547.

Mayer, U.K., Frind, E.O., Blowes, D.W., 2002. Multicomponent reactive transport modeling in variably saturated porous media using a generalized formulation for kinetically controlled reactions. Water Resour. Res. 38, 1174.

McKone, T.E., 1996. Alternative modeling approaches for contaminant fate in soils: uncertainty, variability, and reliability. Reliab. Eng. Syst. Saf. 54, 165-181.

McLachlan, M.S., 1999. Framework for the interpretation of measurements of SOCs in plants. Environ. Sci. Technol. 33, 1799-1804.

Moeckel, C., Nizzetto, L., Strandberg, B., Lindroth, A., Jones, K.C., 2001. Air-boreal forest transfer and processing of polychlorinated biphenyls. Environ. Sci. Technol. 35, 4066-4073.

Moldrup, P., Olesen, T., Gamst, J., Schjønning, P., Yamaguchi, T., Rolston, D.E., 2000. Predicting the gas diffusion coefficient in repacked soil water-induced linear reduction model. Soil Sci. Soc. Am. J. 64, 1588-1594.

Moldrup, P., Olesen, T., Komatsu, T., Schjønning, P., Rolston, D.E., 2001. Division S-1 ─ Soil physics: Tortuosity, diffusivity, and permeability in the soil liquid and gaseous phase. Soil Sci. Soc. Am. J. 65, 613-623.

Morselli, M., Ghirardello, D., Semplice, M., Di Guardo, A., 2011. Modeling short-term variability of semivolatile organic chemicals in air at a local scale: An integrated modeling approach. Environ. Pollut. 159, 1406-1412.

Prevedouros, K., Palm-Cousins, A., Gustafsson, Ö., Cousins, I.T., 2000. Development of a black carbon-inclusive multi-media model: Application for PAHs in Stockholm. Chemosphere 44, 643-654.

Razzaque, M.M., Grathwohl, P., 2008. Predicting organic carbon-water partitioning of hydrophobic organic chemicals in soils and sediments based on water solubility. Water Res. 42, 3775-3780.

Scholtz, M.T., Voldner, E., McMillan, A.C., Van Heyst, B.J., 2002a. A pesticide emission model (PEM) Part I: model development. Atmos. Environ. 36, 5005-5013.

Scholtz, M.T., Voldner, E., Van Heyst, B.J., McMillan, A.C.; Pattey, E., 2002b. A pesticide emission model (PEM) Part II: model evaluation. Atmos. Environ. 36, 5015-5024.

Simonich, S.L., Hites, R.A., 1994a. Vegetation-atmosphere partitioning of polycyclic aromatic hydrocarbons. Environ. Sci. Technol. 28(5), 939-943.

Simonich, S.L., Hites, R.A., 1994b. Importance of vegetation in removing polycyclic aromatic hydrocarbons from the atmosphere. Nature 370, 49-50.

Simonich, S.L., Hites, R.A., 1995. Organic pollutant accumulation in vegetation. Environ. Sci. Technol. 29(2), 2905-2914.

Sinkkonen, S., Paasivirta, J., 2000. Degradation half-life times of PCDDs, PCDFs, and PCBs for environmental fate modeling. Chemosphere 40, 943-949.

Steefel, C.I., Appelo, C.A.J., Arora, B., Jacques, D., et al., 2015. Reactive transport codes for subsurface environmental simulation. Comput. Geosci. 19, 445-478.

Stull, R.B., 2000. Meteorology for scientists and engineers: a technical companion book with Ahrens' meteorology today. Second ed. Brooks/Cole.

Tao, S., Wang, Y., Wu, S., Liu, S., Dou, H., Liu, Y., Lang, C., Hu, F., Xing, B., 2007. Vertical distribution of polycyclic aromatic hydrocarbons in atmospheric boundary layer of Beijing in winter. Atmos. Environ. 41, 9594-9602.

Terzaghi, E., Scacchi, M., Cerabolini, B., Jones, K. C., di Guardo, A., 2015. Estimation of polycyclic aromatic hydrocarbon variability in air using high volume, film, and vegetation as samplers. Environ. Sci. Technol. 49, 5520-5528.

Totten, L.A., Eisenreich, S.J., Brunciak, P.A., 2002. Evidence for destruction of PCBs by OH radical in urban atmospheres. Chemosphere 47, 735-746.

Trapp, S., 2002. Dynamic root uptake model for neutral lipophilic organics. Environ. Toxicol. Chem. 21(1), 203-206.

Trapp, S., 2007. Fruit tree model for uptake of organic compounds from soil and air. SAR/QSAR Environ. Res. 18(3-4), 367-387.

Trapp, S., 2015. Calibration of a Plant Uptake Model with Plant- and Site-Specific Data for Uptake of Chlorinated Organic Compounds into Radish. Environ. Sci. Technol. 49, 395-402.

Trapp, S., Eggen, T., 2013. Simulation of the plant uptake of organophosphates and other emerging pollutants for greenhouse experiments and field conditions. Environ. Sci. Pollut. Res. 20, 4018-4029.

Trapp, S., Matthies, M., 1995. Generic one-compartment model for uptake of organic chemicals by Foliar vegetation. Environ. Sci. Technol. 29, 2333-2338.

van den Berg, F., Leistra, M., 2004. Improvement of the model concept for volatilisation of pesticides from soils and plant surfaces in PEARL (Description and user's guide for PEARL 2.1.1-C1). Alterra, Wageningen, Netherland.

Venkatesan, M.I., 1988. Occurrence and possible sources of perylene in marine sediments – a review. Mar. Chem. 25(1), 1-27.

Wallace, J.C., Hites, R.A., 1996. Diurnal variations in atmospheric concentrations of polychlorinated biphenyls and endosulfan: Implications for sampling protocols. Environ. Sci. Technol. 30, 444-446.

Wegmann, F., Scheringer, M., Möller, M., Hungerbühler, K., 2004. Influence of vegetation on the environmental partitioning of DDT in two global multimedia models. Environ. Sci. Technol. 38, 1505-1512.

Wilcke, W., Amelung, W., Martius, C., Garcia, M.V.B., Zech, W., 1999. Biological sources of polycyclic aromatic hydrocarbons (PAHs) in the Amazonian Rain Forest. Journal of Plant Nutrition and Soil Science-Zeitschrift Fur Pflanzenernahrung Und Bodenkunde 163, 27-30.

Wilcke, W., Krauss, M., Amelung, W., 2002. Carbon isotope signature of polycyclic aromatic hydrocarbons (PAHs): evidence for different sources in tropical and temperate environments? Environ. Sci. Technol. 36, 3530-3535.

Zhang, Y., Deng, S., Liu, Y., Shen, G., Li, X., Cao, J., Wang, X., Reid, B., Tao, S., 2011. A passive air sampler for characterizing the vertical concentration profile of gaseous phase polycyclic aromatic hydrocarbons in near surface air. Environ. Pollut. 159, 694-699.

Chapter 4.

Modeling controls on the chemical weathering of marine mudrocks from the Middle Jurassic (Swabian Alb, Southern Germany)
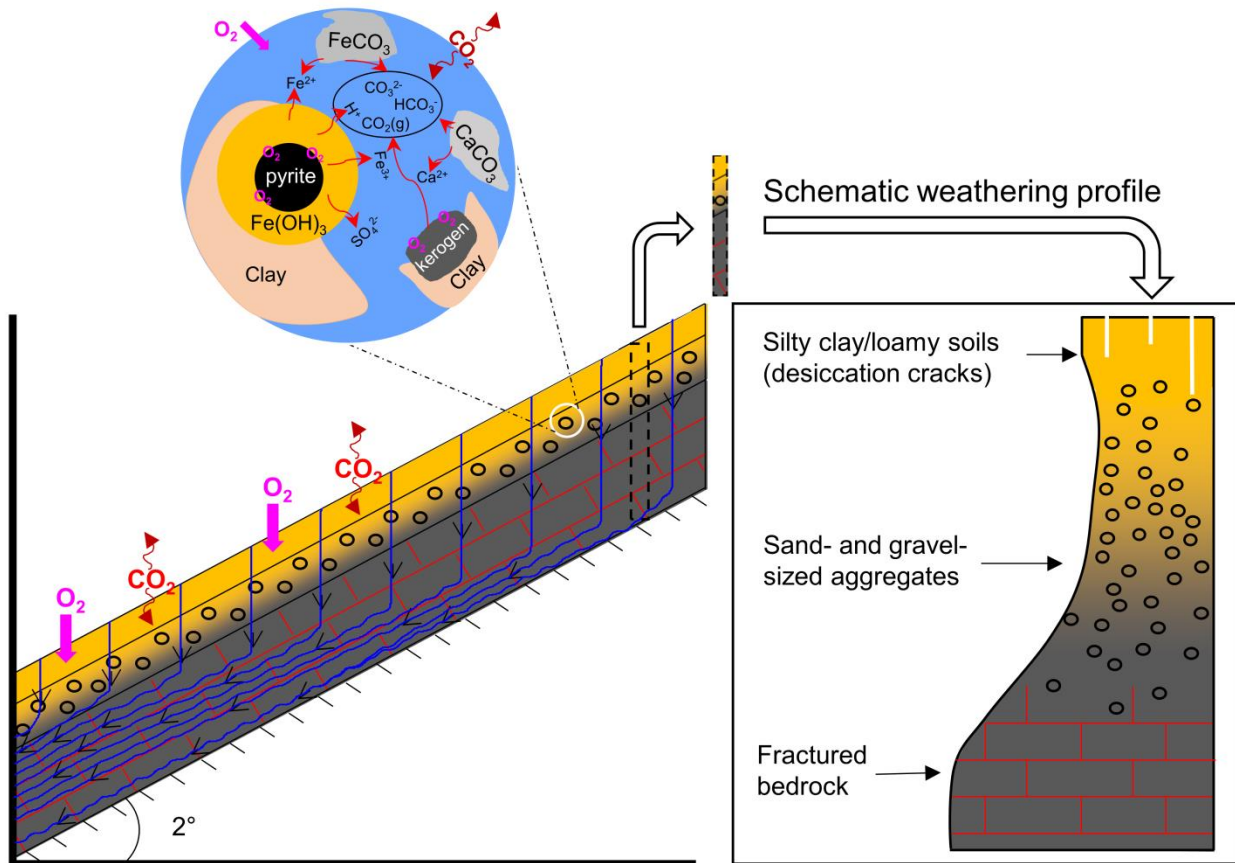
Abstract

Chemical weathering of sedimentary rocks is of great importance in determining seepage water chemistry, carbon, iron and sulfur turnover, as well as mineral transformations. In this study, we used the numerical code MIN3P to investigate controls on the chemical weathering of marine mudrocks. In particular, we focused on the pyrite- and kerogen-bearing formation, Opalinus Clay (with outcrops in the area of the Swabian and Franconian Alb in Southern Germany), a typical fine-grained sedimentary mudrock that had been deposited during the Middle Jurassic in a shallow marine environment. In the geochemical model we considered four reactive minerals, i.e., pyrite, kerogen, calcite and siderite (assuming silicate minerals to be stable), and ran model scenarios over a time period of 10 kyrs (since the last ice age). Our numerical results show that chemical weathering of Opalinus Clay is driven by oxygen ingress (which depends on effective gas diffusion, and thus on water saturation). Due to oxidation of pyrite and kerogen seepage water acidifies, which leads to dissolution of carbonate minerals, i.e. calcite and siderite. As a consequence, porosity and groundwater alkalinity increase, and CO_2 is released into the atmosphere. Following the consumption of primary reactive minerals, iron oxides precipitate in the oxic zone. We compared our model results with field data of water saturation, porosity, and water chemistry. The overall good fit between model results and field data demonstrates the applicability of the numerical code MIN3P to quantify chemical weathering of pyrite bearing sedimentary mudrocks and to predict seepage water chemistry that is impacted by the geochemical water-rock interactions.

Keywords: chemical weathering, oxygen ingress, diffusion, advection, seepage water chemistry, Opalinus Clay

4.1 Introduction

4.1.1 Weathering and models

Sedimentary rocks, i.e. sandstones, limestones and mudstones, form the main landscapes in many parts of central Europe, e.g. Southern Germany and many other continental landscapes. Chemical weathering of sedimentary rocks is of great importance with respect to mineral transformation, thus re-shaping the Earth's surface, regulating atmospheric CO_2 concentrations, and contributing weathering products to biogeochemical cycles at regional and global scales. Chemical weathering may release ions and solutes (depending on the mineral composition of parent bedrocks) into seepage water and eventually groundwater, which poses a strong environmental issue regarding the safety of groundwater as drinking water. Identification of the controls on chemical weathering provides us with a better understanding of soil and groundwater chemistry as well as of biogeochemical cycles. Typically, chemical weathering depends on climate, hydrology, and the geochemistry of rocks (Bluth and Kump, 1994; White and Blum, 1995; West et al., 2005; West, 2012; Li et al., 2014). Rates of chemical weathering (Maher, 2010), and thus the seepage water chemistry or river water chemistry (Torres et al., 2015), are commonly assumed to be controlled by interactions between hydrological processes and geochemical reactions with surrounding rock formation. Particularly, hydrological processes determine water distribution and storage (i.e. flow paths and fluid residence time); this in turn influences aqueous transport and solute concentrations resulting from geochemical water-rock interactions. Bedrock weathering may be additionally constrained by diffusion processes as shown by Lebedeva et al. (2007).

In the past, many researchers have addressed chemical weathering by linking field observations with numerical models and focusing on specific aspects of the real-world problem. For example, most geomorphological models (e.g. Dietrich et al., 1995; Heimsath et al., 2001) focus on erosion and sediment transport without considering geochemistry; and some geochemical weathering models (e.g. Lichtner 1988; White et al., 1998; White et al., 2001) neglect erosion and sediment transport when investigating complex geochemical water-rock interactions. The coupling of erosion and sediment transport with geochemical water-rock interactions to address chemical weathering is

considered in studies e.g. by Brantley et al. (2008), Dixon et al. (2009), Gabet and Mudd (2009), and Navarre-Sitchler et al. (2011). Numerical models coupling the effect of hydrological processes, physical erosion, sediment transport and complex geochemical reactions are of great value in Earth system modeling but raise challenges in numerical stability and computational costs.

In this study, we focused on chemical weathering of marine mudrocks in the Swabian Alb (Southern Germany), with weathering depths of around 1-3 m since the last ice age (around 10 kyrs) and erosion rates of 0.01 to 0.02 mm/yr (Schmidt-Witte and Einsele, 1986). Since the physical erosion rates are much lower than the chemical weathering rate (> 0.1 mm/yr) in the Swabian Alb, coupling of physical erosion and sediment transport with geochemical reactions was neglected. Instead, a hydrogeochemical model was applied to simulate chemical weathering and to investigate the evolution of water chemistry. Hydrogeochemical models that couple hydrological processes and geochemical interactions with the surrounding rock formation are widely used in the fields of natural attenuation of organic pollutants, mining and environmental remediation issues (Nordstrom, 2011; Maier et al., 2013; Nordstrom, 2015; Amos et al., 2015; Torres et al., 2015) to interpret and to predict seepage water and groundwater chemistry in sediments and rocks. Hydrogeochemical modeling can facilitate a better understanding of possible water-rock interactions. Furthermore, it allows predictions of the future evolution of water chemistry. Based on knowledge of the hydrogeological processes and of the dissolution and precipitation of minerals (e.g. calcite and siderite) or the oxidation of sulfide minerals (e.g. pyrite), several reactive transport codes, such as CrunchFlow, TOUGHREACT, and MIN3P (Steefel et al., 2015), have been developed and widely applied to quantitatively address the complex interactions between unsaturated/saturated flow and transport and biogeochemical reactions. In particular, the reactive transport code MIN3P (Mayer et al., 2002) was developed to simulate flow, reactive transport and biogeochemical reactions in the subsurface mainly with respect to seepage water geochemistry and reactive gas transport. Subsequently, the code was extended and applied to various applications (Cheng, 2006; Amos and Mayer, 2006a and 2006b; Molins and Mayer, 2007; Henderson et al., 2009; Bea et al., 2015; Bao et al., 2015; 2016). In the following, we used MIN3P to model the chemical weathering of the pyrite- and kerogen-bearing Opalinus Clay in the

Swabian Alb to elucidate the controlling factors for chemical weathering, seepage water chemistry, and dynamics of carbon, iron and sulfur turnover. Field investigations of the weathering profiles, i.e. vertical distributions of water saturation, porosity and water chemistry collected at various sites in the Swabian Alb, were utilized to parameterize the geochemical model and to validate our model results.

4.1.2 Lithology in the Swabian Alb and conceptual model

The Swabian Alb (Fig. 4.1) is a 200 km long and 40 km wide karstified secondary mountain range between Lake Constance and the Nördlinger Ries. Widely distributed sedimentary rocks in the Swabian Alb are limestones and mudstones from the Jurassic, uplifted by tectonic forces since the end of the Jurassic period. Since prehistoric times, agricultural and cultural activities, physical erosion and transport as well as hydrogeochemical processes were and are currently re-shaping the modern landscapes in the Swabian Alb.
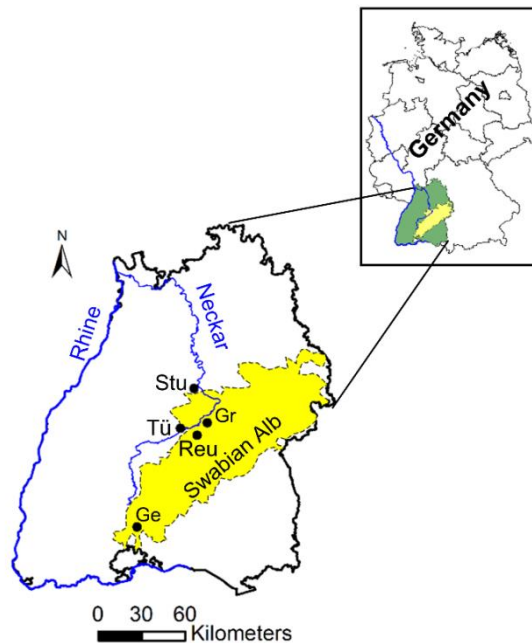
Figure 4.1. Geographic location of the Swabian Alb (yellow zone, obtained from Jurassic sediments) and sites of interest (Stu: Stuttgart, Tü: Tübingen, Reu: Reutlingen, Gr: Grafenberg, and Ge: Geisingen).

Opalinus Clay is widely distributed in the Swabian Alb, but also occurs in Switzerland. This sedimentary rock is a fine-grained pyrite- and kerogen-bearing mudrock deposited about 180 million years ago (Middle Jurassic) in a shallow marine environment. The thickness of the Opalinus Clay layer is 100 to 120 m. In Switzerland, the un-weathered Opalinus Clay formation can be found at large depths and has been considered as a potential location for a subsurface radioactive waste repository (Gautschi, 2001). In Southern Germany Opalinus Clay outcrops; exhumation resulted in expansion fractures near the surface, and thus enhanced hydraulic conductivity. Since the last ice age, i.e. after the end of permafrost, chemical weathering of Opalinus Clay has intensified due to vegetation at the ground surface. Weathering transforms the bedrock into silty clay or loamy materials (fully weathered) as well as sand and gravel sized aggregates (partially weathered) down to a depth of several meters in the subsurface. The weathering profile of Opalinus Clay in Southern Germany is easily recognized by color differences between weathered parts and the original bedrock: the fully weathered zone is yellow-brown (from iron oxides, i.e. ferrihydrite and goethite) while the un-weathered zone is black or dark gray due to high pyrite and kerogen contents.

In 2015, we performed field investigations within the framework of a tunneling project in Reutlingen (Fig. 4.1) to determine the weathering profile of Opalinus Clay in the uppermost meters below the ground surface. The objective was to identify the fully and partially weathered zones as well as the un-weathered bedrock. Moreover, the vertical distribution of water saturation (soil water content) and porosity were determined. Field observations indicated that the subsurface is fully weathered down to a depth of approximately 1 m. Table 4.1 and Fig. 4.2-B give an overview of the typical weathering profile of sedimentary mudrocks in Southern Germany, separated into four layers ranging from fully weathered to un-weathered zones.

Table 4.1. Typical weathering profile of sedimentary mudrocks in Southern Germany.

Weathering profile	Depth [m]	Color	Hydraulic conductivity [m/s]	Description
silty clay/loamy soils	~ 1 m	yellow	- [a]	fully weathered (with seasonally changing desiccation cracks)
sand and gravel sized aggregates	1 – 5 m	yellow to black	- [a]	partially weathered
fractured bedrock	5 – 30 m	black	$5 \times 10^{-8} \sim 10^{-6}$ [b]	un-weathered (fractured)
low permeability bedrock	> 30 m	black	$< 10^{-12}$ [c]	un-weathered

[a]: unsaturated, not determined
[b]: Hekel (1994)
[c]: Gautschi (2001)

Fig. 4.2-A schematically shows the 2-D flow paths of seepage water along a hillslope with three layers (neglecting the low permeability bedrock). As illustrated in Fig. 4.2-A, seepage water primarily penetrates vertically through the uppermost silty clay or loamy soils and the partially weathered layer consisting of sand and gravel sized aggregates or partially weathered rock fragments. In the fractured system a groundwater flow system characterized by lateral flow is established (with possible exfiltration, i.e. springs, at lower locations of the hillslope as frequently observed in the field).
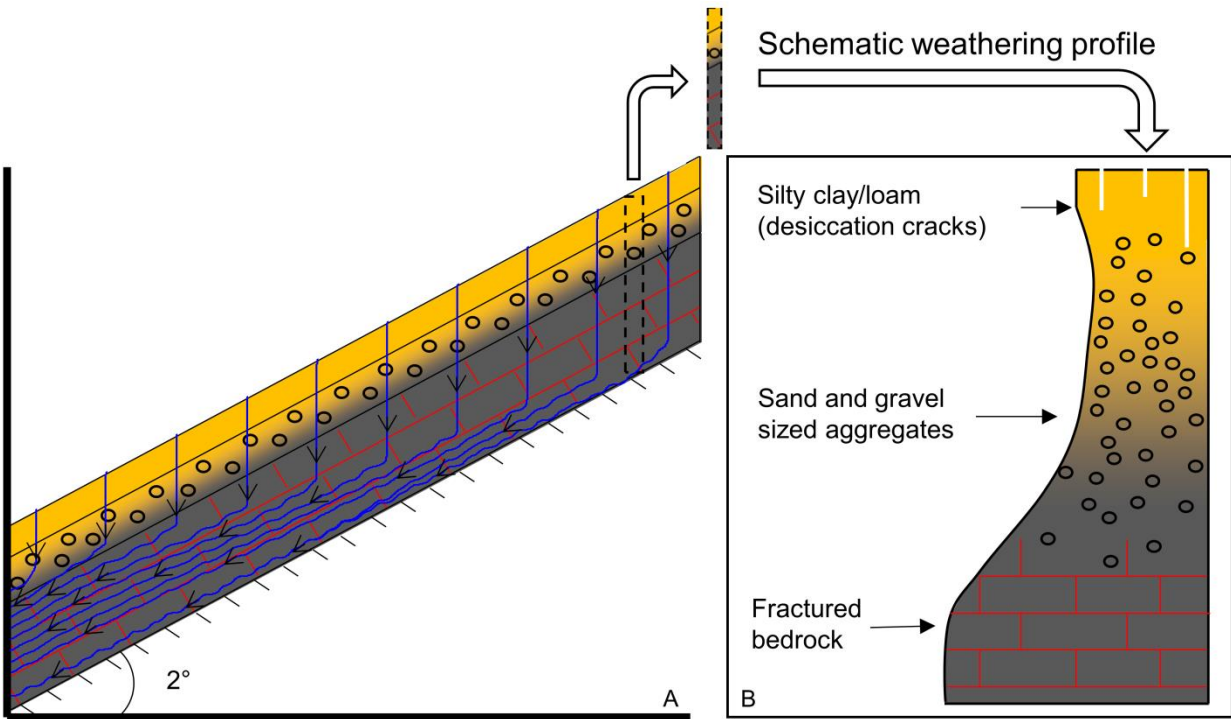
Figure 4.2. (A) 2-D flow paths of seepage water along a hillslope (slope = 2°) with three weathering layers typical for the landscape in the Swabian Alb (horizontal distance: 1,000 m, not drawn to scale); (B) vertical schematic weathering profile for Jurassic mudstones (modified from Einsele et al., 1985 and Wetzel and Einsele et al., 1991).

4.2 Geochemistry and numerical methods

4.2.1 Opalinus Clay

Opalinus Clay is mainly composed of silicate minerals (e.g. illite, quartz, kaolinite, chlorite, smectite and feldspars), reduced phases (pyrite and kerogen), and carbonates (calcite and siderite). Table 4.2 summarizes mineral compositions of Opalinus Clay from near-surface investigations that were performed in recent decades (Grathwohl, 1989; Hekel, 1994; Taubald et al., 2000) in Southern Germany and from deeply buried samples underground (mainly un-weathered bedrock) from the Mont Terri project in Switzerland (Gautschi, 2001; Nagra, 2002). Since the characteristic time in dissolution kinetics of silicate minerals such as quartz and feldspars is much longer than 10 kyrs (Lasaga, 1984; Appelo and Postma, 2005), we simplified the geochemical system focusing on water-rock

interactions of reduced phases and carbonate minerals, while silicate minerals were assumed to be stable over a timescale of 10 kyrs. Kerogen is a mixture of insoluble organic substances finely dispersed in sedimentary rocks. The elemental composition of kerogen varies depending on the origin and diagenesis of sediments. Kerogen content is usually accounted for by the total organic carbon content (TOC wt%). Since mineral composition of Opalinus Clay vary between different sites, model parameters applied in our study are chosen according to literature mean values supplemented by a few laboratory and field measurements (Grathwohl, 1989; Hekel, 1994; Gautschi, 2001; Nagra, 2002; Taubald et al., 2000).

Table 4.2. Mineral composition (wt%) of Opalinus Clay in Southern Germany and Switzerland and selected model parameters.

	Components	Southern Germany		Switzerland		Model parameters selected		Density
		Hekel (1994) wt%	Taubald (2000) wt%	Gautschi (2001) wt%	Nagra (2002) wt%	wt%	vol% $	[g/cm³]
primary minerals	total organic carbon	-	<0.4%	<1%	0.6%	1.5 %[*]	3.34%	0.8
	pyrite	0-3%	-	1-3%	1.1%	2%	0.71%	5.02
	siderite	0-7%	2%	2-3%	4%	2%	0.90%	3.96
	calcite	2-21%	10%	6-40%	16%	15%	9.86%	2.71
secondary minerals	ferrihydrite	-	-	-	-	-	-	4.37
	gypsum	-	-	-	-	-	-	2.32
Silicate minerals (un-reactive)	kaolinite	8-21%	20%	6-20%	17%	20%	13.7%	2.6
	chlorite	2-6%	5%	3-10%	5%	5%	2.97%	3.0
	quartz	21-57%	30%	15-30%	20%	20%	13.44%	2.65
	feldspars	1-10%	-	1-7%	3%	3%	2.07%	2.57
	illite	17-33%	25%	9-29%	18%	25%	16.19%	2.75
	illite/smectite	7-17%	8%	6-40%	14%	6%	-	-

- : not determined.

[*] Total organic carbon (TOC) of field samples retrieved within the framework of a tunneling project in Reutlingen (Fig. 1) and measured by elemental analysis with average values of 0.4 – 0.5 wt% in the fully weathered zone, 0.8 – 1.0 wt% in the partially weathered zone, and 1.2 – 1.5 wt% in the un-weathered zone. Grathwohl (1989) measured 1.5 wt% TOC in the un-weathered mudstone and 0.8 wt% TOC in the fully weathered zone of samples from Southern Germany.

Note: Average grain density of Opalinus Clay, ρ_{OPC} [g/cm³], is 2.74 g/cm³ (Bossart, 2012), density of kerogen is assumed to be 0.8 g/cm³ because only TOC is considered, and densities of other minerals were obtained from the Mineralogy Database (www.webmineral.com), EQ3/6 database and Klein et al. (1993). K-feldspar is chosen as a representative mineral for feldspars. All silicate minerals, i.e. kaolinite, chlorite, quartz, feldspars, illite and illite/smectite, are assumed to be stable.

$ Volume fraction of reactive mineral i, φ_i [-], in the original fractured Opalinus Clay is calculated from weight fraction of reactive mineral i, wt_i [-]:

$$\varphi_i = \frac{V_i}{V_{mudrock}} = \frac{m_i/\rho_i}{m/\rho_{mudrock}} = \frac{m \times wt_i/\rho_i}{m/\rho_{mudrock}} = wt_i \frac{\rho_{mudrock}}{\rho_i} = wt_i \frac{\rho_{OPC} \times (1-n)}{\rho_i}$$

where V_i [L] and $V_{mudrock}$ [L] refer to the volume of reactive mineral i and the mudrock of interest; m_i [kg] and m [kg] are the mass of reactive mineral i and the mudrock; and ρ_i [kg/m³] and $\rho_{mudrock}$ [kg/m³] represent the density of reactive mineral i and the bulk density of the mudrock, respectively. The latter is calculated from $\rho_{mudrock} = \rho_{OPC} \times (1 - n)$, with n [-] referring to the initial porosity with a value of 0.35.

4.2.2 Geochemical model

As shown in Fig. 4.2-A, seepage water mainly penetrates through the weathering profile in the vertical direction before a lateral groundwater flow system builds up. Therefore, chemical weathering of near-surface fractured Opalinus Clay along a 2-D hillslope can be

simplified into a 1-D model domain with seepage water infiltrating vertically at the upper boundary. Fig. 4.3 shows the set-up used to investigate controls on the chemical weathering of Opalinus Clay from the original fractured bedrock (Fig. 4.3-A) to the present weathered profile (Fig. 4.3-B). In the fully weathered zone, un-weathered particle cores of pyrite and sedimentary organic carbon co-exist with coatings of yellow iron oxides such as ferrihydrite and goethite. To simplify numerical simulations we chose ferrihydrite as a representative secondary mineral for iron oxides. Further transformation of ferrihydrite to other iron oxides, such as goethite, was not considered. Besides ferrihydrite gypsum is considered as another secondary mineral (which may precipitate). Residual TOC (the principal composition of kerogen) in the fully weathered zone accounts for around 1/3 of total TOC in the un-weathered mudstone (based on the ratio of TOC analyses from field samples that were retrieved in the fully weathered and un-weathered zones in Reutlingen as well as data from Grathwohl, 1989). Thus, 1/3 of kerogen is assumed to be not reactive in our numerical simulations. Fig. 4.3-C shows the vertical distributions of pyrite, kerogen, calcite, porosity and water-filled porosity obtained from a MIN3P simulation.
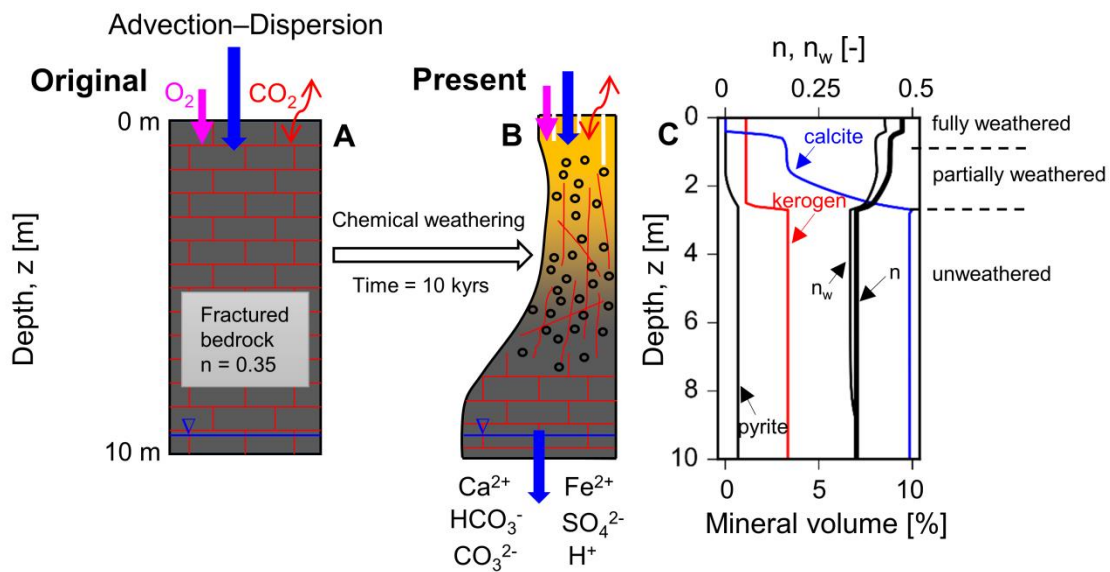
Figure 4.3. Development of a weathering profile (not drawn to scale) in a 10-m thick mudstone since the last ice age (from Plot A to Plot B) as well as vertical distributions (Plot C) of pyrite, kerogen, calcite, porosity (n) and water-filled porosity (n_w) obtained from a MIN3P simulation.

As numerical setup, we considered a 1-D model domain that has a depth of 10 m. Opalinus Clay is uniformly distributed over the whole depth and was assumed to be

fractured. It has an initial porosity of 0.35 (derived from field data in the un-weathered mudstone) as well as an initial hydraulic conductivity of 5×10^{-8} m/s (Hekel, 1994). At the upper boundary we applied fixed partial pressures of reactive gases (i.e. pO_2 = 0.21 bar, pCO_2 = 0.00039 bar), whereas at the bottom (z = 10 m) a free seepage boundary was applied. A mean annual temperature of 10 °C was assumed and the model time is 10 kyrs (since the last ice age). We mainly used a water infiltration rate of q = 100 mm/yr. Reactive mineral content was defined in weight (wt%) and volume (vol%) fractions in accordance to the values given in Table 4.2. In case the water infiltration rate, hydraulic conductivity, van Genuchten parameters or mineral compositions were varied, this is specifically mentioned in the following where applicable. A summary of the physical and hydraulic model parameters applied in this study is given in Table 4.3.

Table 4.3. Overview of physical and hydraulic model parameters for un-weathered fractured Opalinus Clay.

Parameter		Fractured bedrock
Model domain depth, z [m]		10
Initial porosity, n [-]		0.35
	S_{rw} [-]	0.1
van Genuchten	α [1/m]	0.77
parameters of un-weathered Opalinus	N [-]	1.25
Clay [a]	I [-]	0.5
Hydraulic conductivity, K [m/s]		5.0×10^{-8} [b]
Dispersivity for seepage flow, α^* [m]		0.1
Gaseous diffusion coefficient, D_g^* [m²/s]		1.0×10^{-5}
Aqueous diffusion coefficient, D_w^* [m²/s]		1.0×10^{-9}
Water infiltration rate, q [mm/yr]		q = 100 [c]

[a]: detailed investigations of van Genuchten parameters of fractured Opalinus Clay in Southern Germany are missing. Therefore, van Genuchten parameters were calibrated according to grain sizes and field investigations of vertical distributions of water saturation and porosity.
[b]: Hekel (1994).
[c]: as water infiltration rate we applied the same value as for the effective groundwater recharge rate in Southern Germany obtained from the Federal Institute for Geosciences and Natural Resources (BGR).

Model results for water saturation and porosity are compared with field data in Reutlingen; model results for water chemistry are compared with field data in Geisingen and Grafenberg (Hekel, 1994; geographic sites shown in Fig. 4.1). To cover erosion effects (0.1 to 0.2 m over 10 kyrs) and measurement errors when comparing model results with field data, an error of ±0.5 m in depth is considered for values derived from the field. In

addition, an error of ±50% in values of water chemistry and an error of ±10% in values of porosity and water saturation are applied to account for the impact of silicate minerals and measurement errors in field/lab analysis.

4.2.3 Geochemical system

Table 4.4 lists the geochemical reactions and parameters considered in this study. Gas dissolution-exsolution of $O_2(g)$/$O_2(aq)$ as well as $CO_2(g)$ and associated carbonate species follow equilibrium assumptions. For mineral dissolution-precipitation of calcite, siderite, ferrihydrite, and gypsum, surface-controlled reactions are applied. Pyrite oxidation is simulated by the shrinking core model (Wunderly et al., 1996; Mayer et al., 2002). Details on particle sizes, intra-particle diffusion and reaction rate to describe pyrite oxidation in Opalinus Clay, however, are not available in this region. Therefore, empirical parameters were used for the initial and unreacted radii of pyrite particles (Langman et al., 2014). The scaling factor, S_{py} [-], was chosen to account for the uncertainty of intra-particle diffusion coefficient and effective reaction rate of pyrite oxidation when calibrated with field data of water chemistry. Kerogen oxidation follows a Monod kinetic approach; with this respect, representative values of kerogen oxidation in Opalinus Clay, i.e. the half-saturation constant, $K_{1/2S,O_2}$ [mol/L] and the threshold term, K_{thr,O_2} [mol/L], are not known, and hence were adjusted to the values from Mayer et al. (2002). Moreover, Fe^{2+} and Fe^{3+} form a redox couple. Equilibrium constants and effective rate constants for these components are based on values recommended in the literature (Ball and Nordstrom, 1991; Mayer et al., 2002) and are also given in Table 4.4.

Table 4.4. Chemical equations to describe gas dissolution-exsolution, redox reactions with iron, oxidation of reduced phases, and mineral dissolution-precipitation for the chemical weathering of Opalinus Clay.

GAS DISSOLUTION-EXSOLUTION		$\log K_{eq}$ [a]	
O_2(g)/O_2(aq)	$O_2(g) \leftrightarrow O_2(aq)$	-2.898	quasi-equilibrium
CO_2(g)/CO_3^{2-}	$CO_2(g) + H_2O \leftrightarrow CO_3^{2-} + 2H^+$	-18.149	quasi-equilibrium
REDOX REACTION		$\log K_{eq}$ [a]	
redox couple Fe^{2+}/Fe^{3+}	$Fe^{2+} + 0.25O_2(aq) + H^+$ $\rightarrow Fe^{3+} + 0.5H_2O$	8.50	quasi-equilibrium
OXIDATION OF REDUCED PHASES			
pyrite oxidation	$FeS_2 + 3.5O_2(aq) + H_2O$ $\rightarrow Fe^{2+} + 2SO_4^{2-} + 2H^+$	S_{py} = 1×10^{-6} mol/(L • bulk • s) r_{py}^p = 50 µm, r_{py}^r = 49 µm D_{py,O_2} = 2.41×10^{-9} m²/s	
kerogen oxidation	$C + H_2O + O_2(aq) \rightarrow CO_3^{2-} + 2H^+$	k_{C-O_2} = 1×10^{-8} mol/(L • bulk • s) $K_{1/2s,O_2}$ = 3.125 µmol/L K_{thr,O_2} = 1×10^{-10} mol/L	
MINERAL DISSOLUTION-PRECIPITATION		$\log K_{eq}$ [a]	k_{eff} [mol/(L • bulk • s)]
Primary minerals			
calcite	$CaCO_3 \leftrightarrow Ca^{2+} + CO_3^{2-}$	-8.48	1×10^{-6}
siderite	$FeCO_3 \leftrightarrow Fe^{2+} + CO_3^{2-}$	-10.45	1×10^{-9}
Secondary minerals			
ferrihydrite	$Fe^{3+} + 3OH^- \leftrightarrow Fe(OH)_3$	-4.891	1×10^{-8}
gypsum	$CaSO_4 \cdot 2H_2O \leftrightarrow Ca^{2+} + SO_4^{2-} + 2H_2O$	-4.58	1×10^{-6}

[a] calculated based on Ball and Nordstrom, 1991and Mayer et al. (2002).
The symbols used for pyrite and kerogen oxidation are defined in the following.

4.2.4 Reactive transport modeling

The multicomponent reactive transport code MIN3P (Mayer et al., 2002) couples Richard's equation for variably saturated water flow with advective-dispersive transport in the aqueous phase and diffusive transport in the gas phase. Furthermore, multicomponent kinetically controlled and equilibrium biogeochemical reactions are considered.

4.2.4.1 Numerical methods

The equation for variably saturated water flow used in the model is:

$$S_w S_s \frac{\partial h_\psi}{\partial t} + n \frac{\partial S_w}{\partial t} - \frac{\partial}{\partial z}\left[k_{rw} K \frac{\partial}{\partial z} h_\psi\right] = 0 \tag{4.1}$$

in which S_w [-], S_s [1/m], k_{rw} [-], K [m/s], h_ψ [m], n [-], z [m], and t [s] respectively refer to the degree of water saturation, the specific storage coefficient, the relative permeability,

the hydraulic conductivity, the matric potential, the porosity, the vertical coordinate, and the time. Water saturation and relative permeability are parameterized by the van Genuchten model, with $α$ [1/m], N [-], and l [-], being the van Genuchten parameters (see Table 4.3).

The governing equation for advective-dispersive transport in the water phase and diffusive transport in the vapor phase in a variably saturated porous medium is described by a formulation considering the bulk phase:

$$\frac{\partial}{\partial t}[n_w C_w] + \frac{\partial}{\partial t}[n_g C_g] + \frac{\partial}{\partial z}[q C_w] - \frac{\partial}{\partial z}\left[D_{ew}\frac{\partial}{\partial z}C_w\right] - \frac{\partial}{\partial z}\left[D_{eg}\frac{\partial}{\partial z}C_g\right] - Q = 0 \quad (4.2)$$

where n_w [-], and n_g [-] denote the water-filled and the gas-filled porosity, q [m/s] is the infiltration rate of seepage water, and C_g [mol/L] and C_w [mol/L] are the concentrations of the component of interest in the gaseous and aqueous phase. In Eqn. 4.2, D_{eg} [m^2/s] and D_{ew} [m^2/s] denote the effective diffusion coefficients in the gaseous and aqueous phases. The effective diffusion coefficients are corrected following the tortuosity correction method in the subsurface (Moldrup et al., 2000, 2001):

$$D_{eg} = D_g^* \frac{n_g^{2.5}}{n} \quad (4.3)$$

$$D_{ew} = α^* q + D_w^* \frac{n_w^{2.5}}{n} \quad (4.4)$$

where $α^*$ [0.1 m] is the dispersivity for seepage flow, and D_g^* [m^2/s] and D_w^* [m^2/s] are the molecular diffusion coefficients in the free gaseous and aqueous phases.

In Eqn. 4.2 equilibrium gas dissolution-exsolution reactions are integrated in the model by introducing the Henry's law coefficient, H [-]:

$$H = \frac{C_g}{C_w} \quad (4.5)$$

And Q [mol/(L bulk • s)] refers to the source-sink terms from geochemical reactions in the aqueous solution that are computed as the sum of various reactions j:

$$Q = θ \sum R_j v_{i,j} \quad (4.6)$$

where R_j [mol/(L bulk • s)] is the reaction rate, $θ$ [-] refers to the volumetric water content, and $v_{i,j}$ [-] is the stoichiometric coefficient of component i in reaction j.

The overall reaction rate, R_j of surface-controlled mineral dissolution-precipitation (see Table 4.4) follows

$$R_j = -k_{eff,j}\left(1 - \frac{IAP}{K_{eq,j}}\right) \tag{4.7}$$

where $k_{eff,j}$ [mol/(L bulk • s)] and $K_{eq,j}$ refer to the effective rate constant and the equilibrium constant of reaction j, and IAP is the ion activity product.

Based on the shrinking core method, the reaction rate of pyrite oxidation, $R_{py-O_2(aq)}$ [mol/(L bulk • s)] is computed by:

$$R_{py-O_2(aq)} = -10^3 S_{py} D_{py,O_2(aq)} \left[\frac{r_{py}^p}{(r_{py}^p - r_{py}^r)r_{py}^r}\right]\left[\frac{[O_2(aq)]}{v_{py-O_2(aq),O_2(aq)}}\right] \tag{4.8}$$

where r_{py}^p [m] and r_{py}^r [m] are the initial and unreacted particle radii. S_{py} [-] refers to the scaling factor. $D_{py,O_2(aq)}$ [m²/s] denotes the intra-particle diffusion coefficient of oxygen in water, [O₂(aq)] [mol/L] is the total concentration of dissolved oxygen, and $v_{py-O_2(aq),O_2(aq)}$ denotes the stoichiometric coefficient of oxygen in pyrite oxidation.

Oxidation of kerogen follows a Monod kinetic approach:

$$R_{C-O_2(aq)} = -k_{C-O_2} \left[\frac{[O_2(aq)]}{K_{1/2S,O_2} + [O_2(aq)]}\right]\left[\frac{[O_2(aq)]}{K_{thr,O_2} + [O_2(aq)]}\right]^2 \tag{4.9}$$

where k_{C-O_2} [mol/(L bulk • s)] is the effective rate constant, $K_{1/2S,O_2}$ [mol/L] is the Monod term of the half-saturation constant, and K_{thr,O_2} [mol/L] is the threshold term that was applied due to numerical reasons.

Mineral transformations as a result of geochemical water-rock interactions may change the porosity of the porous medium. For numerical simulations, the porosity is updated at each time step based on consumption and accumulation of reactive minerals in the porous medium:

$$n^{t+\Delta t} = n^t + \sum_{i=1}^{N_m} (\varphi_i^{t+\Delta t} - \varphi_i^t) \tag{4.10}$$

where $n^{t+\Delta t}$ [-] and n^t [-] are the porosities at times $t+\Delta t$ and t. In accordance, $\varphi_i^{t+\Delta t}$ [-] and φ_i^t [v-] refer to the volume fractions of reactive mineral i at times $t+\Delta t$ and t. N_m [-] denotes the total number of reactive minerals.

4.3 Results and discussion

4.3.1 Reactive transport modeling of chemical weathering and sensitivity analysis

Oxygen ingress from the atmosphere since the last ice age has resulted in chemical weathering of Opalinus Clay. Reduced phases, such as pyrite and kerogen, have been oxidized. These reactions have resulted in acidification of seepage water, which led to dissolution of siderite and calcite. Fe^{2+} released from pyrite oxidation and siderite dissolution is transformed into Fe^{3+} once exposed to oxygen in the oxic zone. Fe^{3+} then precipitates as yellow-brown colored ferrihydrite. Fig. 4.4 shows the vertical distributions of oxygen concentration and water saturation (S_w) as well as four primary minerals (i.e. pyrite, kerogen, siderite, and calcite) and one secondary mineral (i.e. ferrihydrite) after 10 kyrs of chemical weathering with a water infiltration rate of $q = 100$ mm/yr. In the fully and partially weathered zones where oxygen occurs, siderite, pyrite and reactive kerogen are fully transformed in accordance to the chemical reactions given in Table 4.4. Also ferrihydrite precipitates (gypsum precipitation does not occur because infiltrating water flushes through the weathering profile and dilutes concentrations of Ca^{2+} and SO_4^{2-}). The oxidation front of the reduced phases (pyrite and kerogen) coincides with the dissolution and precipitation fronts of calcite, siderite and ferrihydrite. The location of the oxidation front (as shown by the horizontal dashed line in Fig. 4.4), therefore, can be taken as a quantitative indicator of the weathering depth in field investigations. In summary, pyrite and kerogen oxidation, calcite and siderite dissolution, as well as ferrihydrite precipitation change the original composition of Opalinus Clay, its structure and the volume fractions of reactive minerals and eventually cause an increase of porosity in the fully and partially weathered zones.
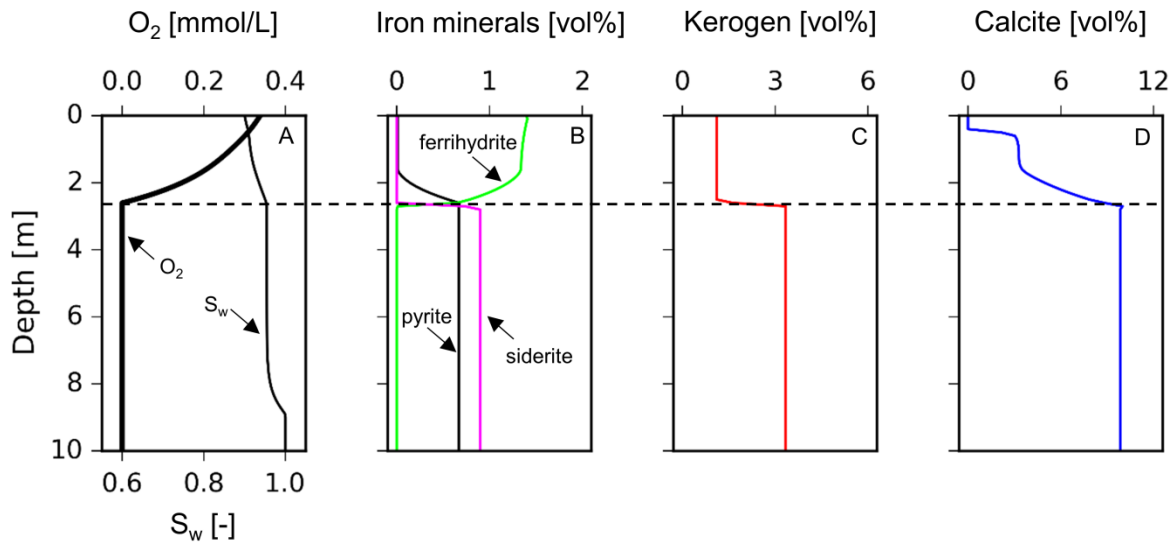
Figure 4.4. Model results of vertical distributions of oxygen ingress and water saturation (S_w) as well as four reactive minerals (i.e. pyrite, kerogen, siderite, and calcite) and one secondary mineral (i.e. ferrihydrite) at Time = 10 kyrs. The horizontal dashed line refers to the oxidation front of pyrite and kerogen, which is in coincidence with the dissolution and precipitation front of carbonates and ferrihydrite.

Field investigations of water saturation and porosity in Reutlingen (Figs. 4.5-A and 4.5-D) indicate that topsoils (i.e. fully weathered residues) are highly water saturated (with water saturation over 90%) and porosity amounts to 0.45 to 0.5. Because water saturations are at a high degree, this restrains effective gas diffusion of oxygen (e.g. Haberer et al., 2011). The effect of the water saturation profile, altered by applying two different values for the van Genuchten parameter N (a measure of the pore size distribution), on oxygen ingress and the vertical distribution of porosity after 10-kyrs weathering is shown in Fig. 4.5. In accordance to Eqn. 4.3, an increase in water saturation (Fig. 4.5-A) reduces the effective gas diffusion of oxygen (Fig. 4.5-B), slows down oxygen transport within the porous medium (Fig. 4.5-C), and thus results in less weathering as indicated by porosity (Fig. 4.5-D). Fig. 4.5 additionally compares model results of water saturation and porosity with field data from Reutlingen. The overall good fit between model results and field data of water saturation and porosity (square symbols) is consistent with our findings and indicates slow chemical weathering of marine mudrocks occurring in Southern Germany

when compared with the equivalent flow depth ($\approx$ 2,000 m, when q = 100 mm/yr and $n \approx$ 0.5) over 10 kyrs.
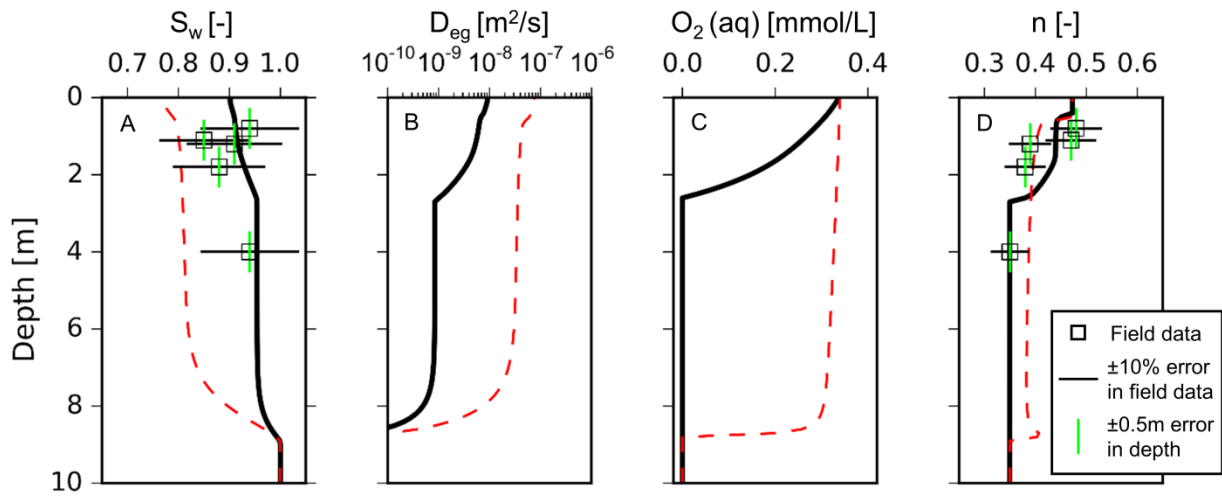
Figure 4.5. Effect of water saturation (S_w) on D_{eg}, oxygen ingress and porosity at Time = 10 kyrs by altering van Genuchten parameter N (N = 1.25: black solid line, N = 1.53: red dashed line). Model results of water saturation and porosity are compared to field data (square symbols) from Reutlingen. Increasing water saturation slows down oxygen transport within the porous medium, and thus results in less weathering.

In Table 4.5 the total amount of oxygen needed to oxidize the reduced phases present in a 1-L representative elementary volume (REV) of fractured un-weathered Opalinus Clay is given and compared with the maximum available amount of dissolved oxygen in the porous medium. Oxidation of reduced phases (neglecting kinetics) strongly retards the propagation of the weathering front. In addition, the limited oxygen supply by gas diffusion results in even slower weathering of the mudrock. Oxygen diffusion, therefore, is the main physical control in the chemical weathering of pyrite- and kerogen-bearing Opalinus Clay. Fig. 4.6 shows the effect of pyrite and kerogen content as well as water saturation on the location of the weathering front after 10 kyrs of chemical weathering. As shown in the first two rows of Fig. 4.6, contents of reduced phases influence oxygen transport in the subsurface slightly, but may impact pH-dependent dissolution of carbonates, and thus porosity in the fully and partially weathered zones. In contrast, weathering front

propagation is clearly determined by gas diffusion, which mainly depends on water saturation (the last row of Fig. 4.6).

Table 4.5. Chemical reactions and amount of oxygen needed to oxidize the reduced phases present in a 1-L representative elementary volume (REV) of un-weathered Opalinus Clay.

Mineral	Mass fraction [wt%]	Mass [mol]	Overall chemical reactions	Total O_2 needed [mol]
pyrite	2%	0.30	$FeS_2 + 3.75O_2(aq) + 3.5H_2O \rightarrow Fe(OH)_3 + 4H^+ + 2SO_4^{2-}$	1.11
kerogen	1.5%	1.48 [*]	$C + H_2O + O_2(aq) \rightarrow CO_3^{2-} + 2H^+ \rightarrow HCO_3^- + H^+$	0.99
siderite	2%	0.31	$FeCO_3 + 0.25O_2(aq) + 2.5H_2O \rightarrow Fe(OH)_3 + H^+ + HCO_3^-$	0.08
Total O_2 needed for oxidation of reduced phases				**2.18** [§]

Average grain density of Opalinus Clay is 2.74 g/cm^3 (Bossart, 2012), densities of pyrite, kerogen and siderite are shown in Table 2.

[*] Only 2/3 of kerogen is reactive.

Note: solubility of dissolved oxygen at 10 °C is 0.339 mmol/L. For the initial porosity $n = 0.35$ and water saturation $S_w = 0.9$ (both are relatively constant during the weathering process), the maximum amount of dissolved oxygen in the 1-L representative elementary volume is 0.107 mmol.

[§] "retardation factor", $R_d = 20,374$, which is the ratio between total oxygen needed for oxidation of reduced phases and available dissolved oxygen in the porous medium.
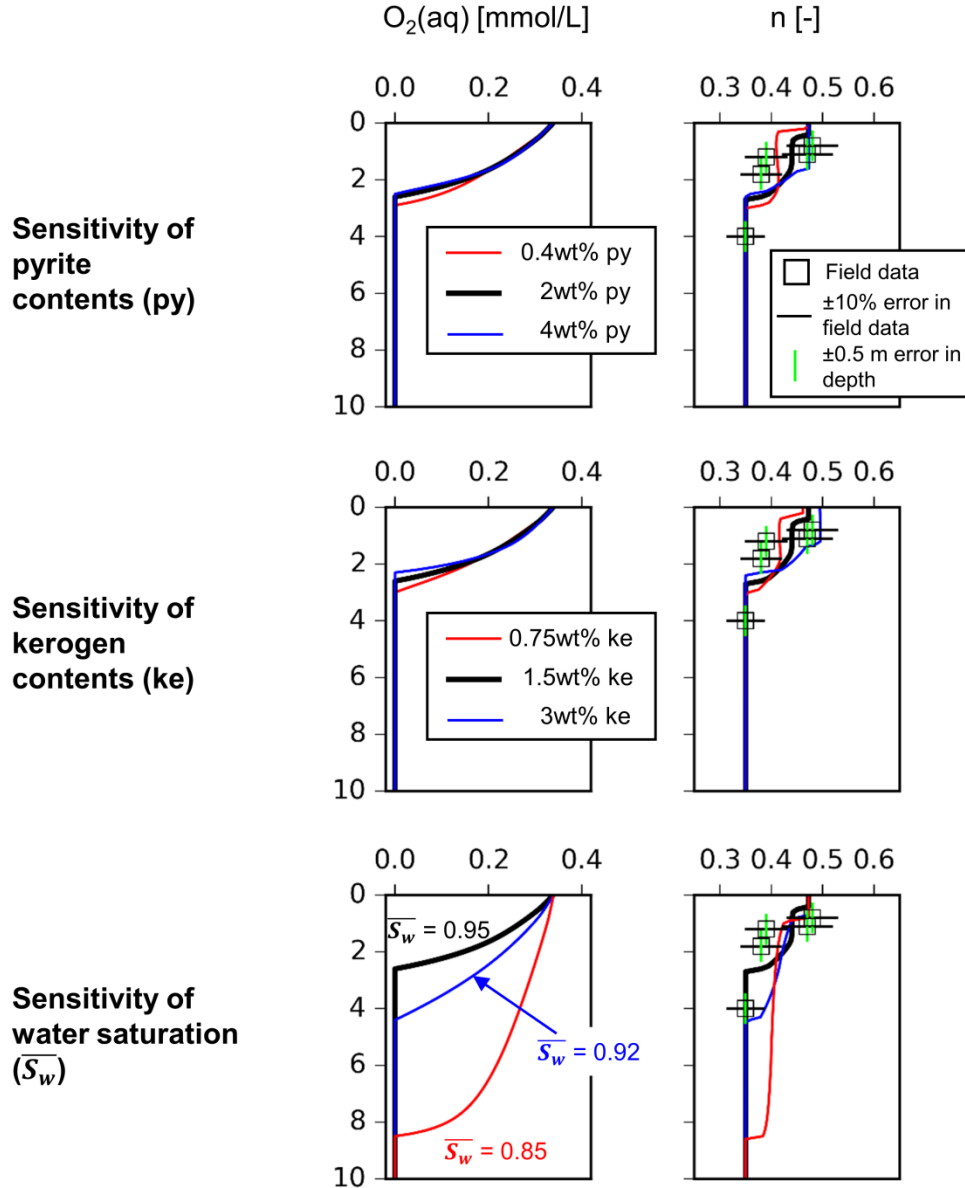
Figure 4.6. Sensitivity of pyrite content (**py**), kerogen content (**ke**) and water saturation ($\overline{S_w}$: average water saturation of the whole model domain) on oxygen ingress in the subsurface and vertical distribution of porosity. Model results for porosity at Time = 10 kyrs are compared with field data from Reutlingen. Water saturation (rather than the content of reduced phases) most significantly impacts effective gas diffusion, and hence determines propagation of the weathering front.

Our previous findings show that the observed weathering processes strongly depend on oxygen ingress into the fresh mudrock by gas diffusion. Solute transport with seepage water of both oxygen and ions released by chemical weathering only plays a minor role. We introduce the Péclet number, Pe [-], to quantify the correlation of diffusive versus advective transport:

$$Pe = \frac{Lv}{D_{eg}} = \frac{L\,q/\theta}{D_g^* n_g^{2.5}/n} = \frac{L\,q/(nS_w)}{D_g^* n_g^{2.5}/n} = \frac{L\,q/S_w}{D_g^* n^{2.5}(1 - S_w)^{1.5}} \tag{4.11}$$

where L [m] is the characteristic length of mass transport (here depth) and v [m/s] refers to the flow velocity. θ [-] and S_w [-] denote volumetric water content and water saturation with $\theta + n_g = n$. In practice, $Pe < 0.1$ indicates a diffusion-limited transport, $Pe > 10$ suggests an advection-dominated regime, while $0.1 < Pe < 10$ indicates coupled effect of advection and diffusion. Since S_w and n are relatively constant in the weathered zone, Fig. 4.7 shows the evolution of Pe as a function of the transport distance for values of S_w and n of 0.9 and 0.45 at three water infiltration rates, i.e. at $0.5q = 50$ mm/yr, $q = 100$ mm/yr, and $1.5q = 150$ mm/yr.
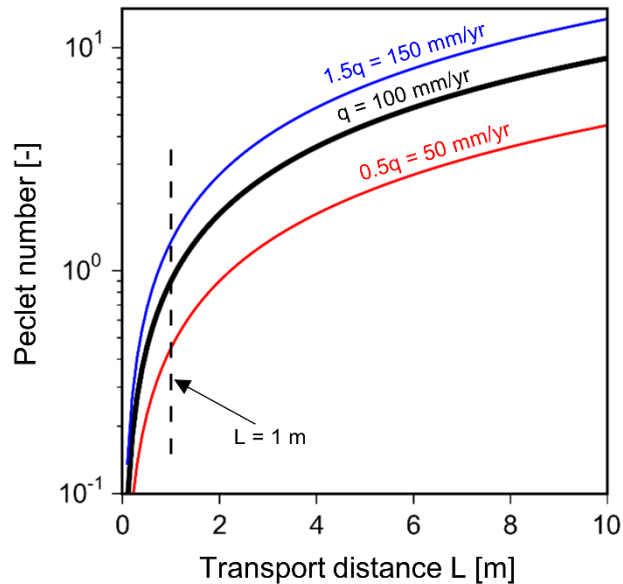
Figure 4.7. Correlation of Péclet number with characteristic length of transport at three water infiltration rates (computed by applying Eqn. 4.11 with $n = 0.45$, $S_w = 90\%$ and $D_g^* = 1\times10^{-5}$ m^2/s at 25 °C but corrected to 10 °C).

For a given water infiltration rate of $q = 100$ mm/yr, $Pe = 0.80$ (when $L = 1$ m). Hence, chemical weathering is influenced by both diffusion-limited transport and advection.

4.3.2 Chemical weathering releasing CO_2 into the atmosphere

Fig. 4.8 shows model results for the evolution of CO_2 outflux from the weathering mudrock into the atmosphere over a time period of 10 kyrs after the start of chemical weathering (the model time was extended accordingly). Pyrite oxidation releases a significant amount of hydrogen ions and strongly acidifies seepage water. Kerogen oxidation and early carbonate dissolution increase the partial pressure of CO_2 (pCO_2) in the subsurface. CO_2 partially outgasses into the atmosphere, while the rest dissolves in seepage water resulting in an increase in groundwater alkalinity:

$$CaCO_3(s) + CO_2(aq) + H_2O \rightarrow Ca^{2+} + 2HCO_3^- \qquad (4.12)$$
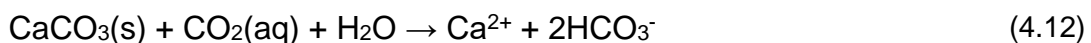
In our model simulations original fresh bedrock is assumed as the initial condition (Fig. 4.3-A). Therefore, CO_2 outflux rates are high at early times (because of short diffusion

distances to the atmosphere) and decrease over time. Since diffusion is one of the main physical controls of chemical weathering, also CO_2 outflux is strongly affected by water saturation and thus water infiltration rates (results not shown). In fact, a high degree of water saturation (wet environment) results in slow oxygen supply, and thus in slow weathering and low CO_2 production (slow calcite dissolution because of low pyrite and kerogen oxidation rates). Fig. 4.8 shows the evolution of CO_2 outflux (F_{CO_2}) over time. Over the first 2 kyrs, $\Delta \log F_{CO_2} / \Delta \log Time \approx$ ½ (red line) indicates that mass transport is diffusion-limited. Subsequently (i.e., after Time ≈ 2 kyrs), CO_2 outflux disproportionally decreases as the diffusion distance increases (Fig. 4.8 and also predicted from Eqn. 4.11). This results from downward spreading of associated carbonate species, which thus reduces the upward outgassing flux of CO_2.
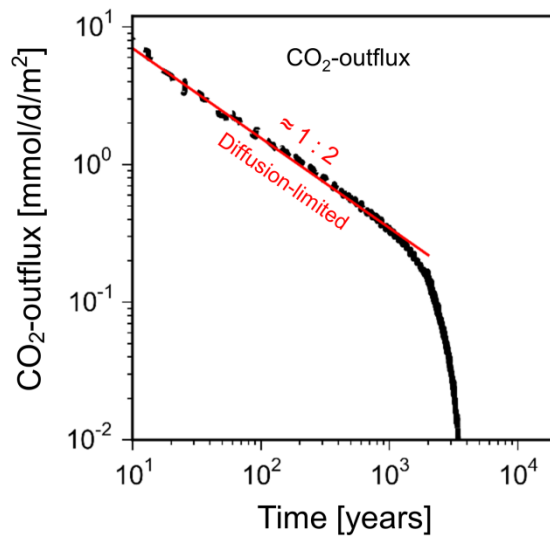
Figure 4.8. Evolution of CO_2–outflux from the weathering mudrock into the atmosphere over a time period of 10 kyrs after the start of chemical weathering; during the first 2 kyrs a CO_2 release into the atmosphere is dominated by diffusion whereas later advection (seepage water) takes over.

4.3.3 Geochemistry of weathering

Chemical weathering not only causes changes in original mineral composition, porosity and water contents, but also affects dynamics of carbon, iron, and sulfur turnover. As a

consequence, also seepage water chemistry, i.e. pH and concentrations of iron species (Fe^{2+} and Fe^{3+}), Ca^{2+}, SO_4^{2-} and HCO_3^-, is affected. Fig. 4.9 shows vertical concentration profiles of the four components $O_2(g)$, $CO_2(g)$, Fe^{2+} and SO_4^{2-} at four time instants, i.e., at 300 yrs, 1 kyr, 3 kyrs, and 10 kyrs, during the chemical weathering of original fresh Opalinus Clay. At Time = 300 yrs (Fig. 4.9-A), O_2 diffuses from the atmosphere into the system and causes pyrite and kerogen to oxidize in the uppermost soil region close to the ground surface. Due to pyrite oxidation, SO_4^{2-} is released to seepage water. The concentration of SO_4^{2-} thereby depends on reaction kinetics and water infiltration rates (results not shown). The oxidation of pyrite and kerogen leads to acidification of seepage water, and thus to the dissolution of siderite and calcite. The concentration of dissolved CO_2 significantly increases and part of the CO_2 outgasses into the atmosphere. Fe^{2+} is released from pyrite oxidation and siderite dissolution. In the oxic zone, Fe^{2+} is oxidized and precipitates as ferrihydrite. When compared with SO_4^{2-} (mmol/L range), Fe^{2+} is only detected in the anaerobic environment in low concentrations (µmol/L range).

Over time (Fig. 4.9-A to Fig. 4.9-D) advection becomes more and more dominant and starts to influence mass transport of solutes and ions. As a consequence, oxygen propagates downward more rapidly than by diffusion alone, CO_2 outgassing decreases, and concentrations of SO_4^{2-} and Fe^{2+} are influenced by the complex interaction between hydrological processes and the geochemical reactions considered (pyrite oxidation, ferrihydrite precipitation, and dissolution of siderite). In the following, we analyzed the influence of water infiltration rates on the propagation of the weathering front and seepage water chemistry and compared the model results with field data (Fig. 4-10).
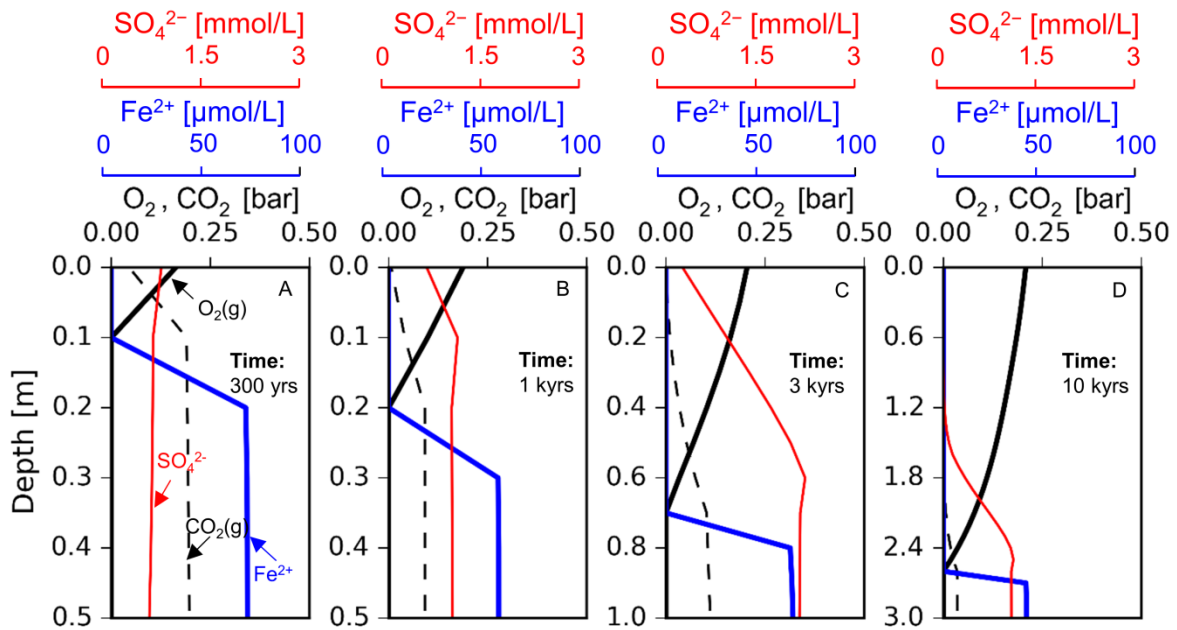
Figure 4.9. Evolution of vertical distributions of $O_2(g)$, $CO_2(g)$ (dashed line), Fe^{2+} and SO_4^{2-} after 300 yrs, 1 kyr, 3 kyrs and 10 kyrs. Note the different vertical scales in the subplots.

4.3.3.1 Comparison with field data

Hekel (1994) carried out comprehensive near-surface investigations of water chemistry from boreholes at various sites in the Swabian Alb. Two boreholes in Geisingen and Grafenberg (Fig. 4.1) were sampled at different depths for pH and concentrations of five ions, i.e. Ca^{2+}, Fe^{2+}, SO_4^{2-}, and HCO_3^-. In Fig. 4.10, these field data are compared with model results at Time = 10 kyrs, considering three water infiltration rates (q = 100 mm/yr, $0.5q$ and $1.5q$), two pyrite contents (Geisingen: 2 wt%; Grafenberg: 0.4 wt%) and two water saturations. Lower water saturation results from 5 times higher values for hydraulic conductivity in Grafenberg than for Geisingen (K = 5×10^{-8} m/s).
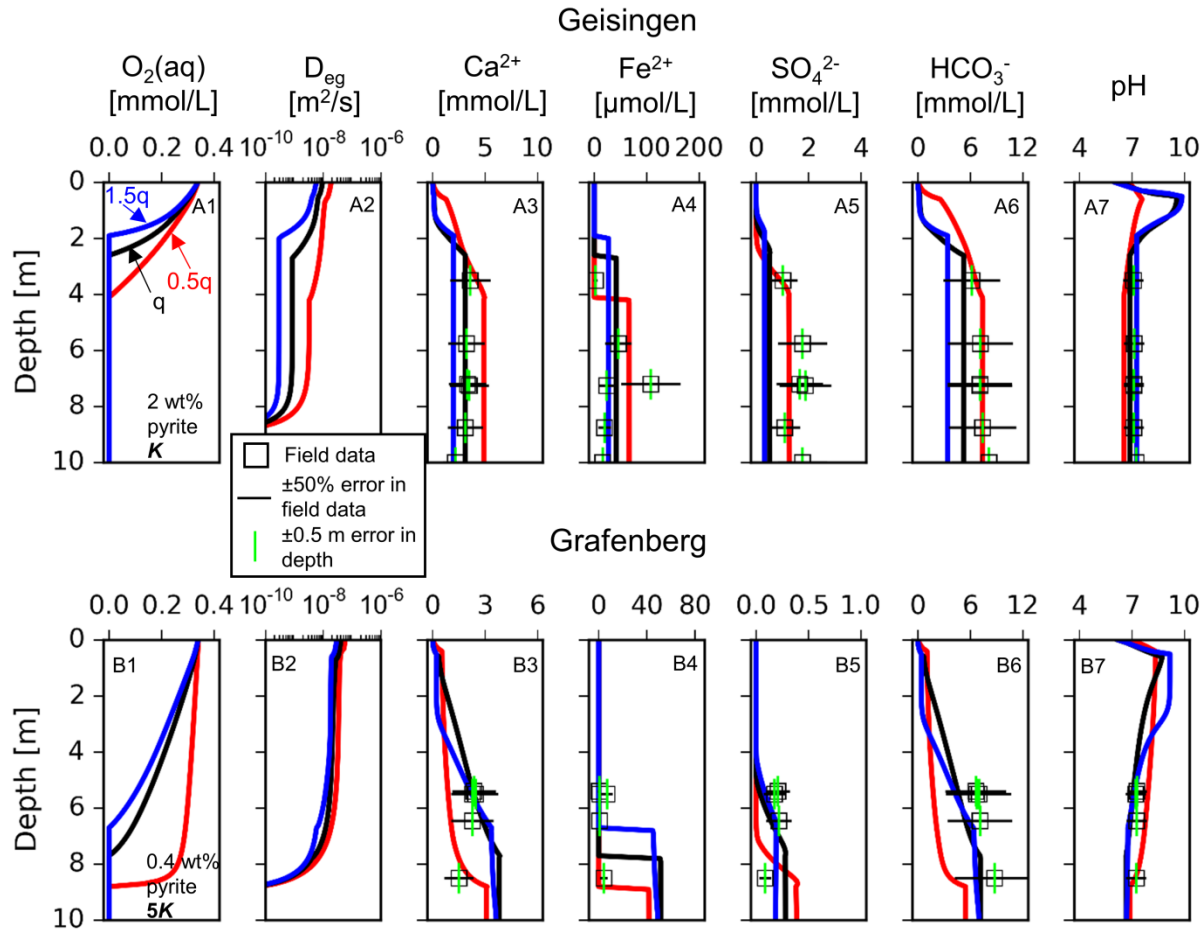
Figure 4.10. Comparison of vertical distributions of water chemistry from two field sites (Hekel, 1994) with model results (at Time = 10 kyrs) considering three water infiltration rates of q = 100 mm/yr, $0.5q$ and $1.5q$, different pyrite contents: 2 wt% (top) and 0.4 wt% (bottom), and hydraulic conductivities: K = 5×10^{-8} m/s (top) and $5K$ (bottom). The measurement error in pH of field data is ±0.5 log units, (hydrolysis of silicate minerals may also buffer pH values). Note: in the subplots different x-axis were applied for Ca^{2+}, Fe^{2+}, and SO_4^{2-}.

In general, oxygen ingress is inversely correlated with water saturation and thus infiltration rates. An increase in water infiltration rate results in an increase in water saturation, and thus in a decrease in effective gas diffusion (Figs. 4.10-A2 and 4.10-B2). Accordingly, the oxygen front propagates into the system more slowly (Figs. 4.10-A1 and 4.10-B1). Since water infiltration rates determine fluid residence time and water contents, it influences concentrations of dissolved species in seepage water. As shown in Fig. 4.10, increasing water infiltration rate from 50 mm/yr (red lines) to 100 mm/yr (black lines), or to 150 mm/yr

(blue lines), results in decreasing concentrations of Ca^{2+}, Fe^{2+}, SO_4^{2-} and alkalinity (HCO_3^-). At the same time pH values increase (more H^+ is exported out of the model domain). At the Grafenberg field site pyrite content is lower than at the Geisingen field site. The lower pyrite content results in less production of H^+, and thus causes less siderite and calcite dissolution. Consequently, less Fe^{2+}, SO_4^{2-} and Ca^{2+} are released into seepage water. High HCO_3^- values (7 ± 3.5 mmol/L) are present at both sites. This is mainly attributed to the production of carbonate species from carbonate dissolution and kerogen oxidation. Field data show an influence of water infiltration rate on water chemistry, especially at the Geisingen field site. Moreover, model results of water chemistry at Time = 10 kyrs generally agree with the field data from both sites Geisingen and Grafenberg when considering $\pm50\%$ measurement error in seepage water chemistry and ±0.5 m in weathering depth as well as uncertainty of water infiltration rates in the Swabian Alb over 10 kyrs.

4.4 Summary and conclusions

The fully coupled numerical model MIN3P was used to simulate water-rock interactions during the chemical weathering of marine mudrocks from the middle Jurassic. In particular, we focused on chemical weathering of fine-grained fractured Opalinus Clay in the Swabian Alb, Southern Germany. Reactive transport simulations of chemical weathering indicate that gas diffusion, coupled with geochemical interactions with Opalinus Clay, strongly influence the propagation of the weathering front, mineral transformation, seepage water chemistry, and dynamics of carbon, iron and sulfur turnover. The weathering process is driven by oxygen ingress from the atmosphere and the oxidation of reduced phases. This acidifies seepage water and changes mineralogical compositions, leading to dissolution of carbonates and precipitation of iron oxides. Field investigations show fully weathered conditions at a depth of around 1 m and high water saturation (over 90%) in weathered as well as in un-weathered bedrock. When compared with water infiltration rate and residence time of seepage water over 10 kyrs, chemical weathering rates of Opalinus Clay are controlled by effective gas diffusion, which depends on water saturation (and thus on water infiltration rates). Pyrite and kerogen oxidation coupled with carbonate dissolution causes release of CO_2 into the atmosphere. The outflux of CO_2

again is influenced by water saturation and water infiltration rates (Singurindy et al., 2012; Amos et al., 2015). Overall, chemical weathering is mainly controlled by re-supply of oxygen from the atmosphere (gas diffusion), while seepage water chemistry is strongly influenced by water infiltration rates on the long term. At strongly reduced water infiltration rates precipitation of gypsum is expected.

Acknowledgements

References

Amos, R.T., Blowes, D.W., Bailey, B.L., Sego, D.C., Smith, L., Ritchie, A.I.M., 2015. Waster-rock hydrogeology and geochemistry. Appl. Geochem. 57, 140-156.

Amos, R.T., Mayer, K.U., 2006a. Investigating the role of gas bubble formation and entrapment in contaminated aquifers: Reactive transport modeling. J. Contam. Hydrol. 87, 123-154.

Amos, R.T., Mayer, K.U., 2006b. Investigating ebullition in a sand column using dissolved gas analysis and reactive transport modeling. Environ. Sci. Technol. 40, 5361-5367.

Appelo, C.A.J., Postma, D., 2005. Geochemistry, groundwater and pollution. CRC press.

Ball, J.W., Nordstrom, D.K., 1991. User's manual for WATEQ4F, with revised thermodynamic data base and test cases for calculating speciation of major, trace, and redox elements in natural waters. U.S. Geological Survey, Open-file report 91-183.

Bain, J.G., Mayer, K.U., Blowes, D.W., Frind, E.O., Molson, J.W.H., Kahnt, R., Jenk, U., 2001. Modeling the closure-related geochemical evolution of groundwater at a former uranium mine. J. Contam. Hydrol. 52, 109-135.

Bao, Z., Haberer, C., Maier, U., Beckingham, B., Amos, R.T., Grathwohl, P., 2015. Modelling long-term uptake and re-volatilization of semi-volatile organic compounds (SVOCs) across the soil–atmosphere interface. Sci. Total Environ. 538, 789-801.

Bao, Z., Haberer, C.M., Maier, U., Beckingham, B., Amos, R.T., Grathwohl, P., 2016. Modeling short-term concentration fluctuations of semi-volatile pollutants in the soil–plant–atmosphere system. Sci. Total Environ. 569-570, 159-167.

Bea, S.A., Mayer, K.U., MacQuarrie, K.T.B., 2015. Reactive transport and thermo-hydro-mechanical coupling in deep sedimentary basins affected by glaciation cycles: model development, verification, and illustrative example. Geofluids, 1-22.

BGR. Mittlere järhliche Grundwasserneubildung (Tafel 5.5). Bundesanstalt für Geowissenschaften und Rohstoffe (BGR) in Hannover. Access time: Jan. 5, 2016. URL: www.bgr.bund.de.

Bluth, G.J.S., Kump, L.R., 1994. Lithologic and chimatologic controls of river chemistry. Geochim. Cosmochim. Ac. 58, 2341-2359.

Bossart, P., 2011. Characteristics of the Opalinus Clay at Mont Terri. Access time: Jan. 5, 2016. URL: http://www.mont-terri.ch/internet/mont-terri/de/home/geology/key_characteristics.parsys.49924.DownloadFile.tmp/characteristicsofopa.pdf

Brantley, S.L., Bandstra, J., Moore, J., White, A.F., 2008. Modelling chemical depletion profiles in regolith. Geoderma 145(3-4), 494-504.

Cheng, L., 2006. Dual porosity reactive transport modeling (PhD dissertation). University of Sheffield.

Dietrich, W.E., Reiss, R., Hsu, M.-L., Montgomery, D.R., 1995. A process-based model for colluvial soil depth and shallow landsliding using digital elevation data. Hydrol. Process. 9, 383-400.

Dixon, J.L., Heimsath, A.M., Amundson, R., 2009. The critical role of climate and saprolite weathering in landscape evolution. Earth Surf. Proc. Land. 34, 1507-1521.

Einsele, G., Heitfeld, K.-H., Lempp, C., Schetelig, K., 1985. Auflockerung und Verwitterung in der Ingenieurgeologie: Übersicht, Feldansprache, Klassifikation (Verwitterungsprofile) – Einleitender Beitrag. In Heitfeld, K.-H., 1985. Ingenieur geologische Probleme im Grenzbereich zwischen Locker und Festgesteinen. Springer-Verlag Berlin, Heidelberg.

Gabet, E.J., Mudd, S.M., 2009. A theoretical model coupling chemical weathering rates with denudation rates. Geology 37, 151-154.

Gautschi, A., 2001. Hydrogeology of a fractured shale (Opalinus Clay): Implications for deep geological disposal of radioactive wastes. Hydrogeol. J. 9, 97-107.

Grathwohl, P., 1989. Verteilung unpolarer organischer Verbindungen in der wasserungesättigten Bodenzone am Beispiel leichtflüchtiger aliphatischer Chlorkohlenwasserstoffe (Modellversuche). (PhD Dissertation) Tübinger Geowissenschaftliche Arbeiten, Reihe C, Nr. 1; 106 S.

Haberer, C.M., Rolle, M., Liu, S., Cirpka, O.A., Grathwohl, P., 2011. A high-resolution non-invasive approach to quantify oxygen transport across the capillary fringe and within the underlying groundwater. J. Contam. Hydrol. 122(1-4), 26-39.

Heimsath, A.M., Dietrich, W.E., Nishiizumi, K., Finkel, R.C., 2001. Stochastic processes of soil production and transport: erosion rates, topographic variation and cosmogenic nuclides in the Oregon Coast Range. Earth Surf. Proc. Land. 26, 531-552.

Hekel, U., 1994. Hydrogeologische Erkundung toniger Festgesteine am Beispiel des Opalinustons (Unteres Aalenium). (PhD dissertation) Institut und Museum für Geologie und Paläontologie der Universität Tübingen.

Henderson, T.H., Mayer, K.U., Parker, B.L., Al, T.A., 2009. Three-dimensional density-dependent flow and multicomponent reactive transport modeling of chlorinated solvent oxidation by potassium permanganate. J. Contam. Hydrol. 106, 195-211.

Klein, C., Hurlbut, C.S., Dana, J.D., Mineraloge, G., 1993. Manual of mineralogy. Vol. 527., Wiley, New York.

Langman, J.B., Moore, M.L., Ptacek, C.J., Smith, L., Sego, D., Blowes, D.W., 2014. Diavik waste rock project: evolution of mineral weathering, element release, and acid generation and neutralization during a five-year humidity cell experiment. Minerals 4(2), 257-278.

Lasaga, A. C., 1984. Chemical kinetics of water-rock interactions. J. Geophys. Res. – Sol. Ea. 89, 4009-4025.

Levedeva, M.I., Fletcher, R.C., Balashov, V.N., Brantley, S.L., 2007. A reactive diffusion model describing transformation of bedrock to saprolite. Chem. Geol. 244, 624-645.

Li, D.D., Jacobson, A.D., McInerney, D.J., 2014. A reactive-transport model for examining tectonic and climatic controls on chemical weathering and atmospheric CO_2 consumption in granitic regolith. Chem. Geol. 365, 30-42.

Lichtner, P.C., 1988. The quasi-stationary state approximation to coupled mass transport and fluid-rock interaction in a porous medium. Geochim. Cosmochim. Ac. 52, 143-165.

Maher, K., White, A.F., Steefel, C.I., Stonestrom, D.A., 2009. The role of secondary minerals and reaction affinity in regulating weathering rates at the Santa Cruz marine terrace chronosequence. Geochim. Cosmochim. Ac. 73, 2804-2831.

Maher, K., 2010. The dependence of chemical weathering rates on fluid residence time. Earth Planet. Sc. Lett. 294, 101-110.

Maher, K., 2011. The role of fluid residence time and topographic scales in determining chemical fluxes from landscapes. Earth Planet. Sc. Lett. 312, 48-58.

Maier, U., Flegr, M., Rügner, H., Grathwohl, P., 2013. Long-term solute transport and geochemical equilibria in seepage water and groundwater in a catchment cross section. Environ. Earth Sci. 69, 429-441.

Mayer, U.K., Frind, E.O., Blowes, D.W., 2002. Multicomponent reactive transport modeling in variably saturated porous media using a generalized formulation for kinetically controlled reactions. Water Resour. Res. 38, 1174.

Mazurek, M., Alexander, W.R., MacKenzie, A.B., 1996. Contaminant retardation in fractured shales: matrix diffusion and redox front entrapment. J Contam. Hydrol. 21, 71-84.

Moldrup, P.; Olesen, T.; Gamst, J.; Schjønning, P.; Yamaguchi, T.; Rolston, D.E., 2000. Predicting the gas diffusion coefficient in repacked soil water-induced linear reduction model. Soil Sci. Soc. Am. J. 64, 1588-1594.

Moldrup, P.; Olesen, T.; Komatsu, T.; Schjønning, P.; Rolston, D.E., 2001. Division S-1 — Soil physics: Tortuosity, diffusivity, and permeability in the soil liquid and gaseous phase. Soil Sci. Soc. Am. J. 65, 613-623.

Molins, S., Mayer, K.U, 2007. Coupling between geochemical reactions and multicomponent gas and solute transport in unsaturated media: A reactive transport modeling study. Water Resour. Res. 43, W05435.

Nagra, 2002. Projekt Opalinuston – Synthese der geowissenschaftlichen Untersuchungsergebnisse. Entsorgungsnachweis für abgebrannte Brennelemente, verglaste hochaktive sowie langlebige mittelaktive Abfälle. Nagra Technical Report NTB 02-03. Nagra, Wettingen, Switzerland.

Navarre-Sitchler, A., Steefel, C. I., Sak, P. B., Brantley, S.L., 2011. A reactive-transport model for weathering rind formation on basalt. Geochim. Cosmochim. Ac. 75(23), 7644-7667.

Nordstrom, D.K., 2011. Hydrogeochemical processes governing the origin, transport and fate of major and trace elements from mine wastes and mineralized rock to surface waters. Appl. Geochem. 26, 1777-1791.

Nordstrom, D.K., Blowes, D.W., Ptacek, C.J., 2015. Hydrogeochemistry and microbiology of mine drainage: An update. Appl. Geochem. 57, 3-16.

Schmidt-Witte, H., Einsele, G., Rezenter und holozäner Feststoffaustrag aus den Keuper-Lias-Einzugsgebieten des Naturparks Schönbuch. In Einsele, G. 1986. Das landschaftsökologische Forschungsprojekt Naturpark Schönbuch: Wasser- und Stoffhaushalt, bio-, geo- u. Forstwirtschaftl. Studien in Südwestdeutschland / DFG, Deutsche Forschungsgemeinschaft. VCH Verlagsgesellschaft mbH, Weinheim.

Singurindy, O., Lorca, M.E., Peterson, H.E., Hirsche, T., Javadi, M., Blackmore, S.R., Aranda, C., Mayer, K.U., Beckie, R.D., Smith, L., 2012. Spatial and temporal variations of O_2 and CO_2 pore gas

concentrations in an experimental waste rock pile at the Antamina mine, Peru. In: Proceedings International Conference on Acid Rock Drainage (ICARD) Ottawa, 9th, Canada, 20-24 May, 2012.

Steefel, C.I., Appelo, C.A.J., Arora, B., and et al., 2015. Reactive transport codes for subsurface environmental simulation. Computat. Geosci. 19, 445-478.

Steefel, C.I., DePaolo, D.J., Lichtner, P.C. Reactive transport modeling: An essential tool and a new research approach for the Earth Sciences. Earth Planet. Sc. Lett. 240, 539-558.

Taubald, H., Bauer, A., Schäfer, T., Geckeis, H., Satir, M., Kim, J.I., 2000. Experimental investigation of the effect of high-pH solutions on the Opalinus Shale and the Hammerschmiede Smectite. Clay Miner. 35(3), 515-524.

Torres, M.A., West, A.J., Clark, K.E., 2015. Geomorphic regime modulates hydrologic control of chemical weathering in the Andes-Amazon. Geochim. Cosmochim. Ac. 166, 105-128.

Torres, M.A., West, A.J., Li, G., 2014. Sulphide oxidation and carbonate dissolution as a source of CO_2 over geological timescales. Nature 507, 346-349.

West, A.J., Galy, A., Bickle, M., 2005. Tectonic and climatic controls on silicate weathering. Earth Planet. Sc. Lett. 235, 211-228.

West, A.J., 2012. Thickness of the chemical weathering zone and implications for erosional and climatic drivers of weathering and for carbon-cycle feedbacks. Geology 40, 811-814.

Wetzel, A., Einsele, G., 1991. On the physical weathering of various mudrocks. Bulletin of the International Association of Engineering Geology-Bulletin de l'Association Internationale de Géologie de l'Ingénieur 44(1), 89-100.

White, A.F., Blum, A.E., 1995. Effects of climate on chemical weathering in watersheds. Geochim. Cosmochim. Ac. 59, 1729-1747.

White, A.F., Blum, A.E., Schulz, M.S., Vivit, D.V., Stonestrom, D.A., Larsen, M., Murphy, S.F:, Eberl, D., 1998. Chemical weathering in a tropical watershed, Luquillo Mountains, Puerto Rico: I. Long-term versus short term weathering fluxes. Geochim. Cosmochim. Ac. 62(2), 209-226.

White. A.F., Bullen, T.D., Schulz, M.S., Blum, A.E., Huntington, T.G., Peters, N.E., 2001. Differential rates of feldspar weathering in granitic regoliths. Geochim. Cosmochim. Ac. 65(6), 847-869.

Wunderly, M.D., Blowes, D.W., Frind, E.O., Ptacek, C.J., 1996. Sulfide mineral oxidation and subsequent reactive transport of oxidation products in mine tailings impoundments: A numerical model. Water Resour. Res. 32(10), 3173-3187.

Chapter 5.

Modeling gypsum precipitation below buildings founded in pyrite bearing mudstones in Southern Germany
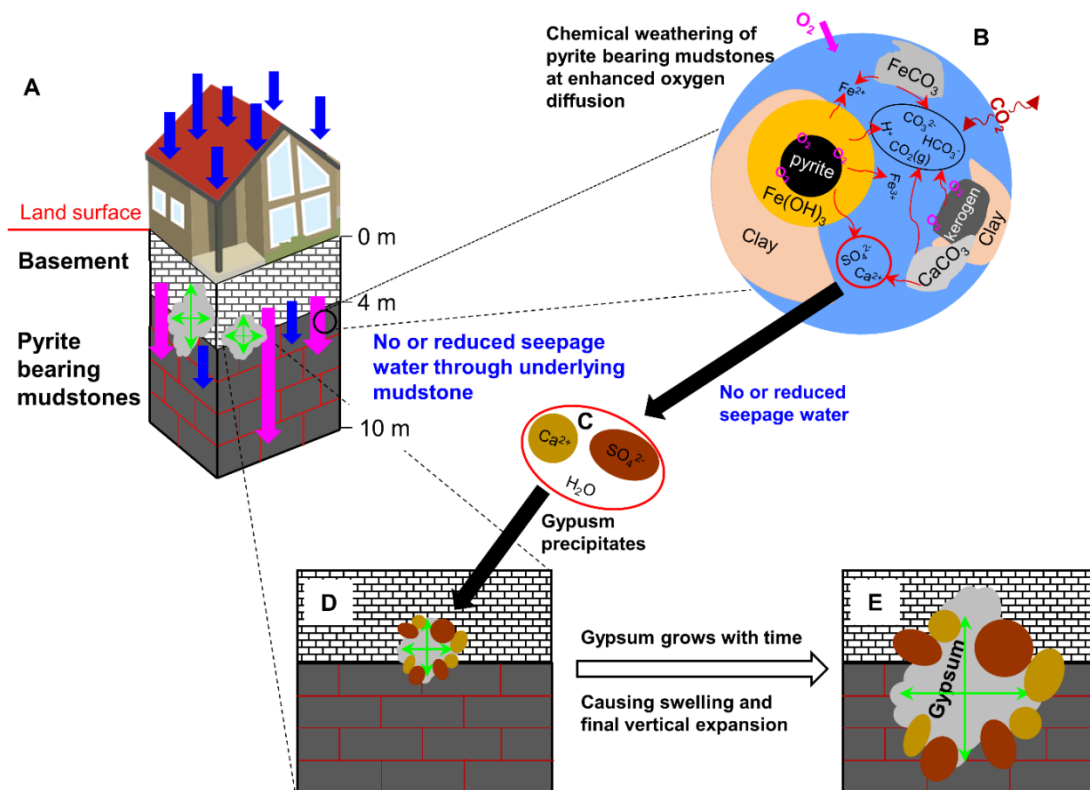
Abstract

Geotechnical consequence of gypsum precipitation below buildings founded in pyrite bearing mudstones in Southern Germany has been widely detected. Swelling of gypsum below buildings causes vertical expansion in the subsurface and eventually serious damages of buildings, e.g. irregular uplift or inclination above ground and cracks in walls. In this study, we used the reactive transport code MIN3P to investigate controls and sensitive parameters on gypsum precipitation due to weathering of pyrite containing rocks. We focused on a widely distributed marine mudrock - Opalinus Clay in Southern Germany, and considered four reactive minerals (i.e. pyrite, kerogen, calcite and siderite) and two secondary minerals - gypsum and ferrihydrite (assuming major clay minerals are stable). Model results show that, since buildings prohibit or reduce seepage water infiltrating through the pyrite bearing mudstones, concentrations of dissolved species, especially Ca^{2+} and SO_4^{2-}, released due to the weathering process (oxidation of pyrite, reduction of pH, and dissolution of calcite) continuously increase, and finally gypsum precipitates. The rate and amount of gypsum precipitation depend on water saturation (and thus effective gas diffusion) in porous media as well as pyrite oxidation rate and pyrite content. Concentrations of dissolved species are diluted by water infiltration, thus irrigation of the underlying bedrock could technically prevent gypsum precipitation.

Keywords: chemical weathering, diffusion, gypsum precipitation, Opalinus Clay

5.1 Introduction

Swelling of mudrocks have attracted a lot of attention since many serious geotechnical problems occur in tunnel engineering (e.g. Einstein, 1996; Berdugo et al., 2009a, 2009b; Anagnostou et al., 2010; Butscher et al., 2016) and geothermal applications (Goldscheider and Bechtel, 2009; Sass and Burbaum, 2010; Grimm et al., 2014) at various sites, such as in Southern Germany, Switzerland, etc.. Transformation of anhydrite to gypsum is well known and accompanied by a volume increase of 61% (the molar volumes of anhydrite and gypsum are 46 cm^3 and 74 cm^3, Sass and Burbaum, 2010; Butscher et al., 2016). In Southern Germany, damages of buildings founded above anhydritic claystones (i.e. irregular uplift or inclination of buildings above ground and some cracks in walls of buildings) are well documented (Goldscheider and Bechtel, 2009; Sass and Burbaum, 2010; Grimm et al., 2014). Other reasons for such damages e.g. oxidation of pyrite followed by gypsum precipitation are not much understood. Weathering of the mudstones typically causes pyrite oxidation and consequently high sulfate contents in seepage water. If seepage water recharge rates are low, which is typical below buildings, concentrations of ions may exceed the solubility limit of gypsum which then precipitates. Objective of this study is to quantify controls and sensitive parameters (oxygen diffusion, groundwater recharge rate and pyrite content) on gypsum precipitation below buildings founded in pyrite bearing strata using the numerical code MIN3P. As a consequence, a minimum irrigation rate is identified which would prevent gypsum precipitation.

5.2 Modeling

5.2.1 Background and conceptual model

In Southern Germany, since the last ice age (around 10 kyrs) chemical weathering of near-surface mudstones formed loamy or silty clay soils (fully weathered zone) and sand- and gravel-sized aggregates (partially weathered zone). A previous study (Bao et al., 2016) showed that chemical weathering of pyrite bearing marine mudrocks in Southern Germany is driven by oxygen ingress from the atmosphere. Mass transfer of oxygen is mainly controlled by effective gas diffusion (determined by water saturation of the soil). Model results validated with field data clearly show that fully weathered depth is around

1 m below ground while partially weathered zones may extend from 2 to 8 m below ground depending on site-specific parameters, i.e. vertical distributions of water saturation, fractures and hydraulic parameters (Hekel, 1994). Buildings typically are founded in this partially or un-weathered zone which contains significant amounts of pyrite depending on the rock formations. Fig. 5.1-A shows conceptual setup of our model for buildings founded in pyrite bearing mudstones in a depth of 4 m (fully and partially weathered zones removed). Since sealed surfaces reduce infiltration of water we account for decreasing groundwater recharge rates far less than 100 mm/yr (see Fig. 5.1-A).
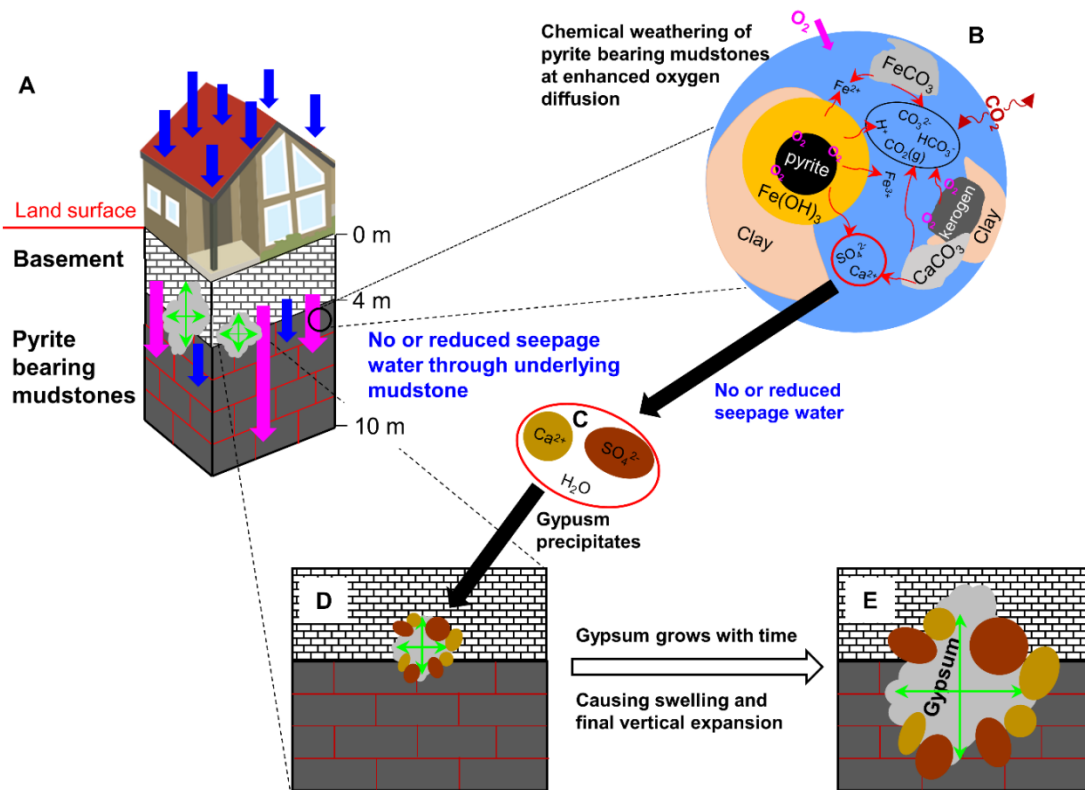
Figure 5.1. Conceptual setup of modeling gypsum precipitation below buildings founded in pyrite bearing mudstones (A, not drawn to scale). Chemical weathering (oxidation) of pyrite and (dissolution) of calcite (B) cause increasing concentrations of Ca^{2+} and SO_4^{2-} in seepage water (C), and finally gypsum precipitates (D) if water infiltration rates are too low to allow for sufficient dilution; the latter causes swelling and vertical expansion in the subsurface (E).

5.2.2 Chemical weathering and gypsum precipitation

Chemical weathering of pyrite bearing mudstones is mainly driven by oxidation. and causes changes of original mineral composition, increase of porosity, release of CO_2 into the atmosphere, and an increase of dissolved species in seepage water (Bao et al., 2016). Geochemical water-rock interactions during the weathering process are shown in Fig. 5.1-B. Pyrite oxidation causes strong acidification of seepage water and increases of concentrations of iron species and sulfate (SO_4^{2-}). Calcite dissolution releases Ca^{2+} and carbonate species into seepage water. Depending on effective groundwater recharge (net water infiltration from precipitation minus evapotranspiration, surface runoff, and lateral flow) water saturation in the porous medium strongly influences oxygen diffusion rates. In case sufficient infiltration or groundwater recharge rates exist, concentrations of Ca^{2+} and SO_4^{2-} are kept low (i.e. 2-4 mmol/L of Ca^{2+} and < 50 mmol/L of SO_4^{2-}) and gypsum does not precipitate (saturation index, SI < 1). However, if seepage water infiltration rates are reduced or fully prohibited (e.g. due to sealed surface below buildings, Fig. 5.1-A), diffusion of oxygen continuously drives chemical weathering of pyrite which significantly elevates concentrations of dissolved species, i.e. of Ca^{2+} and SO_4^{2-}. If dissolved species are not effectively flushed out from the model domain into groundwater, oversaturation of Ca^{2+} and SO_4^{2-} may lead to gypsum precipitation (Figs. 5.1-D and 5.1-E):

$$Ca^{2+} + SO_4^{2-} + 2H_2O \leftrightarrow CaSO_4 \cdot 2H_2O \qquad \log K_{eq,gyp} = 4.58 \qquad (5.1)$$

where $K_{eq,gyp}$ [-] is the equilibrium constant of the reaction.

Typically, gypsum precipitates and grows in the bedding plane of pyrite bearing strata below buildings and swelling of gypsum may lead to vertical expansion. In case uneven swelling occurs below buildings, irregular uplift and inclination of buildings are a consequence often causing cracks in walls.

5.2.3 Numerical methods and model parameters

In order to elucidate controls of gypsum precipitation below buildings the numerical code MIN3P (May et al., 2002; Bao et al., 2016) was used which allows to model chemical weathering of pyrite bearing mudstones accounting for oxygen (gas) diffusion and unsaturated flow. The governing equations of flow and reactive transport as well as

kinetical and equilibrium controlled water-rock interactions are given in Bao et al., 2016. Effective diffusion coefficients in gas and water were estimated from empirical relationships (e.g. following Moldrup et al. 2000 and 2001).

In particular, we focused on widely distributed pyrite- and kerogen-bearing Opalinus Clay in Southern Germany and considered four reactive minerals, i.e. pyrite, kerogen, calcite and siderite, and two secondary minerals, i.e. ferrihydrite and gypsum (assuming major clay minerals are stable). Kinetics of pyrite oxidation follow the shrinking core model (Wunderly et al., 1996; Mayer et al., 2002), while kerogen oxidation follows a Monod kinetic approach (reaction rates and parameters taken from Mayer et al., 2002 and Bao et al., 2016). Surface-controlled reactions of mineral precipitation and dissolution are applied for calcite, siderite, ferrihydrite and gypsum (effective reaction rates and equilibrium constants taken or calculated from Ball and Nordstrom, 1991 and from Mayer et al., 2002). For instance, the reaction rate of gypsum precipitation and dissolution, R_{gyp} [mol/(L • bulk • s)] is calculated by:

$$R_{gyp} = -k_{eff,gyp}(1 - \frac{IAP}{K_{eq,gyp}}) \hspace{3cm} (5.2)$$

where $k_{eff,gyp}$ [mol/(L • bulk • s)] denotes the effective rate of the reaction, and IAP is the ion activity product.

Fe^{2+} and Fe^{3+} form a redox couple, and gas dissolution-exsolution of $O_2(g)/O_2(aq)$ and $CO_2(g)$/carbonate species are assumed to be at equilibrium state.

Table 5.1 shows mineral compositions in weight (wt%) and volume (vol%) fractions selected for numerical simulations based on literature data (Grathwohl,1989; Hekel, 1994; Taubald, 2013; Gautschi, 2001; Nagra, 2002; Bao et al., 2016).

Table 5.1. Mineral compositions (wt% vs vol%) of pyrite bearing mudstones (Opalinus Clay) selected.

	Minerals	wt%	vol%	Density [g/cm³]
primary minerals	total organic carbon	1.5%	3.34%	0.8
	pyrite	2%	0.71%	5.02
	siderite	2%	0.90%	3.96
	calcite	15%	9.86%	2.71
secondary minerals	ferrihydrite	-	-	4.37
	gypsum	-	-	2.32

-: not determined.

Table 5.2 lists physical and hydrological parameters (e.g. van Genuchten parameters, initial porosity and hydraulic conductivity) used for numerical simulations. Buildings and heating systems in the subsurface can additionally enhance gas diffusion and promote oxygen transport to larger depth, and thus we considered enhanced diffusion coefficients in the free gas ($D_g^* = 5.0\times10^{-5}$ m^2/s) and water ($D_w^* = 5.0\times10^{-9}$ m^2/s) phases.

Table 5.2. Overview of model parameters for un-weathered pyrite bearing mudstones.

Physical and hydrological parameters		
Model domain depth, z [m]		6
Initial porosity, n [-]		0.35
	S_{rw} [-]	0.1
van Genuchten	α [1/m]	0.77
parameters of un-weathered Opalinus	N [-]	1.25
Clay [a]	I [-]	0.5
Hydraulic conductivity, K [m/s]		5.0×10^{-8} [b]
Dispersivity, α^* [m]		0.1
Temperature, [°C]		10
Gaseous diffusion coefficient, D_g^* [m^2/s]		5.0×10^{-5} [c]
Aqueous diffusion coefficient, D_w^* [m^2/s]		5.0×10^{-9} [c]

[a]: van Genuchten parameters were taken Bao et al., (2016).
[b]: Hekel (1994).
[b]: enhanced diffusion coefficients in the free gas and water phases were assumed below buildings.

At low water infiltration rates the model predicts the amount of gypsum precipitated. Vertical expansion caused by precipitation of gypsum is quantified by calculating the potential volume of gypsum per square meter surface area, V_{gyp} [m^3/m^2]:

$$V_{gyp}(t) = n_{gyp}(t) \times \Delta V_{gyp} \tag{5.3}$$

where t [year] is the time, n_{gyp} [moles/m^2] refers to the total mass of gypsum per square meter surface area below buildings (which is obtained from MIN3P simulations), and ΔV_{gyp} [74 cm^3/mol] is the molar volume of gypsum.

In modeling, we focus on evolution of concentrations of Ca^{2+} and SO$_4^{2-}$ and gypsum precipitation for the scenarios of pure oxygen diffusion and with different water infiltration rates. Consequences of water saturation, effective gas diffusion, pyrite contents as well as water infiltration rates are discussed in the following.

5.3 Results and discussion

5.3.1 Gypsum precipitation

Fig. 5.2 shows evolution of oxidation front in pyrite bearing mudstones, concentrations of Ca^{2+} and SO_4^{2-}, effective gas diffusion (D_{eg}), gypsum precipitation (in volume fraction, vol%) and potential volume caused by swelling of gypsum following chemical weathering for the pure diffusion scenario (no infiltration of water) at five time instants, i.e. initial condition, 1 yr, 3 yr, 10 yr and 30 yr. We started model simulations with original mudstones (mineral compositions in Table 5.1), water contents (predicted by Richard's equation with van-Genuchten parameters in Table 5.2) and initially no dissolved species, i.e. Fe^{2+}, HCO_3^-, H^+, Ca^{2+} and SO_4^{2-} (see the first row of Fig. 5.2). Due to fast pyrite oxidation and quasi-equilibrium calcite dissolution, concentrations of Ca^{2+} and SO_4^{2-} immediately pop up to saturation levels at the weathering front and precipitate as gypsum (the second row of Fig. 5.2, SI > 0). During progress of the weathering front gypsum continuously accumulates (see 1 yr, 3 yr, 10 yr and 30 yr, last column of Fig. 5.2). For the example given here, model results indicate that potential volume of gypsum per square meter surface area achieve 0.015 m^3/m^2 (at 1 yr), 0.024 m^3/m^2 (3 yr), 0.038 m^3/m^2 (10 yr) and 0.062 m^3/m^2 (30 yr).

Clearly, gypsum precipitation depends on concentrations of Ca^{2+} and SO_4^{2-} in the water, both of which are released from chemical weathering due to pyrite oxidation and calcite dissolution. In the following we discuss how water saturation (and thus effective gas diffusion) and the effect of pyrite oxidation rates and pyrite contents can influence gypsum precipitation and potential volume of gypsum in the subsurface at Time = 10 yr.
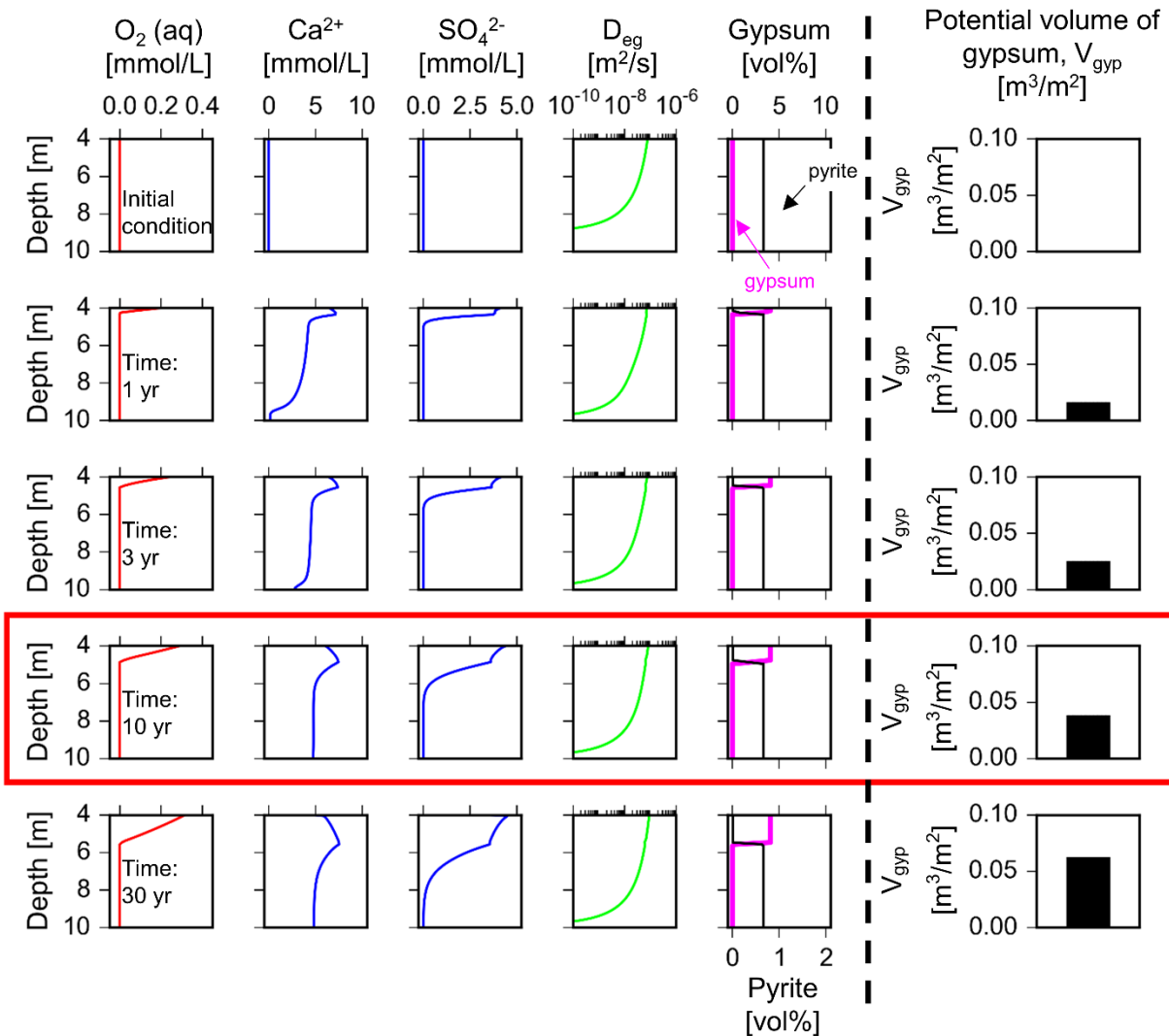
Figure 5.2. Evolution of oxygen, Ca^{2+}, and SO_4^{2-} vertical concentration profiles, effective gas diffusion (D_{eg}) and gypsum precipitation from model simulations as well as potential volume of gypsum expected at five time instants, i.e. initial condition, 1 yr, 3 yr, 10 yr and 30 yr in the subsurface.

5.3.1.1 Effect of water saturation and pyrite content

Water saturation in porous media depends on grain size distribution (or van Genuchten parameters) and water infiltration rates. Effective gas diffusion coefficients are highly sensitive to water saturation (Moldrup et al. 2000 and 2001). Fig. 5.3 compares the effect of two water saturation scenarios (i.e. van Genuchten parameters α/N: 0.77/1.25 (black

line) vs. 5.0/2.0 (red line)) on effective oxygen diffusion, pyrite oxidation, gypsum precipitation, and potential volume of gypsum at Time = 10 yr. As shown in Fig. 5.3, decreasing water saturation (Fig. 5.3-A) enhances effective gas diffusion (Fig. 5.3-B) and thus accelerates oxygen ingress (Fig. 5.3-C), and consequently speeds up oxidation of pyrite (Fig. 5.3-D) and enhances precipitation of gypsum (Fig. 5.3-E), which finally causes larger volume of gypsum (Fig. 5.3-F) and potentially more vertical expansion after the same time period (10 yr).
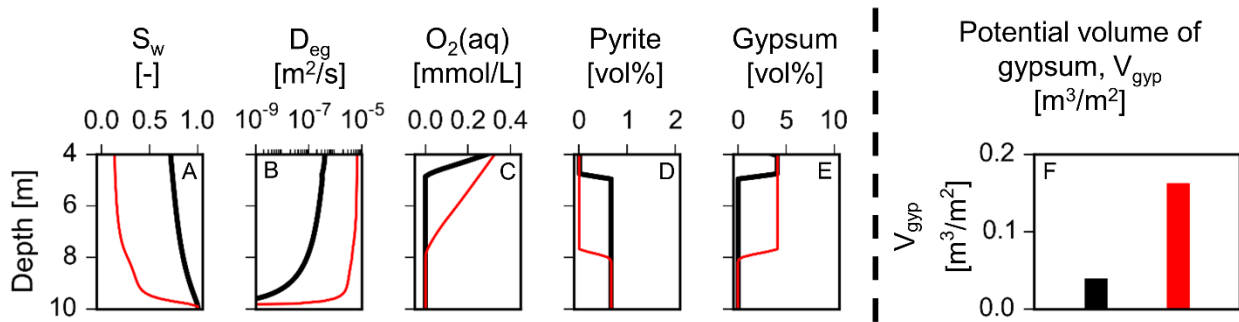
Figure 5.3. Effect of water saturation (S_w) on D_{eg}, oxygen ingress, pyrite oxidation, and gypsum precipitation and potential volume of gypusm at Time = 10 yr.

Clearly, oxygen diffusion is the main factor driving the weathering front, and thus the total amount of gypsum precipitation and vertical expansion in the subsurface. Enhanced gas diffusion caused by low water contents or higher temperatures (e.g. because of elevated temperatures below buildings) result in more gypsum precipitation and faster vertical expansion.

Fig. 5.4 shows the effect of increasing pyrite contents (2 wt%: black bar vs. 5 wt%: red bar) on the potential volume caused by gypsum precipitation at Time = 10 yr. Higher pyrite contents release more SO_4^{2-} and thus increase the amount of gypsum precipitation and thus vertical expansion.
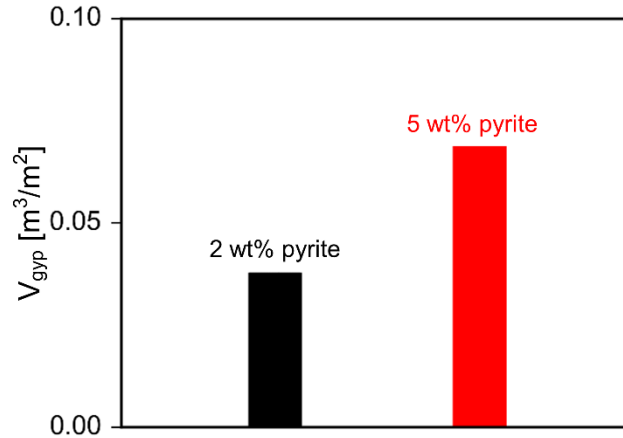
Figure 5.4. Effect of pyrite contents on potential volume of gypsum in the subsurface at Time = 10 yr.

5.3.2 Leaching of sulfate and prevention of gypsum precipitation by water infiltration

At low water flow rates increasing concentrations of Ca^{2+} and SO_4^{2-} (no or limited leaching by seepage water) cause gypsum precipitation. In case seepage water is allowed, water saturation is increased and concentrations of Ca^{2+} and SO_4^{2-} are diluted depending on water infiltration rates. Fig. 5.5 shows this effect for different water infiltration rates of 0 mm/yr, 3 mm/yr, 10 mm/yr, 30 mm/yr and 100 mm/yr at Time = 10 yr. Increasing water infiltration rates dilute concentrations of Ca^{2+} and SO_4^{2-} in seepage water and finally less gypsum precipitation and thus vertical expansion are expected. Gypsum precipitation is significantly eliminated if the water infiltration rate reaches 100 mm/yr in the scenario modelled here. Water infiltration rates to prohibit gypsum precipitation depend much effective diffusion coefficients of oxygen, pyrite contents and reaction rates. In summary, gypsum precipitation might be prohibited by (*i*) irrigation systems to flush out dissolved species released from the weathering process and (*ii*) oxygen diffusion barriers below buildings (unrealistic).
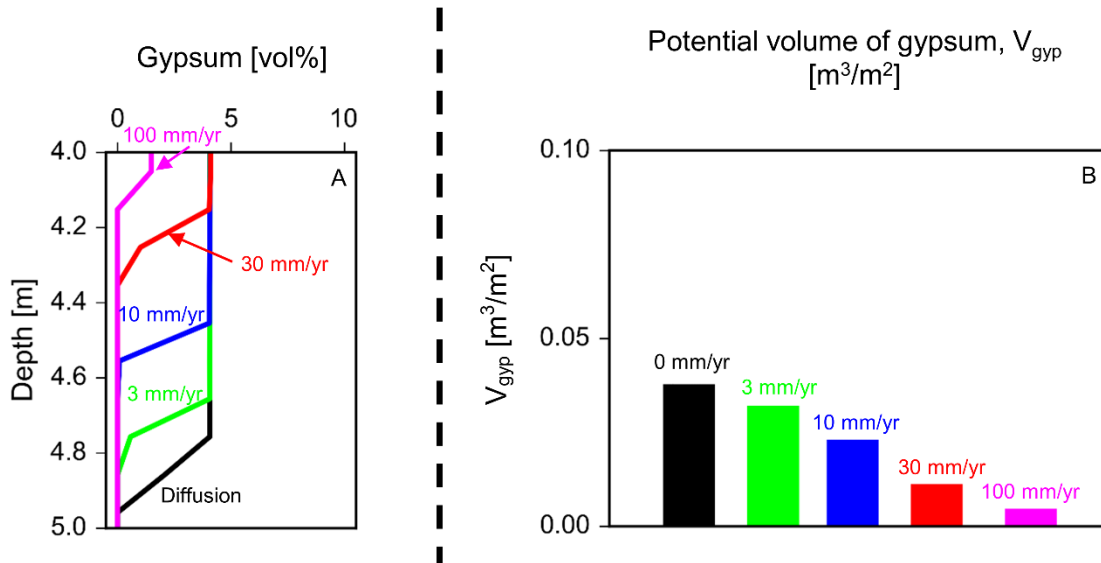
Figure 5.5. Gypsum precipitation (A) and potential volume of gypsum (B) as a function of water infiltration rates at Time = 10 yr.

5.4 Conclusions

Chemical weathering of pyrite bearing mudstones below buildings is mainly driven by oxygen transport. It leads to release of dissolved species, i.e. iron species (Fe^{2+} and Fe^{3+}), carbonate species, and Ca^{2+} and SO_4^{2-} into seepage water. Aqueous concentrations of these solutes depend on water infiltration rates. If water infiltration rates are much less than 100 mm/yr, elevated concentrations of dissolved species, especially Ca^{2+} and SO_4^{2-}, have to be expected which consequently leads to gypsum precipitation. The rate and amount of gypsum precipitation depend on pyrite contents and oxidation kinetics as well as water saturation (controlling effective oxygen diffusion). Irrigation systems or oxygen diffusion barriers could help to eliminate gypsum precipitation below buildings. Coupled models such as MIN3P as presented here help in analyzing hydrogeochemical controls of gypsum precipitation of pyrite bearing strata.

References

Anagnostou, G., Pimentel, E., Serafeimidis, K., 2010. Swelling of sulphatic claystones: some fundamental questions and their practical relevance. Geomechanics and Tunnelling. 3(5), 567-572.

Ball, J.W., Nordstrom, D.K., 1991. User's manual for WATEQ4F, with revised thermodynamic data base and test cases for calculating speciation of major, trace, and redox elements in natural waters. U.S. Geological Survey, Open-file report 91-183.

Bao, Z., Maier, U., Haberer, C., Amos, R.T., Blowes, D.W., Grathwohl, P., 2016. Modeling controls on the chemical weathering of marine mudrocks from the Middel Jurassic (Swabian Alb, Southern Germany). Chem. Geol. (Submitted).

Berdugo, I. R., Alonso, E. E., Romero, E., Gens, A., 2009a. Tunneling and swelling in Triassic sulphate-bearing rocks. Part I: case studies from Baden-Württemberg. Revista Epsilon. 12, 1-17.

Berdugo, I. R., Alonso, E. E., Romero, E., Gens, A., 2009b. Tunneling and swelling in Triassic sulphate-bearing rocks. Part II – Case studies from Jura Mountains. Revista Epsilon. 12, 18-30.

BGR. Mittlere järhliche Grundwasserneubildung (Tafel 5.5). Bundesanstalt für Geowissenschaften under Rohstoffe (BGR) in Hannover. Access time: May 22, 2016. URL: www.bgr.bund.de.

Bossart, P., 2011. Characteristics of the Opalinus Clay at Mont Terri. Access time: Jan. 5, 2016. URL: http://www.mont-terri.ch/internet/mont-terri/de/home/geology/key_characteristics.parsys.49924.DownloadFile.tmp/characteristicsofopa.pdf

Butscher, C., Mutschler, T., Blum, P., 2016. Swelling of clay-sulfate rocks: A review of processes and controls. Rock Mech. Rock Eng. 49(4), 1533-1549.

Einstein, H.H., 1996. Tunnelling in difficult ground: swelling behavior and identification of selling rocks. Rock Mech. Rock Eng. 29(3), 113-124.

Gautschi, A., 2001. Hydrogeology of a fractured shale (Opalinus Clay): Implications for deep geological disposal of radioactive wastes. Hydrogeol. J. 9, 97-107.

Goldscheider, N., Bechtel, T.D., 2009. Editors' message: the housing crisis from underground-damage to a historic town by geothermal drillings through anhydrite, Staufen, Germany. Hydrogeol. J. 17(3), 491-493.

Grimm, M., Stober, I., Kohl, T., Blum, P., 2014. Schadensfallanalyse von Erdwärmesondenbohrungen in Baden-Württemberg (Damage event analysis of drilling borehole heat exchangers in Baden-Württemberg, Germany). Grundwasser. 19, 275-286.

Hekel, U. Hydrogeologische Erkundung toniger Festgesteine am Beispiel des Opalinustons (Unteres Aalenium). (PhD dissertation) Institut und Museum für Geologie und Paläontologie der Universität Tübingen, 1994.

Klein, C., Hurlbut, C.S., Dana, J.D., Mineraloge, G., 1993. Manual of mineralogy. Vol. 527. Wiley, New York.

Langman, J.B., Moore, M.L., Ptacek, C.J., Smith, L., Sego, D., Blowes, D.W., 2014. Diavik waste rock project: evolution of mineral weathering, element release, and acid generation and neutralization during a five-year humidity cell experiment. Minerals 4(2), 257-278.

Mayer, U.K., Frind, E.O., Blowes, D.W., 2002. Multicomponent reactive transport modeling in variably saturated porous media using a generalized formulation for kinetically controlled reactions. Water Resour. Res. 38, 1174.

Moldrup, P.; Olesen, T.; Gamst, J.; Schjønning, P.; Yamaguchi, T.; Rolston, D.E., 2000. Predicting the gas diffusion coefficient in repacked soil water-induced linear reduction model. Soil Sci. Soc. Am. J. 64, 1588-1594.

Moldrup, P.; Olesen, T.; Komatsu, T.; Schjønning, P.; Rolston, D.E., 2001. Division S-1 — Soil physics: Tortuosity, diffusivity, and permeability in the soil liquid and gaseous phase. Soil Sci. Soc. Am. J. 65, 613-623.

Nagra, 2002. Projekt Opalinuston – Synthese der geowissenschaftlichen Untersuchungsergebnisse. Entsorgungsnachweis für abgebrannte Brennelemente, verglaste hochaktive sowie langlebige mittelaktive Abfälle. Nagra Technical Report NTB 02-03. Nagra, Wettingen, Switzerland.

Sass, I., Burbaum, U., 2010. Damage to the historic town of Staufen (Germany) caused by geothermal drillings through anhydrite-bearing formations. Acta Carsologica. 39(2), 233-245.

Wunderly, M.D., Blowes, D.W., Frind, E.O., Ptacek, C.J., 1996. Sulfide mineral oxidation and subsequent reactive transport of oxidation products in mine tailings impoundments: A numerical model. Water Resour. Res. 32(10), 3173-3187.

Chapter 6.

Conclusions and Future Outlook

In this study, reactive transport modeling was applied to analyze the effect of coupled physical, biological, geochemical and hydrological processes on diffusive gas exchange across the soil-atmosphere interface as well as on soil and groundwater chemistry. The multicomponent reactive transport code MIN3P (May et al., 2002), originally developed to model flow, reactive transport and biogeochemical reactions in the subsurface, was extended with the atmospheric boundary layer where eddy diffusion and photochemical transformation of photosensitive pollutants (in the vapor phase) occur. In addition, a plant layer was considered as well as heat transport in the subsurface and temperature-dependent multiphase partitioning. Mass transport of semi-volatile compounds across the soil-atmosphere interface is controlled by the concentration gradient and effective gas diffusion coefficient following Fick's laws. With MIN3P, mass fluxes and vertical concentration profiles across the soil-atmosphere interface are obtained. In two case studies, we selected two groups of semi-volatile compounds to investigate gas exchange across the soil-atmosphere interface; we focussed on concentrations of solutes and/or ions in soils and groundwater:

- Vertical transport of SVOCs across the soil-(plant-)atmosphere interface with focus on
  - i. long-term soil pollution from atmospheric deposition and
  - ii. diurnally temperature-driven concentration fluctuations.
- Oxygen ingress into pyrite- and kerogen-bearing mudstones during the chemical weathering process, with
  - i. dynamics in oxidation, mineral transformation, carbon, iron and sulfur turnover and CO_2 release, as well as
  - ii. diffusion-driven gypsum precipitation.

6.1 Conclusions

The main conclusions drawn from the four subtopics of this PhD study are summarized in the following:

Long term environmental fate of SVOCs. Soil-atmosphere exchange is of vital importance for the environmental fate and atmospheric transport of SVOCs. Due to turbulent mixing of vapor phase pollutants in the atmosphere and strong retardation in the subsurface (caused by the affinity of SVOCs to soil organic matter), long term soil-atmosphere exchange of SVOCs is limited by the soil compartment, depending on physicochemical parameters for the compound of interest, soil properties, and effective groundwater recharge rate. Diffusion and sorption significantly influence the accumulation and spreading of pollutants in soils at early time periods, whereas microbial degradation and groundwater recharge determine the long term mass transfer in the subsurface. As a consequence, for undisturbed soils, soils are contaminated by gas and wet atmospheric deposition following temporal variations of atmospheric pollution from anthropogenic emissions. The time period required to reach steady state with respect to soil pollution depends on physicochemical parameters of the transported compound and on soil properties, e.g. soil organic matter and soil thickness.

Diurnal concentration fluctuations of SVOCs between different compartments. We investigated temperature-driven cycling of semi-volatile pollutants between soils, plants, and the atmosphere. To do so we considered heat transport, effective gas diffusion, sorption and biodegradation in soils as well as eddy diffusion and photochemical transformation in the atmospheric boundary layer with changing heights over a day and night cycle. PCB-52 and phenanthrene were chosen as representative compounds for PCBs and PAHs. We compared atmospheric concentration fluctuations of PCB-52 with field data (from Lee et al., 1998) in the soil–plant–atmosphere system. We found that temperature-mediated soil-atmosphere exchange cannot account for strong atmospheric concentration fluctuations of vapor phase pollutants as observed. Instead we observed that a rapidly-exchanging compartment above ground, such as plants may act as the source/sink term responsible for significant diurnal atmospheric concentration fluctuations.

Chemical weathering of pyrite- and kerogen-bearing mudrocks. Numerical simulations show that diffusion is the main control of chemical weathering of pyrite- and kerogen-bearing mudrocks in the Swabian Alb, Southern Germany. Oxidation of pyrite and kerogen by oxygen causes acidification of seepage water and release of H^+ and iron species, which consequently dissolve carbonates and precipitate as iron oxides, i.e. ferrihydrite. Water infiltration rate determines water saturation in the porous medium and thus influences effective gas diffusion and oxygen ingress. Eventually, water infiltration rate also controls the propagation of the weathering front. Chemical weathering of near-surface mudstones thus changes mineral composition, re-shapes soil structure, increases porosity and influences seepage water and finally groundwater chemistry. Model results in porosity, water saturation, and water chemistry were validated with field data obtained in Reutlingen and with data from Hekel (1994). We found that seepage water and groundwater chemistry are strongly influenced by advection. For instance, higher water infiltration rate results in lower concentrations of ions in seepage water and groundwater.

Gypsum precipitation below buildings founded in pyrite bearing mudstones. In Southern Germany, buildings founded in pyrite bearing mudstones reduce or inhibit water infiltrating through the underlying bedrock, which is still exposed to atmospheric oxygen. As a result, chemical weathering of the underlying bedrock is enhanced. Dissolved species, especially Ca^{2+} and SO_4^{2-}, released from chemical weathering, accumulate and finally precipitate as gypsum. The rate and amount of gypsum precipitation depend on water saturation of the underlying bedrock, reaction rate of pyrite oxidation as well as pyrite content. Since concentrations of Ca^{2+} and SO_4^{2-} are determined by advection, developing a drainage system (i.e. 'irrigation'), can technically reduce or limit gypsum precipitation for future buildings founded in pyrite bearing strata.

6.2 Future outlook

The numerical model developed in this PhD study couples physical, biological, geochemical and hydrological processes to investigate the impact of these processes on mass transfer within/across different environmental compartments. The model can be applied to simulate environmental fate of legacy organic pollutants, such as PAHs, PCBs

and pesticides. In addition, the model is also applicable to quantify environmental pathways of emerging organic pollutants, e.g. pharmaceuticals and personal care products (PPCPs) as well as poly- and perfluorinated compounds (PFCs). It was demonstrated that the numerical model can also be applied to problems where flow and reactive transport in the porous medium are coupled with biogeochemical reactions of inorganic volatile gases, i.e. O_2, CO_2, NH_3 and CH_4. Hence, the numerical model may serve as a tool to establish or adapt environmental regulations or specifications for management and engineering applications.

As many assumptions had to be made and physicochemical processes had to be simplified, the complexity of the subject regarding diffusive gas exchange across the soil-atmosphere interface and its impact on soil and groundwater chemistry are shown. Based on the scenarios presented above, a future outlook on modeling environmental fate of SVOCs and chemical weathering of pyrite bearing mudstones are given separately in the following.

6.2.1 Environmental fate of SVOCs

For the sake of simplicity, a linear sorption isotherm, temperature-independent microbial degradation and photochemical transformation following first-order kinetics, and local equilibrium of plant-air partitioning of phenanthrene and PCB-52 were assumed for numerical simulations. Validation of our model results with field data was limited. In particular, measurements of atmospheric PAH concentrations over long time periods or at high temporal resolution and with stable patterns on the short term are missing in literature. Therefore, validation of our model results with actual field measurements is worthy further investigation. Obtaining field data, especially with respect to short-term atmospheric concentration fluctuations of PAHs, is currently challenging due to strong photochemical transformations of PAHs, nearby ongoing and unstable anthropogenic emissions, and difficulties in field sampling by passive or active samplers.

The numerical model illustrates strong capability to model environmental fate of hydrophobic organic pollutants. These hydrophobic organic pollutants (legacy and emerging organic pollutants) may partition similarly due to their affinity to soil organic matter (sorption), volatility from soil solids or water into vapor phase as well as resistance

to microbial degradation and photochemical oxidation. Mackay (2001) proposed the idea of chemical space to identify and group environmental fate of SVOCs into different categories between different environmental compartments. However, this approach is mainly limited to linear models (or nonlinear models with analytical solutions), and many details (e.g. flux across compartments and concentration profiles) are neglected. Therefore, it is necessary to develop novel numerical approaches, such as a global sensitivity analysis, to combine chemical space with nonlinear environmental fate models at affordable computational costs.

6.2.2 Chemical weathering of pyrite bearing mudstones

When modeling chemical weathering of pyrite- and kerogen-bearing mudstones in Southern Germany, we focussed on diffusive gas exchange of O_2 and CO_2 across the mudstone-atmosphere interface, carbon, iron and sulfur turnover, seepage water and groundwater chemistry, mineral transformation (i.e. consumption of reactive minerals, and precipitation of ferrihydrite and gypsum) and increase of porosity. All clay minerals in pyrite bearing mudstones were assumed to be stable. However, ion exchange between seepage water and clay minerals and concentrations of other dissolved species may pose influences on concentrations of Fe^{2+}, Ca^{2+}, SO_4^{2-}, HCO_3^- and pH (Appelo and Postma, 2005). As a consequence, this may again impact mineral precipitation and dissolution. Dissolved species released from chemical weathering were assumed to leach into deeper groundwater in a 1-D vertical model; a free seepage boundary was applied at the bottom of the model domain. Further research may be necessary to evaluate how transport of these dissolved species occurs in 2-D hillslope or 3-D catchment scale models.

Investigating gypsum precipitation below buildings founded in pyrite bearing mudstones in Southern Germany, special attention was on hydrogeochemical controls of rate and amount of gypsum precipitation and potential swelling caused by gypsum while interactions with other clay minerals were neglected. To develop new reactive transport models that can couple geochemical water-rock interactions with swelling of clay minerals is required to better understand swelling potential of claystones in geotechnical applications.

References

Appelo, C.A.J., Postma, D., 2005. Geochemistry, groundwater and pollution. CRC press.

Hekel, U., 1994. Hydrogeologische Erkundung toniger Festgesteine am Beispiel des Opalinustons (Unteres Aalenium). (PhD dissertation) Institut und Museum für Geologie und Paläontologie der Universität Tübingen.

Lee, R.G.M., Hung, D., Mackay, D., Jones, K.C., 1998. Measurement and modeling of the diurnal cycling of atmospheric PCBs and PAHs. Environ. Sci. Technol. 32, 2171-2179.

Mackay, D., 2001. Multimedia environmental models: the fugacity approach. CRC press.

Mayer, U.K., Frind, E.O., Blowes, D.W., 2002. Multicomponent reactive transport modeling in variably saturated porous media using a generalized formulation for kinetically controlled reactions. Water Resour. Res. 38, 1174.

Supporting Information

S1 Modeling long-term uptake and re-volatilization of semi-volatile organic compounds (SVOCs) across the soil-atmosphere interface

Verification of the numerical model.

S1.1 Transport by advection-dispersion and diffusion

To verify the numerical code, we modeled transport through a 5 m thick homogeneous soil column (porosity = 0.33; organic carbon content = 0.3%; temperature = 10 °C) and compared the results of our numerical simulations with corresponding analytical solutions for advective-dispersive transport (Ogata and Banks, 1961) and diffusion into a semi-infinite porous medium with linear sorption (Grathwohl, 1998).

The analytical solution for advective-dispersive transport (Ogata and Banks, 1961) in a water-saturated porous medium is:

$$\frac{C}{C_0} = \frac{1}{2} \left[erfc\left(\frac{|z| - \frac{q}{n}\,t}{2\,\sqrt{Dt}} \right) + exp\left(\frac{\frac{q}{n}\,|z|}{D} \right) erfc\left(\frac{|z| + \frac{q}{n}\,t}{2\,\sqrt{Dt}} \right) \right] \tag{S1.1}$$

where C/C_0 [-] is the normalized concentration of a conservative tracer, $|z|$ [m] refers to the soil depth (i.e. $z = 0$ at the ground surface), q [m/s] is the steady-state seepage water recharge rate (here 200 mm/year), n [-] denotes the total porosity, and t [s] is the time. D [m^2/s] denotes the hydrodynamic dispersion coefficient:

$$D = \frac{\alpha^*|q|}{n} + D_w^*\,n^{0.5} \tag{S1.2}$$

where α^* [m] refers to the dispersivity of the porous medium (here: $\alpha^* = 0.01$ m) and Dw^* [m^2/s] is the molecular diffusion coefficient of the compound of interest in water (phenanthrene: 6.71×10^{-10} m^2/s).

For pure diffusive transport we compared the numerical results with the analytical solution for retarded diffusion into a partially water-saturated semi-infinite porous medium (Grathwohl, 1998):

$$\frac{C}{C_0} = erfc\left(\frac{|z|}{2\sqrt{D_a t}} \right) \tag{S1.3}$$

where D_a [m^2/s] denotes the apparent diffusion coefficient of a vapor phase compound in porous media:

$$D_a = \frac{D_{eg}}{n_g + \frac{n_w}{H} + \frac{\rho(1-n)K_d}{H}} = \frac{D_g^* \frac{n_g^{2.5}}{n}}{n_g + \frac{n_w}{H} + \frac{\rho(1-n)K_d}{H}} \qquad \text{(S1.4)}$$

where D_{eg} [m²/s] and D_g^* [m²/s] are the effective and the molecular gas diffusion coefficients, n_g [-] and n_w [-] are the gas-filled and the water-filled porosity, and H [-], ρ [kg/m³], K_d [L/kg], S_g [-], and S_w [-] denote the Henry's law coefficient, the density of the particles, the sorption distribution coefficient, the gas saturation, and the water saturation, respectively.

Our results for the two cases are shown in Fig. S1.1. For both cases we achieved excellent agreement between the numerical model results and the analytical solutions. Besides numerical accuracy, this confirms accurate implementation of transport parameters (recharge, dispersion and diffusion coefficients, sorption, air/water partitioning, etc.).
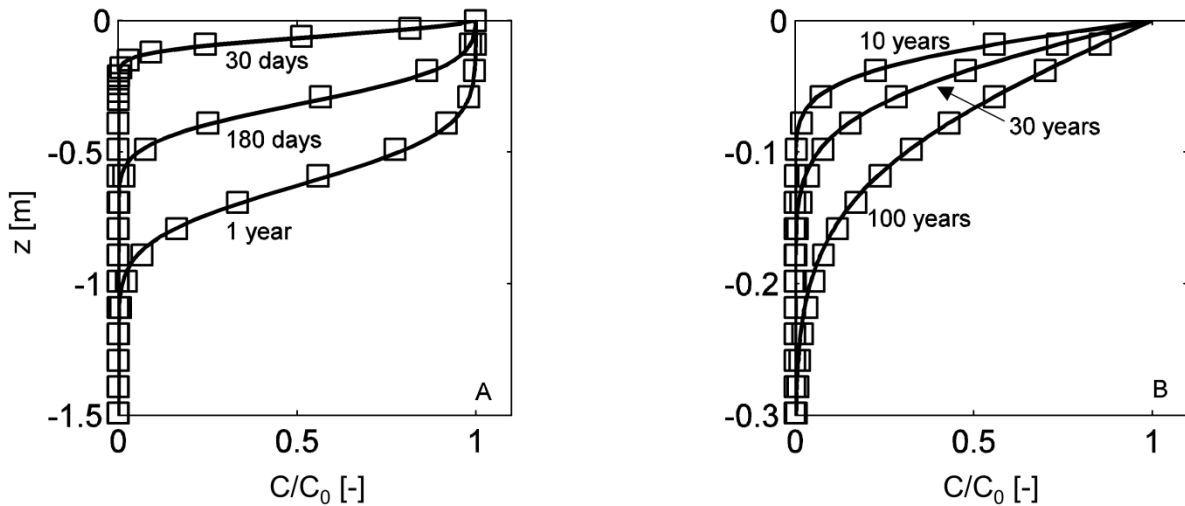

Figure S1.1. Verification of MIN3P (symbols) with analytical solutions (lines) for fixed concentration at the top boundary: (A) conservative advective-dispersive transport under water-saturated conditions, (B) retarded diffusion in the unsaturated soil (K_d = 78.3 L/kg).

S1.2 Characteristic time scales, steady-state concentrations and Damköhler numbers

For estimation of characteristic time scales to achieve steady state and corresponding concentration levels an analytical solution was derived using a simple box model. As described above, a uniform, water-saturated 5 m thick soil compartment was considered (porosity = 0.33; organic carbon content = 0.3%; temperature = 10 °C). Taking into account only groundwater recharge (which dominates over diffusion in the long term), linear sorption, and first-order biodegradation, the total solute mass change per area, $\frac{dM}{dt}$ [mg/(m^2·s)], in the soil results in the following differential equation:

$$\frac{dM}{dt} = input - decay - output = qC_{w,in} - \lambda C_w \theta h - qC_w \qquad \text{(S1.5)}$$

h [m] is the thickness of the soil layer considered and q [m/s] denotes the infiltration rate, which at steady state is equal to the groundwater recharge rate. $C_{w,in}$ [kg/m^3] and C_w [kg/m^3] refer to the aqueous concentration at the inflow boundary and the aqueous concentration leaving the system. θ [-] represents the volumetric water content in the porous medium, and λ [1/s] is the rate constant of first-order biodegradation.

The total mass in a soil column, e.g. after breakthrough at depth h, is given by:

$$M = C_w\theta h + C_g(n - \theta)h + C_s\rho(1 - n)h = C_w h(\theta + (n - \theta)H + \rho(1 - n)K_d) \qquad \text{(S1.6)}$$

where C_g [kg/m^3], and C_s [kg/kg bulk phase] respectively are the concentrations in the gas, and solid phase, and ρ [kg/m^3] denotes the solids density (2650 kg/m^3).

Since phenanthrene preferentially is present in the solid phase, M in Eqn. S1.6 can be simplified by neglecting the terms representing the gas and water phases ($M = h\rho(1 - n)K_d c_w$). Integration of Eqn. S1.6 with respect to C_w and t yields:

$$\int_0^{C_w} \frac{dC_w}{(q + \lambda h\theta)C_w - qC_{w,in}} = -\int_0^t \frac{dt}{h\rho(1 - n)K_d} \qquad \text{(S1.7)}$$

Thus,

$$\frac{C_w}{C_{w,in}} = \frac{1}{1 + \lambda h\theta/q}(1 - \exp(-\frac{q + \lambda h\theta}{h\rho(1 - n)K_d}t)) \qquad \text{(S1.8)}$$

In Eqns. S1.7 and S1.8, C_w is the averaged concentration in the aqueous phase across the soil depth. At $t = 0$, $C_w = 0$. Similarly, when $t \to \infty$ the steady-state concentration, $C_{w,s\text{-}s}$ [kg/m^3], is reached:

$$C_{w,s-s} = \frac{1}{1 + \lambda h\theta/q} C_{w,in} \qquad (S1.9)$$

A characteristic time, t_c [s], to reach steady state may be defined for an argument of one in the exponential function of Eqn. S1.8:

$$t_c = \frac{h\rho(1-n)K_d}{q + \lambda h\theta} \qquad (S1.10)$$

Since 1 – exp(-1) = 0.6321, the characteristic time to reach steady state is defined as the point in time when 63.21% of $C_{w,s-s}$ is achieved.

To evaluate if groundwater recharge or biodegradation, or both, are the decisive factors for the steady-state concentration levels, we use the Damköhler number (Damköhler, 1936), Da [-], which relates the time scale of flow ($t_a = h\,\theta/q$) to the time scale of biodegradation ($t_r = 1/\lambda$):

$$Da = \frac{t_a}{t_r} = \frac{\lambda\theta h}{q} \qquad (S1.11)$$

The Da term is included in the denominator of Eqn. S1.10. If $Da \ll 1$, the long-term steady state is dominated by groundwater recharge, and the output concentration equals the input concentration; if $Da > 1$, the long-term steady state is dominated by both groundwater recharge and biodegradation and for $Da > 100$, biodegradation takes over. Fig. S1.2 shows the comparison of our numerical model outcomes (symbols) accounting for all processes (advection, dispersion, diffusion, biodegradation and sorption) with the simple analytical solution for the box model (line, Eqn. S1.8). In this case, $Da \approx 31$, which indicates that biodegradation is important. Except for small differences at early times (which is due to diffusion/dispersion not covered in the analytical solution), an excellent match of our numerical model results with the analytical solution is achieved. Furthermore, the characteristic time (Eqn. S1.10), derived from the analytical solution, can be applied to estimate the time period needed to reach steady state.
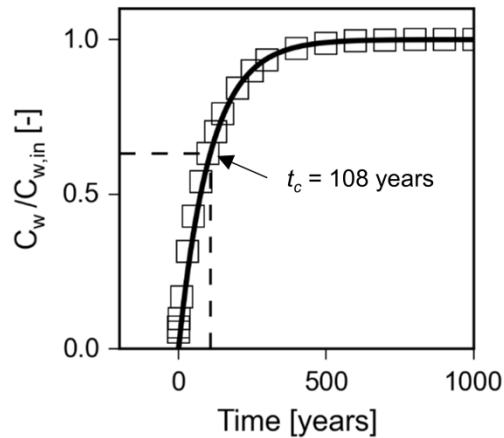
Figure S1.2. Model comparison of MIN3P (symbols) with the analytical solution of a simplified one-box model (line) accounting only for recharge and biodegradation (Eqn. S1.8). $C_w/C_{w,s-s}$ refers to the normalized concentration in the aqueous phase and values of the box model parameters applied are $h = 5$ m, $q = 200$ mm/year, $\theta = 0.33$, $\lambda = 1.2 \times 10^{-6}$ /s and $K_d = 78.3$ L/kg, respectively.

References

Damköhler G., 1936. Einflüsse der Strömung, Diffusion und des Wärmeübergangs auf die Leistung von Reaktionsöfen. Zeitschrift Elektrochemie 42(12), 846-862.

Grathwohl P., 1998. Diffusion in natural porous media: contaminant transport, sorption/desorption and dissolution kinetics. Kluwer, Boston, Massachusetts.

Ogata A., Banks R.B., 1961. A solution of the differential equation of longitudinal dispersion in porous media, USGS Professional Paper 411-A.

S2 Modeling short-term concentration fluctuations of semi-volatile pollutants in the soil–plant–atmosphere system

S2.1 Physico-chemical properties of PCB-52 and phenanthrene

Table S2.1 compiles all physicochemical properties of the two compounds at 25 °C.

Table S2.1. Physicochemical properties of PCB-52 and phenanthrene at 25 °C.

Parameter	PCB-52	Phenanthrene
Chemical formula	$C_{12}H_6Cl_4$	$C_{14}H_{10}$
Molecular weight, MW [g/mol]	292.0	178.2
Henry's law coefficient, $\log H$ [-]	-2.14 [a]	-3 [b]
Subcooled liquid solubility, S_{scl} [g/m³]	0.145 [c]	3.05 [d]
Organic carbon-water partition coefficient, $\log K_{OC}$ [L/kg]	5.26 [e]	4.14 [e]
Octanol-air partition coefficient, $\log K_{OA}$	7.73 [f]	7.60 [f]
Plant-air partition coefficient, $\log K_{PA}$ for a lipid content of 1% (= K_{OC}x0.01/H)	5.40	5.14
Enthalpy of air-water partitioning, ΔH_{aw} [kJ/mol]	48.44 [g]	47 [h]
Enthalpy of sorption, $\Delta H_{sorption}$ [kJ/mol]	-37.56 [g]	-30 [i]
Enthalpy of plant-air partitioning, ΔH_{PA} [kJ/mol]	86.6 [f]	71.4 [j]
Overall half-life of biodegradation, $t_{1/2, biodeg}$ [years]	4.81 [k]	0.18 [k]
Half-life of photochemical oxidation, $t_{1/2, photodeg}$ [hours]	1500 [l]	5.6 [m]
Aqueous diffusion coefficient, D_w^* [m²/s]	5.4×10⁻¹⁰ [n]	6.7×10⁻¹⁰ [n]
Gaseous diffusion coefficient, D_g^* [m²/s]	5.2×10⁻⁶ [n]	6.0×10⁻⁶ [n]

[a]: EPI Suite
[b]: Verschueren (1993)
[c]: Razzaque and Grathwohl (2008)
[d]: Liu et al. (2013)
[e]: calculated following Razzaque and Grathwohl (2008)
[f]: Böhme et al. (1999)
[g]: Beyer et al. (2002); the enthalpy of sorption between organic carbon and water was assumed the same as the internal energy change between octanol and water.
[h]: Schwarzenbach et al. (2003)
[i]: Wang and Grathwohl (2013)
[j]: Simonich and Hites (1994)
[k]: Gouin et al. (2000)
[l]: Sinkkonen and Paasivirta (2000)
[m]: Atkinson and Arey (1994)
[n]: calculated using the Fuller-Schettler-Gidding (FSG) method for the gaseous phase and the equation from Hayduk and Laudie (1974) for the aqueous phase

S2.2 Effective gas and eddy diffusion coefficients in soils and in the atmosphere

Fig. S2.1 shows the vertical profile of effective and eddy diffusion coefficients for PCB-52 at 23.1 ± 4.9 °C as calculated from empirical relationships for gas diffusion in soils and eddy diffusion in the atmosphere (Foken, 2008). These coefficients are used to describe vertical mass transfer of vapor phase pollutants. In case the empirical relationship from Foken (2008) is extrapolated, D_{eg} reaches values of 1.03 m²/s at 10 m, 10.3 m²/s at 100 m, and 102.8 m²/s at 1,000 m height in the atmosphere during daytime and at 23.1 °C. For a more detailed description see Bao et al. (2015).
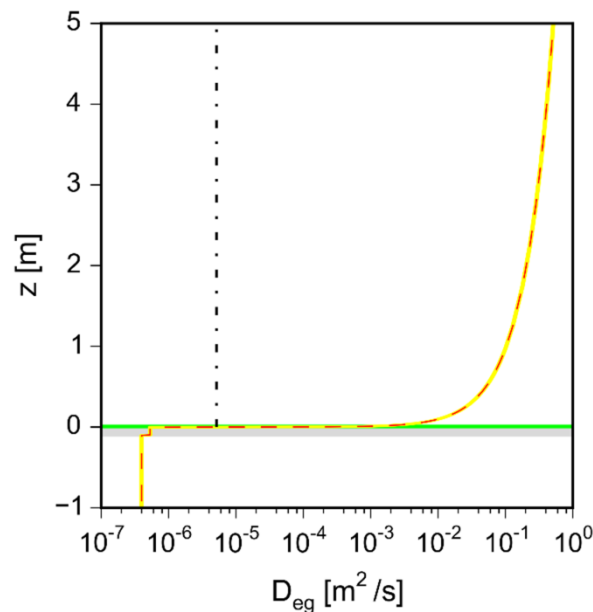
Figure S2.1. Vertical profile of effective gas and eddy diffusion coefficients for PCB-52 across the soil-atmosphere interface (red dashed line for T_A = 23.1 °C; the yellow area shows the impact of temperature changes with A = ± 4.9 °C on D_{eg}; vertical black dot-dashed line represents the molecular gas diffusion coefficient for PCB-52). The horizontal grey-shaded area marks the topsoil layer enriched in organic carbon, and the green-shaded area marks the 1 L/m² plant layer with an equivalent height of 1 cm in the model.

S2.3 Modeling vertical soil water contents

Water contents in soils control gas diffusion coefficients and thus are important for pollutant fluxes. The governing flow equation considering variable water saturation and used in the model is:

$$S_w S_s \frac{\partial h_\psi}{\partial t} + n \frac{\partial S_w}{\partial t} - \frac{\partial}{\partial z}\left[k_{rw} K \frac{\partial}{\partial z} h_\psi\right] = 0 \tag{S2.1}$$

in which S_w [-], S_s [1/m], k_{rw} [-], K [m/s], h_ψ [m], n [-], z [m], and t [s] respectively refer to the degree of water saturation, the specific storage coefficient, the relative permeability, the hydraulic conductivity, the matric potential, the porosity, the vertical coordinate, and the time. Water saturation and relative permeability are parameterized by the van Genuchten model, with α [1/m], N [-], and l [-], being the van Genuchten parameters (van Genuchten, 1980; Wösten and van Genuchten, 1988). Eqn. S2.1 is solved for long-term pollution and regulation (Bao et al., 2015) considering a Neumann boundary condition with $\frac{\partial q}{\partial z}\big|_{z=1000\ m}$ = 500 mm/yr. For short-term simulations, the numerical model result for water saturation is kept constant in this study.

S2.4 Modeling diurnal temperature changes in the soil

In the model we assumed that temperatures sinusoidally vary over a day in the atmosphere. Soil temperatures, T [°C] were updated in the vertical 1-D model using the analytical solution of the heat transport equation (Hillel, 1998):

$$T(z,t) = T_A + A\, exp\left(\frac{-|z|}{\sqrt{\frac{K_T \tau}{\pi}}}\right) sin\left(\frac{2\pi}{\tau}t - \frac{|z|}{\sqrt{\frac{K_T \tau}{\pi}}}\right) \text{ for } z < 0$$

$$T(z,t) = T_A + A\, sin\left(\frac{2\pi}{\tau}t\right) \text{ for } z \geq 0 \tag{S2.2}$$

where z [m] refers to the distance from the ground surface (where at the ground surface $z = 0$ m, below the ground surface $z < 0$, above the ground surface $z > 0$) and t [s] is the time. The characteristics of the temperature changes are described by the average temperature, T_A [°C], the amplitude, A [°C], and the period, τ [s]. In Eqn. S2.2, the thermal diffusivity, K_T [m^2/s], is estimated by applying Eqns. S2.3 to S2.8 (Hu et al., 2001; Balland and Arp, 2005; Lu et al., 2007):

$$K_T = \frac{\lambda_t}{c\rho(1-n)} \tag{S2.3}$$

$$\lambda_t = (\lambda_{t,sat} - \lambda_{t,dry})K_e + \lambda_{t,dry} \tag{S2.4}$$

$$K_e = 0.1811 \ln(S_w) + 0.9878 \tag{S2.5}$$

$$\lambda_{t,dry} = 0.039\, n^{-2.2} \tag{S2.6}$$

$$\lambda_{t,sat} = \lambda_{t,solid}^{1-n}\lambda_{t,water}^{n} \tag{S2.7}$$

$$c = (1 - n)c_s + n_w c_w + n_g c_g \tag{S2.8}$$

where λ_t [J/(m·K·s)], $\lambda_{t,sat}$ [J/(m·K·s)], and $\lambda_{t,dry}$ [J/(m·K·s)] are the thermal conductivities for a variably saturated porous medium, a saturated porous medium, and a dry porous medium, respectively. $\lambda_{t,solid}$ [J/(m·K·s)] and $\lambda_{t,water}$ [J/(m·K·s)] are the thermal conductivities for the solid and the aqueous phase, with values of 8.8 J/(m·K·s) (quartz material) and 0.57 J/(m·K·s) (water) (Hillel, 1998). ρ [kg/m³] and S_w [-] refer to the solids density (2,650 kg/m³) and the degree of water saturation, and K_e [-] is an empirical correction factor. c [kJ/(kg·K)] refers to the specific heat capacity of the porous medium of interest, c_s [kJ/(kg·K)], c_w [kJ/(kg·K)] and c_g [kJ/(kg·K)] are the specific heat capacities for the solid material, the aqueous phase and the gaseous phase, which are 2,120 kJ/(kg·K) for quartz, 4,185 kJ/(kg·K) for water and 1.3 kJ/(kg·K) for air (Hillel, 1998), and n_w [-] and n_g [-] are the water-filled and the gas-filled porosity.

Fig. S2.2 shows the temperature changes at different depths in the soil calculated with Eqn. S2.2 (T_A = 23.1 °C; A = 4.9 °C). At time = 0 we started with the average temperature, which is again reached after 12 hours. In the subsurface an increasing phase shift and dampening of the peak temperature is observed with increasing depth. The maximum and the minimum temperatures in the atmosphere are observed after 6 hours (+6 h) and 18 hours (+18 h), respectively. In case the plant layer was considered in a model scenario, the temperature within the plant layer (i.e. plant tissues) was assumed to be the same as in the atmosphere.
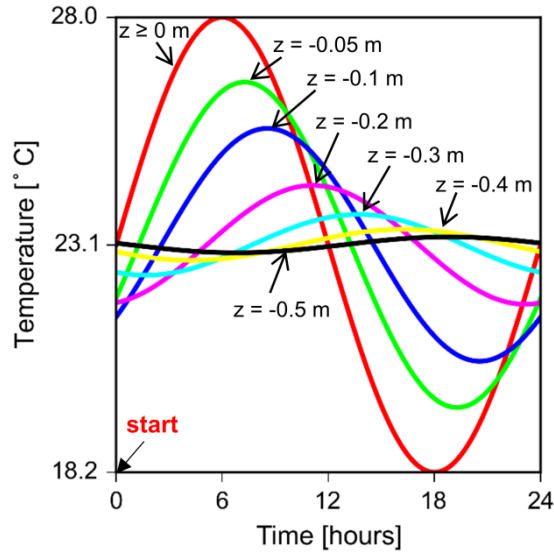
Figure S2.2. Diurnal temperature changes at 7 depths in the soil and in the atmosphere.

S2.5 Temperature dependence of sorption, partitioning, and diffusion

To account for the temperature dependence of sorption, changes in the distribution coefficient, K_d [L/kg], were determined based on the van't Hoff equation (Schwarzenbach et al., 2003):

$$\frac{K_d(T)}{K_d(T_0)} = \exp[-\frac{\Delta H_{sorption}}{R}(\frac{1}{T} - \frac{1}{T_0})] \tag{S2.9}$$

where T [K] and T_0 [K] are the specified temperature of interest and the standard temperature (298.15 K). $\Delta H_{sorption}$ [kJ/mol] denotes the enthalpy of sorption and R [8.314 J/(mol K)] is the ideal gas constant. Similarly, the van't Hoff equation was also utilized to calculate changes of Henry's law coefficient, H [-]:

$$\frac{H(T)}{H(T_0)} = \exp[-\frac{\Delta H_{aw}}{R}(\frac{1}{T} - \frac{1}{T_0})] \tag{S2.10}$$

ΔH_{aw} [kJ/mol] denotes the enthalpy of air-water partitioning.

Similarly, temperature dependence of plant-air partition coefficient, K_{PA} [L/kg], was also modeled following the van't Hoff relationship by applying the enthalpy of phase change between plants and air, ΔH_{PA} [kJ/mol].

Temperature dependence of diffusion coefficients in the aqueous, D_w [m²/s], and the gaseous, D_g [m²/s], phases was accounted for directly by implementing temperatures into empirical relationships from literature (Atkins, 1986; Lyman et al., 1990):

$$\frac{D_w(T)}{D_w(T_0)} = \frac{T}{T_0} \times 10^{\frac{247.8(T-T_0)}{(T-140)(T_0-140)}} \tag{S2.11}$$

$$\frac{D_g(T)}{D_g(T_0)} = \left(\frac{T}{T_0}\right)^{1.75} \tag{S2.12}$$

S2.6 Setting the initial conditions for volatilization/deposition of PCB-52 and phenanthrene

Initial conditions for the short-term model simulations were derived based on the procedure that we had developed to evaluate the long-term environmental fate of semi-volatile pollutants (Bao et al., 2015) for undisturbed soils. We assume that pollutants accumulated in topsoils during a pollution period, which is followed by a regulation period. The relevant model parameters as well as the boundary conditions for the selected semi-volatile pollutants (PCB-52 and phenanthrene) are summarized in Table S2.2 and shown in Fig. S2.3. Mean annual temperatures, seepage rates and the atmospheric concentrations of both compounds were taken from the literature (Lee et al., 1998). Fig. S2.3 also shows vertical concentration profiles, which were used for the short-term (diurnal) simulations.

Table S2.2. Model parameters used for long-term simulations of PCB-52 and phenanthrene.

Compound	Mean annual temperature [°C]	Seepage rate [mm/year]	Atm. concentrations		Time scale	
			Pollution period	Regulation period	Pollution period	Regulation period up to the time of interest (1995)
PCB-52	10 [a]	500 [b]	106.5 pg/m^3 [d]	21.3 pg/m^3 [c]	1930-1970 (40 years)	1970-1995 (25 years)
Phenanthrene	10 [a]	500 [b]	10.6 ng/m^3 [e]	5.3 ng/m^3 [c]	1870-1970 (100 years)	1970-1995 (25 years)

[a] data from the UK Climate, Met Office
[b] data from the UK Groundwater Forum
[c] averaged concentration according to Lee et al. (1998)
[d] five times the concentration at regulation period, considering historically stronger emissions at the pollution period and strict regulation measures at present for PCB-52 according to Stockholm Convention when compared with PAHs
[e] two times the concentration at regulation period according to Gocht and Grathwohl (2004)
Note, different time scales of pollution period were considered for PCB-52 and phenanthrene considering different emissions characteristics. Year 1995 was selected as the time of interest because we compared atmospheric concentration fluctuations of PCB-52 between model results and field measurements obtained in 1995 (Lee et al., 1998).

Figs. S2.3-A1 and S2.3-B1 show the accumulation and loss of the compounds of interest at selected vertical locations for the bare soil and the soil & plant scenarios over time. For the two compounds, rapid mass accumulation in soils during the pollution period and a decline during the regulation period are observed at the shallow depth of z = -0.01 m in the subsurface. Due to strong sorption in the topsoil, pollutants predominantly accumulate in the topsoil. Thus, plants and the underlying subsoil are much less affected (see overlap of blue dashed and red lines, and smaller concentration change at deeper depth in Figs. S2.3-A1 and S2.3-B1). Vertical concentration profiles (Figs. S2.3-A2 and S2.3-B2) show that the peak concentration of the pollutants is located at a shallow depth below the ground surface, which in principle fits field observations (Cousins et al., 1999a and 1999b; Gocht et al., 2001; Vikesøe et al., 2002; Atanassova and Brümmer, 2004). In the long term soils stay sinks for atmospheric pollutants even when the concentration in the atmosphere is reduced to a certain extent (Bao et al., 2015).
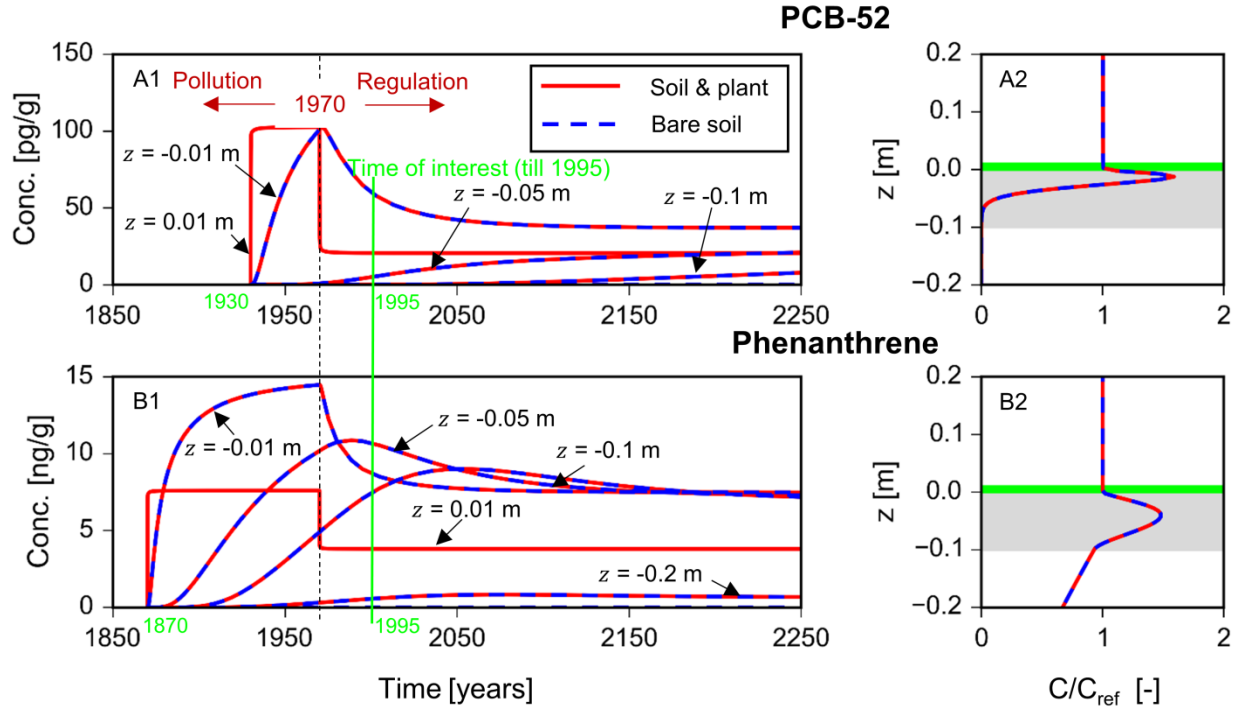
Figure S2.3. Uptake of atmospheric pollutants in soils ($z < 0$ m) without plants (bare soil, blue dashed lines) and with plants (soil & plant, red solid lines), and above ground in plants ($z = 0.01$ m). Left column A1, B1: Concentrations during the pollution period and the subsequent regulation period at selected depths in the subsurface ($z < 0$ m) and at the plant-atmosphere interface ($z = 0.01$ m). Right column A2, B2: vertical concentration profiles at the time of interest (in the year 1995). These concentration profiles were used as the initial conditions for the subsequent short-term (diurnal) simulations. The grey-shaded area represents the topsoil layer (2% f_{OC}), while the green-shaded area refers to the plant layer (1% lipid content). For normalization the initial concentrations at the upper boundary at 1.5 m height in the atmosphere were used ($C_{ref} = 21.3$ pg/m^3 for PCB-52 and $C_{ref} = 5.3$ ng/m^3 for phenanthrene).

S2.7 Mass balance in the soil–plant–atmosphere system

The effective diffusive depth, h_{eff} [m], of semi-volatile pollutants by diffusion from a semi-infinite source (plane sheet) at elevated periodic temperature changes is calculated by:

$$h_{eff} = \sqrt{\frac{D_{ag}t}{\pi}}$$

(S2.13)

in which t [0.5 d] is the time, D_{ag} [m^2/s] is the apparent diffusion coefficient which is calculated following $D_{ag} = D_{eg}/\alpha$, and α refers to the capacity factor, calculated by:

129

$$\alpha = n_g + \frac{n_w}{H} + \frac{\rho(1-n)K_d}{H} \qquad \text{(S2.14)}$$

As an example, the diffusive depth is only 0.1 mm considering f_{oc} = 2% in the topsoil for PCB-52 where ρ = 2,650 kg/m³, n = 0.4, n_g = 0.28 and n_w = 0.12 (and thus D_{eg} = 5.5×10⁻⁷ m²/s; $\alpha \approx 7.99 \times 10^5$) at 28 °C. This calculation agrees with our modelling results indicating that only a few millimeters of top soil are involved in diurnal soil-atmosphere mass exchange. The total mass of the compound of interest over one square meter land surface, X_{tot} [kg/m²], is mainly comprised by fractions in the atmosphere, plants, atmospheric particles, and soils:

$$X_{tot} = C_g h_{ABL} + C_{plant}\rho_{plant}V_{plant} + C_{particle}\omega_{particle}h_{ABL} + C_s\rho(1-n)h_{eff} \qquad \text{(S2.15)}$$

where C_g [kg/m³], $C_{particle}$ [kg/kg bulk phase], C_{plant} [kg/kg bulk phase], and C_s [kg/kg bulk phase] are the concentrations of the compound of interest in gas phase in the atmosphere, in the atmospheric particles, in the plant layer, and in the soil. V_{plant} [m³/m²] is the effective volume of the plant layer per square meter land surface, $\omega_{particle}$ [kg/m³] is the concentration of atmospheric particles, h_{ABL} [m] is the thickness of the atmospheric boundary layer and ρ_{plant} [kg/m³] is the density of plants.

Introducing the appropriate partioning coefficients K_{PA} [L/kg], $K_{particle-air}$ [L/kg] and K_{SG} [L/kg], and employing the local equilibrium approach, C_g in Eqn. S2.15 can be expressed as:

$$C_g = \frac{X_{tot}}{h_{ABL} + K_{PA}\rho_{plant}V_{plant} + K_{particle-air}\omega_{particle}h_{ABL} + K_{SG}\rho(1-n)h_{eff}} \qquad \text{(S2.16)}$$

where K_{PA}, $K_{particle-air}$ and K_{SG} represent the plant-air, particle-air, and soil-air partitioning coefficients.

For a rough estimate on mass fractions of PCB-52 in air, plants, atmospheric particles, and soils, the following parameterization was chosen: $K_{PA} \approx K_{particle-air} \approx 10^{5.4}$ (Table S2.1), K_{SG} = 2×10⁵·⁴, $\omega_{particle}$ = 0.1 mg/m³ which was chosen as a large, conservative value given reported limits of atmospheric particles with values less than 0.1 mg/m³ for some regions and countries, e.g. EU (European Commission), Australia (Australian Government), the United States (US EPA), V_{plant} = 1 L/m², ρ_{plant} = 1,000 kg/m³, and h_{ABL} = 1,000 m. The

resulting distribution is: 76% of PCB-52 in the atmosphere, 19% in plants, 2% in atmospheric particles, and 3% in a topsoil layer of 0.1 mm thickness. Obviously, the effective biomass above ground is of vital importance for short-term temperature-driven atmospheric concentration fluctuations of SVOCs.

Depending on the site-specific concentrations of particles in the atmosphere and compound-specific particle-air partitioning, pollutants sorbed to atmospheric particles (Eqn. S2.16) may also have some impact on atmospheric concentration fluctuations. Using the van't Hoff equation (see Eqn. S2.9) to calculate temperature-dependent plant-air parition coefficient K_{PA} for PCB-52 where $\log K_{PA}$ =5.40 and ΔH_{PA} = 86.6 kJ/mol, by changing from an average temperature of 23.1°C to 28°C the maximum release of PCB-52 from historically loaded plants is found to be 43.3%. Therefore, using mass balance, around half of the mass of PCB-52 from the plant layer could contribute to diurnal atmospheric concentration fluctuations. Here at temperature changes of 23.1±4.9 °C atmospheric concentration fluctuations of maximum 40% are observed; more biomass (i.e. higher plant coverage or more sorption) would increase this effect and cause higher fluctuations.

S2.8 Sensitivity analysis in the thickness of the stagnant air layer in the bare soil scenario

In the literature, two values in the thickness of the stagnant air layer, δ [m], were applied. Jury et al. (1983), McKone (1996) and Loizeau et al. (2014) applied a value of 5 mm while Davie-Martin et al. (2012) used a value of 1 mm. Fig. S2.4 compares model results of normalized concentration fluctuations of vapor phase PCB-52 in the bare soil scenario in a height of 1.5 m in the atmosphere with δ = 5 mm and δ = 1 mm. A smaller stagnant air layer enhances mass transfer coefficient by reducing diffusion distance across the soil-atmosphere interface, and thus relatively strong atmospheric concentration fluctuation is obtained when δ = 1 mm. However, compared with field measurements (black dots in Fig. S2.4, and from Lee et al., 1998), re-volatilization of semi-volatile pollutants from soils over a day and night cycle cannot account for the strong atmospheric concentration fluctuations of PCB-52 and the conclusion is valid regardless the thickness of the stagnant air layer.
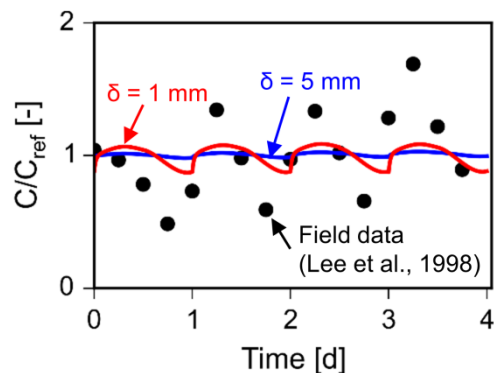
Figure S2.4. Impact of the thickness of the stagnant air layer (δ [m]) on the diurnal temperature-driven concentration fluctuations of vapor phase PCB-52 at 1.5 m height in the atmosphere in the bare soil scenario. Filed data of PCB-52 obtained in Hazelrigg (UK) is normalized to the reference concentration C_{ref} = 21.3 pg/m^3 (black dots, from Lee et al., 1998).

S2.9 Vertical concentration profiles up to 1 m height in the atmosphere and atmospheric concentration fluctuations of PCB-52 and phenanthrene at 3 heights in both scenarios

Fig. S2.5 shows the vertical concentration profiles in the atmosphere from the soil surface up to a height of 1 m above ground (profiles across the compartmental interfaces are shown in Fig. 4.2). The most pronounced vertical concentration gradients are observed for phenanthrene, with photochemical oxidation occurring during daytime and where the plant layer is present.
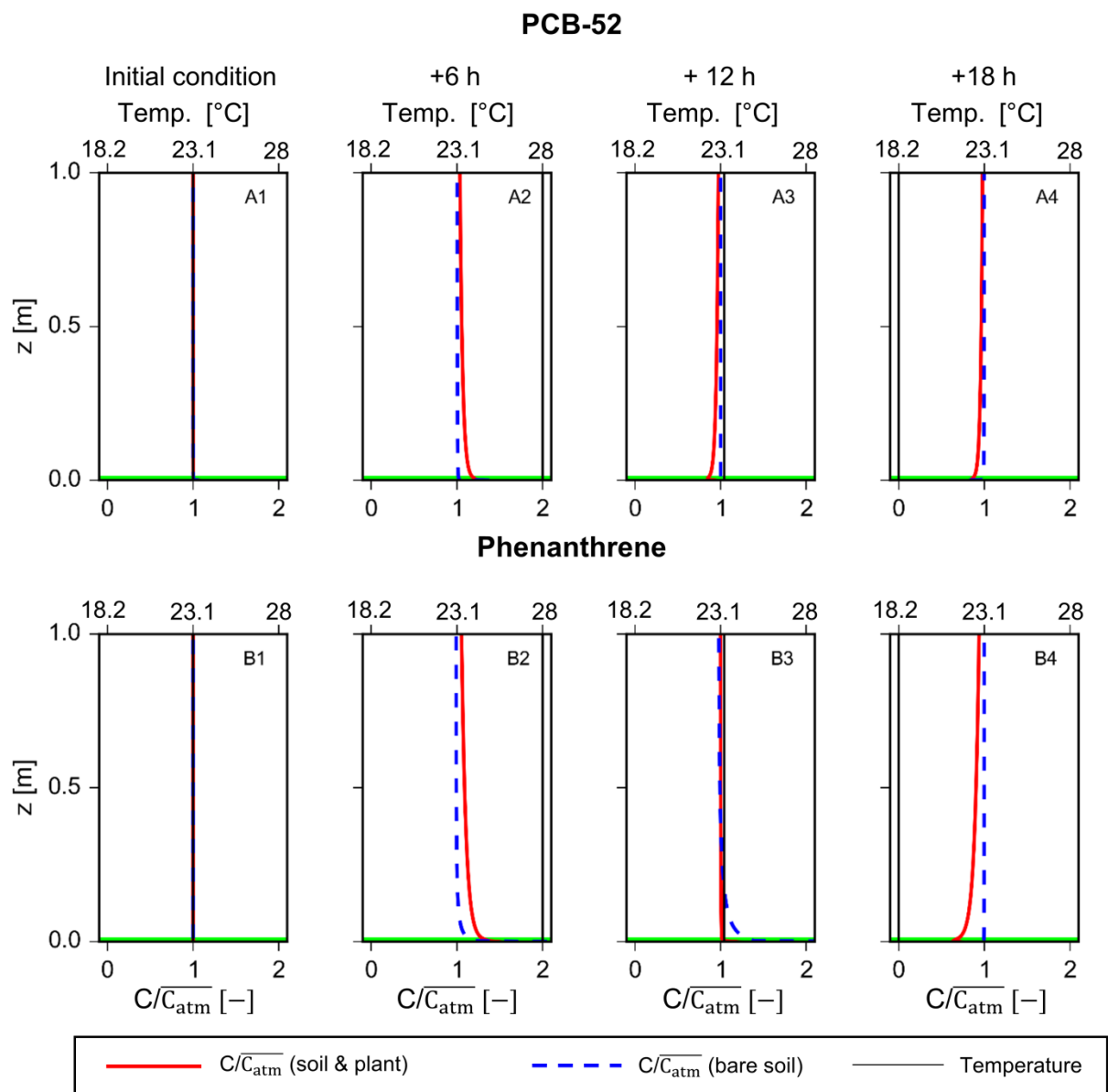
Figure S2.5. Vertical concentration profile of PCB-52 (top) and phenanthrene (bottom) in the atmosphere up to 1 m height at four time points when quasi-stable atmospheric concentrations were achieved (start: initial condition, +6 h, +12 h, +18 h) in the bare soil and the soil & plant scenarios. Concentrations were normalized to the average concentrations in the atmosphere at each time point, $\overline{C_{atm}}$ [mass/volume].

Fig. S2.6 shows short-term concentration fluctuations at 3 different heights in the atmosphere, i.e. at 0.005 m, 1.5 m and 10 m above ground over a time period of 4 days (Fig. 4.3 shows concentration fluctuations close to the compartmental interfaces).
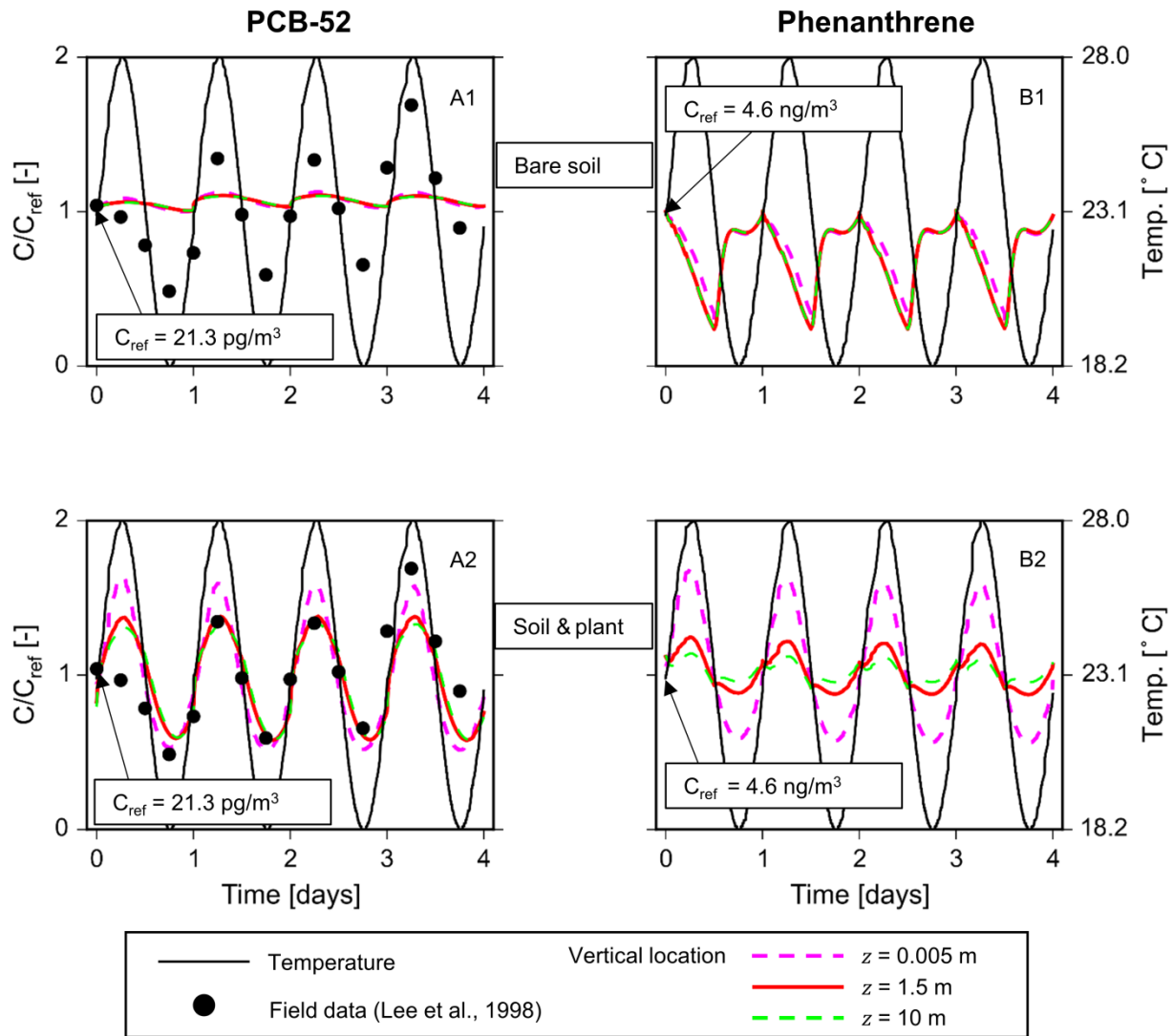

Figure S2.6. Concentration fluctuations of atmospheric PCB-52 and phenanthrene over four days at 3 heights in the atmosphere: 0.005 m (laminar layer), 1.5 m and 10 m height; first row A1, B1: the bare soil scenario; second row A2, B2: the soil & plant scenario. PCB-52 results are compared with data obtained in Hazelrigg, UK (black dots, from Lee et al., 1998 normalized to 21.3 pg/m^3). Different reference concentrations, C_{ref} [mass/volume], were chosen for normalization. Note that quasi-stable atmospheric concentration of phenanthrene is slightly lower than the initial concentration applied in Table S2.2 because of photochemical oxidation, ongoing emissions and plant regulation.

References

Australian Government. "National standards for criteria air pollutants in Australia – Air quality fact sheet". Access time: May 14, 2016. URL: http://www.environment.gov.au/protection/publications/factsheet-national-standards-criteria-air-pollutants-australia.

Atkins P.W., 1986. Physical chemistry. 3rd ed. Oxford University, New York.

Atanassova, I., Brümmer G.W., 2004. Polycyclic aromatic hydrocarbons of anthropogenic and biopedogenic origin in a colluviated hydromorphic soil of Western Europe. Geoderma 120(1-2), 27-34.

Balland, V., Arp, P.A., 2005. Modelling soil thermal conductivities over a wide range of conditions. J. Environ. Eng. Sci. 4(6), 549-58.

Bao, Z., Haberer, C., Maier, U., Beckingham, B., Amos, R.T., Grathwohl, P., 2015. Modelling long-term uptake and re-volatilization of semi-volatile organic compounds (SVOCs) across the soil-atmosphere interface. Sci. Total Environ. 538, 789-801.

Beyer, A., Wania, F., Gouin, T., Mackay, D., Matthies, M., 2002. Selecting internaly consistent physicochemical properties of organic compounds. Environ. Toxicol. Chem. 21(5), 941-953.

Cousins, I.T., Gevao, B., Jones, K.C., 1999a. Measuring and modelling the vertical distribution of semi-volatile organic compounds in soils. 1: PCB and PAH soil core data. Chemosphere 39, 2507-2518.

Cousins, I.T., Gevao, B., Jones, K.C., 1999b Measuring and modelling the vertical distribution of semi-volatile organic compounds in soils. 2: model development. Chemosphere 39, 2519-2534.

Cousins, I.T., Mackay, D., 2000. Strategies for including vegetation compartments in multimedia models. Chemosphere 44, 643-654.

EL-Saeid M.H., Al-Turki, A., Nadeem, M.E.A., Hassanin, A.S., Al-Wabel, M.I., 2015. Photolysis degradation of polyaromatic hydrocarbons (PAHs) on surface sandy soil. Environ. Sci. Pollut. Res. 22(13), 9603-9616.

European Commission. "Air Quality Standards". Access time: May 14, 2016. URL: http://ec.europa.eu/environment/air/quality/standards.htm.

Foken, T., 2008. Micrometeorology. Springer-Verlag: Heidelberg, Germany.

Gocht, T., Grathwohl, P., 2004. Polyzyklische aromatische Kohlenwasserstoffe aus diffusen Quellen. Umweltwissenschaften und Schadstoff-Forschung. 16, 245-254.

Gouin, T., Mackay, D., Webster, E., Wania, F., 2000. Screening chemicals for persistence in the environment. Environ. Sci. Technol. 34, 881-884.

Hayduk, W., Laudie, H., 1974. Prediction of diffusion coefficients for nonelectrolytes in dilute aqueous solutions. American Institute of Chemical Engineers Journal. 20(3), 611-615.

Hillel, D., 1998. Environmental Soil Physics: Fundamentals, applications, and environmental considerations. Academic Press, CA, USA.

Hu, X., Du, J., Lei, S., Wang, B., 2001. A model for the thermal conductivity of unconsolidated porous media based on capillary pressure-saturation relation. Int. J. Heat Mass Tran. 44, 247-251.

Lee, R.G.M., Hung, D., Mackay, D., Jones, K.C., 1998. Measurement and modeling of the diurnal cycling of atmospheric PCBs and PAHs. Environ. Sci. Technol. 32, 2171-2179.

Liu, L., Wu, F., Haderlein, S., Grathwohl, P., 2013. Determination of the subcooled liquid solubilities of PAHs in partitioning batch experiments. Geosci. Front. 4, 123-6.

Lu, S., Ren, T., Gong, Y., Horton, R., 2007. An improved model for predicting soil thermal conductivity from water content at room temperature. Soil Sci. Soc. Am. J. 71, 8-14.

Lyman W.L., Reehl W.F., Rosenblatt D.H., 1990. Handbook of chemical property estimation methods: Environmental behavior of organic compounds. 2nd. ed. Mc Graw – Hill, New York.

Mackay, D., 2001. Multimedia environmental models: the fugacity approach. CRC press.

Met Office. UK climate. Met Office in Exeter, UK. Access time: May 28, 2015. URL: http://www.metoffice.gov.uk.

Razzaque, M.M., Grathwohl, P., 2008. Predicting organic carbon-water partitioning of hydrophobic organic chemicals in soils and sediments based on water solubility. Water Res. 42, 3775-80.

Schwarzenbach, R.P., Gschwend, P.M., Imboden, D.M., 2003. Environmental organic chemistry. (2nd ed.) John Wiley & Sons Inc., New Jersey.

Simonich, S.L., Hites, R.A., 1994. Vegetation-atmosphere partitioning of polycyclic aromatic hydrocarbons. Environ. Sci. Technol. 28(5), 939-943.

Sinkkonen, S., Paasivirta, J., 2000. Degradation half-life times of PCDDs, PCDFs, and PCBs for environmental fate modeling. Chemosphere 40, 943-949.

UK Groundwater Forum. Groundwater resources. UK Groundwater Forum in Oxfordshire, UK. Access time: May 28, 2015. URL: http://www.groundwateruk.org.

US EPA. "Environmental Protection Agency – Particulate Matter (PM-10)". Access time: May 14, 2016. URL: https://www3.epa.gov/airtrends/aqtrnd95/pm10.html.

Van Genuchten, M.T., 1980. A closed-form equation for predicting the hydraulic conductivity of unsaturated soils. Soil Sci. Soc. Am. J. 44, 892-898.

Verschueren, K., 1993. Handbook of Environmental Data on Organic Chemicals. (2nd ed.) van Nostrand Reinhold Company Inc., New York.

Vikesøe, J., Johansen, E., Thomsen, M., Carlsen, L., 2002. Persistent organic pollutants in soil, sludge and sediment: a multianalytical field study of selected organic chlorinated and brominated compounds. National Environmental Research Institute Denmark. Roskilde. Report no. 402.

Wang, G., Grathwohl, P., 2013. Isosteric heats of sorption and desorption of phenanthrene in soils and carbonaceous materials. Environ. Pollut. 175, 110-6.

Wösten, J.H.M., van Genuchten, M.T., 1988. Using texture and other soil properties to predict the unsaturated soil hydraulic functions. Soil Sci. Soc. Am. J. 52, 1762-1770.

- **Movie S2.1** Dynamics of vertical concentration profile of vapor phase PCB-52 across the soil-atmosphere interface in the bare soil scenario.
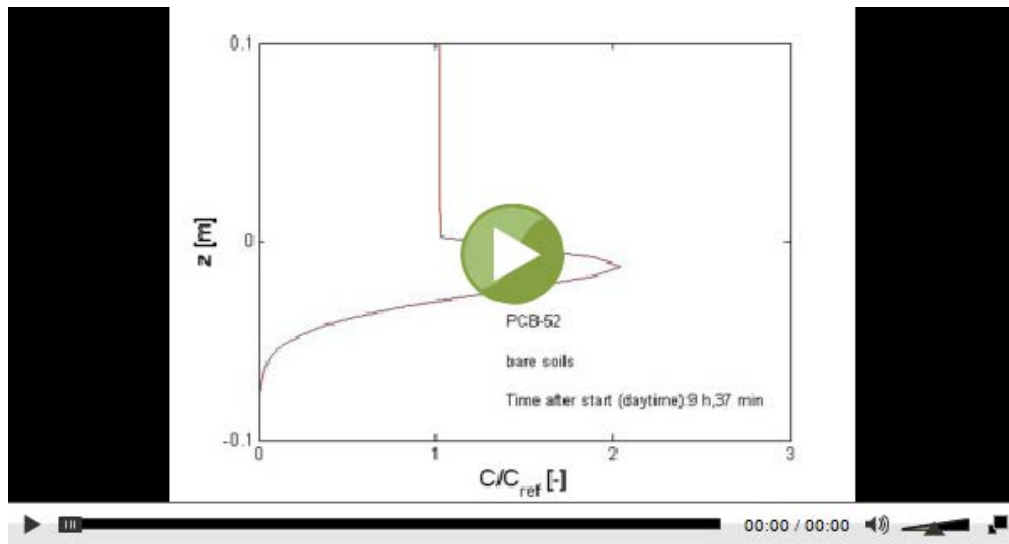
- **Movie S2.2** Dynamics of vertical concentration profile of vapor phase PCB-52 across the soil-atmosphere interface in the soil & plant scenario.